

TKK Dissertations 190  
Espoo 2009

# **MODELLING THE ATTACHED PLANE JET IN A ROOM**

Doctoral Dissertation

**Guangyu Cao**



**Helsinki University of Technology  
Faculty of Engineering and Architecture  
Department of Energy Technology**

TKK Dissertations 190  
Espoo 2009

## **MODELLING THE ATTACHED PLANE JET IN A ROOM**

Doctoral Dissertation

**Guangyu Cao**

Dissertation for the degree of Doctor of Science in Technology to be presented with due permission of the Faculty of Engineering and Architecture for public examination and debate in Auditorium K216 at Helsinki University of Technology (Espoo, Finland) on the 13th of November, 2009, at 12 noon.

**Helsinki University of Technology  
Faculty of Engineering and Architecture  
Department of Energy Technology**

**Teknillinen korkeakoulu  
Insinööritieteiden ja arkkitehtuurin tiedekunta  
Energiatekniikan laitos**

Distribution:

Helsinki University of Technology  
Faculty of Engineering and Architecture  
Department of Energy Technology  
Heating, Ventilating and Air-Conditioning  
P.O. Box 4400  
FI - 02015 TKK  
FINLAND

URL: <http://ene.tkk.fi/>

Tel. +358-9-451 3601

Fax +358-9-451 3418

E-mail: [guangyu.cao@tkk.fi](mailto:guangyu.cao@tkk.fi)

E-mail: [guangyu.cao@vtt.fi](mailto:guangyu.cao@vtt.fi)

© 2009 Guangyu Cao

ISBN 978-952-248-134-4

ISBN 978-952-248-135-1 (PDF)

ISSN 1795-2239

ISSN 1795-4584 (PDF)

URL: <http://lib.tkk.fi/Diss/2009/isbn9789522481351/>

TKK-DISS-2660

Multiprint Oy

Espoo 2009



ABSTRACT OF DOCTORAL DISSERTATION		HELSINKI UNIVERSITY OF TECHNOLOGY P.O. BOX 1000, FI-02015 TKK <a href="http://www.tkk.fi">http://www.tkk.fi</a>	
Author Guangyu Cao			
Name of the dissertation Modelling the attached plane jet in a room			
Manuscript submitted 25.02.2009		Manuscript revised 31.08.2009	
Date of the defence 13.11.2009			
<input type="checkbox"/> Monograph		<input checked="" type="checkbox"/> Article dissertation (summary + original articles)	
Faculty	Faculty of Engineering and Architecture		
Department	Department of Energy Technology		
Field of research	HVAC-technology		
Reviewers	Associate Professor Arsen K. Melikov, Technical University of Denmark, Denmark D.Sc.(Tech.) Kim Hagström, Halton Oy, Finland		
Opponent(s)	Professor Hazim B. Awbi, University of Reading, UK D.Sc.(Tech.) Kim Hagström, Halton Oy, Finland		
Supervisor	Professor Olli Seppänen (2006–2008), Helsinki University of Technology, Finland Professor Kai Sirén (2008–2009), Helsinki University of Technology, Finland		
Instructor	Docent D.Sc.(Tech.) Jarek Kurnitski, Helsinki University of Technology, Finland		
<b>Abstract</b> The application of the attached plane jet has proved to be an effective way to resolve the draught problem and to create a comfortable indoor environment. The objective of this thesis is to give a basis for improving the existing modelling and calculation method applied to predict the jet velocity in both ventilated and air-conditioned rooms using attached plane jet diffusers to avoid the draught problem. A special consideration is to set up models that could be used to predict the jet velocity along the surface more easily, more accurately and more efficiently than the existing methods under attachment and separation conditions.  Jet velocity modelling and full-scale experimental measurement have been done to complete the above objectives. Through two measurement phases the whole flow field of the attached plane jet has been investigated experimentally in two full-scale test chambers. A large amount of data on jet velocity, temperature and turbulence intensity has been obtained; beyond that the visualization results are complementary to the understanding of turbulent buoyant jet characteristics.  The results showed that: the superimposing model and the free convection velocity are capable of predicting the maximum air jet velocities along the wall under the conditions of the straight downward jet flow and the corner effect jet flow, respectively; the calculated corner-jet velocity profiles by the corner model obtained a good agreement with the measured results; the maximum velocity calculated by the model for the transition zone can be used to predict the maximum velocity decay.  This work reveals that the turbulent attached plane jet behaves in a different way compared with the high Reynolds number turbulent jet in a ventilated and air-conditioned room. From the modelling viewpoint, the jet velocity models constructed here can be used to predict the maximum jet velocity decay and velocity profiles from the corner effect region in the indoor airflow studies. The detailed jet information obtained can contribute to the corresponding CFD simulation for further linear slot diffuser development.			
Keywords attached plane jet, draught, impingement, airflow modelling, air velocity			
ISBN (printed)	978-952-248-134-4	ISSN (printed)	1795-2239
ISBN (pdf)	978-952-248-135-1	ISSN (pdf)	1795-4584
Language	English	Number of pages	82 p. + app. 93 p.
Publisher Helsinki University of Technology			
Print distribution Helsinki University of Technology			
<input checked="" type="checkbox"/> The dissertation can be read at <a href="http://lib.tkk.fi/Diss/2009/isbn9789522481351/">http://lib.tkk.fi/Diss/2009/isbn9789522481351/</a>			

To my beloved wife Feng

## **PREFACE**

The thesis was prepared in the HVAC-technology laboratory, Department of Energy Technology, Helsinki University of Technology during the years of 2006-2009. All of the experimental works in the study were done in the Indoor Air Research Centre of Halton Oy. The principal financial supports were provided by the Helsinki University of Technology and Halton Oy; and they are gratefully acknowledged for sponsoring this work. The financial support provided by the CIMO Foundation, the L.V.Y. Foundation, the Finnish Work Environment Foundation and the K.V. Lindholm Foundation are also gratefully acknowledged.

I express my gratitude and thanks to my supervisor, Professor Olli Seppänen, for his constructive advices, encouragement and invaluable comments on my published papers. I wish to thank Docent Jarek Kurnitski, my practical supervisor, for his continuous assistance and plenty of great comments on the published papers. I thank my supervisor, Professor Kai Sirén, for his guidance and motivation in the thesis finalization process.

Many thanks to Associate Professor Arsen K. Melikov from the Department of Civil Engineering, Technical University of Denmark and to Dr. Kim Hagström from Halton Oy for their positive feedback and constructive comments on the thesis.

I wish to thank PhD Mika Ruponen, M.Sc. Panu Mustakallio and Dr. Risto Kosonen from Halton Oy for their comprehensive advices and enthusiastic help during the experimental period, and constructive comments on my publications. In addition, I express warm thanks to my friends and colleagues at Halton Oy, Ismo Grövall, Risto Paavilainen, Maija Virta and many others besides. Their collaboration and support enabled me to complete the experimental research at Kausala, Halton Oy Indoor Air Research Centre, in the most pleasant, helpful and friendly atmosphere.

In addition, I wish to thank Dr. Rauno Holopainen from Finnish Institute of Occupational Health for his earlier collaboration and support. I would like to thank all my colleagues at Helsinki University of Technology, especially Dr. Juha Jokisalo, Senior Researcher Jari Palonen, Dr. Ala Ali Hasan, Lab. Manager Markku Sivukari, Dr. Targo Kalamees, Dr. Kari Alanne, M.Sc. Lari Eskola, and Secretary Mirka Seppälä, for the discussions, assist and pleasant working atmosphere during the past four years.

I wish to thank Professor Guohui Feng from Shenyang Jianzhu University for the continuous stimulation and support since my father passed away in 2003.

I would like to dedicate the thesis to the memory of my father, Yubin Cao who brought me up in a cultivated and well-educated environment. Special thanks to my mother Weiqing Zhang, for her encouragement and motivation, and for engendering in me a sense of discipline from an early age.

Finally, I want to thank my beloved wife, Feng Wang, who came to Finland beside me and has gone through all the difficult times with great patience, tolerance and support.

Espoo, June 2009  
Guangyu Cao

# TABLE OF CONTENTS

PREFACE.....	1
TABLE OF CONTENTS .....	2
LIST OF ORIGINAL PUBLICATIONS .....	4
ABBREVIATIONS .....	5
NOMENCLATURE .....	5
1 INTRODUCTION.....	8
1.1 Indoor air distribution .....	8
1.2 General thermal comfort in rooms.....	8
1.3 Air distribution and local thermal discomfort - draught .....	9
1.4 Different air distribution systems and air diffusers.....	11
1.5 The attached plane jet application.....	13
1.6 Objectives and contents of this thesis .....	15
2 TURBULENT ATTACHED PLANE JET FLOW .....	17
2.1 Literature review .....	17
2.2 The structure of the attached plane jet .....	19
2.2.1 Isothermal attached plane jet.....	19
2.2.2 Non-isothermal attached plane jet.....	20
2.3 Attached plane jet mean flow equations .....	21
3 EXPERIMENTAL SETUP .....	25
3.1 The test chambers and the air supply devices.....	25
3.1.1 The test chambers.....	25
3.1.2 Air diffusers for discharging jet flow .....	27
3.2 Measurement conditions .....	28
3.3 The supply air duct system and the cooling & heating source .....	29
3.4 The measurement points distribution.....	30
3.5 Measuring instruments and accuracy.....	31
3.5.1 Anemometer and calibration .....	31
3.5.2 Temperature sensor .....	32
3.5.3 Traversing device .....	32
3.5.4 Estimation of measurement accuracy.....	33
4 ISOTHERMAL AND NON-ISOTHERMAL JET VELOCITY MODELLING.....	34
4.1 Corner region modelling.....	34
4.2 Non-corner region modelling.....	35
4.2.1 Isothermal model.....	35
4.2.2 Free convection model .....	38
4.2.3 Buoyancy superimposing model .....	40
5 CALCULATION AND MEASUREMENT RESULTS .....	42
5.1 Jet flow field visualization.....	42
5.2 Jet velocity distribution in the developing region.....	44
5.2.1 Measurement results.....	44
5.2.2 Calculation results .....	46
5.3 Jet velocity distribution in the developed region .....	47
5.3.1 Measurement results.....	47
5.3.2 Calculation results .....	50
5.4 Jet velocity distribution in the corner region .....	53

5.4.1 Measurement results.....	53
5.4.2 Calculation results.....	54
5.5 Jet velocity distribution after the corner impingement.....	56
5.5.1 Measurement results.....	56
5.5.2 Calculation results.....	57
6 DISCUSSION.....	61
6.1 The limitation of the conventional jet model.....	61
6.2 The attached plane jet thickness.....	64
6.3 The corner effect on jet flow.....	67
6.4 Jet potential core.....	68
6.5 The buoyant jet regions and self similarity.....	70
7 CONCLUSIONS.....	73
REFERENCES.....	75
ORIGINAL PUBLICATIONS.....	82



## LIST OF ORIGINAL PUBLICATIONS

This thesis is completed on the basis of the following eight original publications, which are referred to in the text by their Roman numbers I-VIII.

- I Cao, G.Y., Kurnitski, J., Mustakallio, P. and Seppänen, O. (2008). Active Chilled Beam Wall Jet Prediction by the Free Convection Model. *International Journal of Ventilation*, Vol. 7(2), pp:169-178.
- II Cao, G.Y., Kurnitski, J., Ruponen, M., Mustakallio, P. and Seppänen, O. (2009). Plane-air-jet corner zone modelling in a room ventilated by an active chilled beam. *International Journal of Ventilation*, Vol. 7(4), pp:287-298.
- III Cao, G.Y., Kurnitski, J., Ruponen, M. and Seppänen, O. (2009). Modelling and experimental investigation of the turbulent attached plane jet in the transition process. *HVAC&R Research*, Vol. 15(3), pp:489-508.
- IV Cao, G.Y., Kurnitski, J., Ruponen, M. and Seppänen, O. (2009). Modelling and experimental investigation of a buoyant attached plane jet. *Applied Thermal Engineering*, Vol. 29(13-14), pp:2790-2798.
- V Cao, G.Y., Kurnitski, J. and Mustakallio, P. (2007). Draught risk evaluation in rooms with chilled beams, In: *Proceedings of Roomvent 2007*, pp:101-110, June 13-15, 2007, Helsinki, Finland.
- VI Cao, G.Y., Kurnitski, J., Mustakallio, P. and Seppänen, O. (2007). Performance of chilled beam air distribution close to the wall. In: *Proceedings of Roomvent 2007*, pp:79-86, June 13-15, 2007, Helsinki, Finland.
- VII Cao, G.Y., Kurnitski, J., Mustakallio, P. and Seppänen, O. (2007). Chilled beam's air distribution measurements and plane wall jet modelling, In: *Proceedings of the 5th International Symposium on Heating, Ventilating and Air Conditioning - ISHVAC 2007*, pp:288-295, September 7-8, 2007, Beijing, China.
- VIII Kurnitski, J., Cao, G.Y. and Mustakallio, P. (2007). Draft assessment for ceiling vs. wall mounted chilled beams. In: *Proceedings of Roomvent 2007*, pp:11-18, June 13-15, 2007, Helsinki, Finland.

The thesis author is the principal author of the seven publications (I-VII). He has written completely the publications (I-VII) and completed most of the experiments, the calculations and the modelling in (I-VII). In (I) and (III) the co-author Jarek Kurnitski participated in the model development. In (I-II) the co-author Panu Mustakallio took part in the measurement work and the co-author Mika Ruponen participated in and contributed to the experiments in (III-IV). All the other authors made contributions through comments and discussions on the analysis and the conclusions in (I-VII). In (VIII), the thesis author made a contribution to the results and the discussion.

## ABBREVIATIONS

DV	Displacement Ventilation
DR	Draught Rate
CFD	Computation Fluid Dynamics
PD	Percentage Dissatisfied Index
PIV	Particle Image Velocimetry
PMV	Predicted Mean Vote
PPD	Predicted Percentage of Dissatisfied
MV	Mixing Ventilation
TCV	Task Conditioning Ventilation

## NOMENCLATURE

The International System of units (SI) is used throughout the thesis

## NORMAL SYMBOLS

$a$	acceleration ( $\text{m}^2/\text{s}$ )
$Ar$	Archimedes number
$b$	distance between the geometrical origin of the jet and the wall (m)
$C_0$	velocity coefficient
$D_p$	growth rate of the jet per unit distance from the inlet
$F_b$	buoyancy force (N)
$g$	gravitational acceleration ( $9.81 \text{ m}^2/\text{s}$ )
$Gr$	Grashof number
$h$	slot height of the plane wall jet (m)
$H$	height of the room (m)
$I$	turbulence intensity (%)
$K$	velocity coefficient of jet model
$K_\theta$	temperature coefficient in jet velocity model
$K_l$	jet velocity constant in conventional jet model
$K^e$	temperature decay coefficient
$l$	length of the active-chilled-beam slot (m)
$L_x$	distance from the ceiling (m)
$L^*$	geometry characteristic of the office room (m)
$p$	similarity exponent of the jet velocity
$P-c$	total cooling power (W)
$Pr$	Prandtl number
$Pr_t$	turbulent Prandtl number
$q$	similarity exponent of the jet boundary layer thickness
$q_s$	supply air flow rate (L/s)
$Q$	air volume flow rate (L/s)
$Q'$	volume element of airflow (L)
Re	Reynolds number

$S$	slot area (m <sup>2</sup> )
$T$	temperature (°C)
$u$	jet velocity (m/s)
$u'$	standard deviation of the turbulent velocity
$U_{slot}$	slot initial air velocity (m/s)
$v_M$	coefficient in mean flow momentum equation
$W$	width of the test room (m)
$x$	jet horizontal traveling distance (m)
$x_0$	distance to virtual origin (m)
$x_p$	jet potential core distance (m)
$y$	vertical distance from initial point (m)
$y_{1/2}$	the distance from the wall where the air velocity is equal to half of the maximum air velocity (m)

### GREEK SYMBOLS

$\alpha$	finite angle of the jet boundary layer on a wall encounters a concave corner
$\alpha_H$	eddy diffusivities for heat transfer
$\rho$	density of fluid (kg/m <sup>3</sup> )
$\eta$	non dimensional distance from the wall
$\theta$	non dimensional temperature
$\nu$	kinematic viscosity (m <sup>2</sup> /s)
$\delta$	boundary layer thickness (m)
$\delta_a^1$	separation distance before the first corner (m)
$\delta(x)$	local boundary layer thickness (m)
$\delta$	uncertainty in measurement (%)
$\mu$	dynamic viscosity (kg/(s·m))
$\beta$	thermal expansion rate
$\omega$	air flow vorticity in the corner zone
$\psi$	stream function
$\tau$	shear stress (Pa)
$\varepsilon_M$	eddy diffusivities for momentum transfer (m <sup>2</sup> /s)
$\varepsilon_H$	eddy diffusivities for heat transfer (m <sup>2</sup> /s)

### Subscripts

$0$	initial situation
$a$	ambient air
$c$	cooling
$H$	heat transfer
$j$	jet
$l$	local
$m$	maximum
$p$	potential core
$ref$	buoyancy reference
$slot$	jet slot
$t$	turbulent

$w$	wall surface
$x$	distance on x axis
$y$	distance on y axis

*Superscripts*

$e$	temperature decay
'	standard deviation
*	geometry characteristic
$l$	the first corner

# 1 INTRODUCTION

## 1.1 Indoor air distribution

Office and commercial buildings require fresh air and the removal of heat, contaminated gases and particles that are emitted in the buildings, which may cause ‘sick building syndrome’ (SBS) (Awbi 1991). In the past, natural ventilation was used to achieve a good indoor environment (Loomens 1998). However, the natural ventilation method could not guarantee sufficient fresh air in each individual room. In many cases, an efficient air distribution system should be designed to create a more comfortable environment in the occupied zone (Nielsen 2007). In particular, the air distribution should reach the parts of the occupied zone where occupants will be present. The fresh air supplied by a properly designed system could contribute to the improvement of indoor productivity and to the reduction of airborne infectious diseases (Seppänen et al. 2006 and Seppänen 2008).

The early 1970s energy crisis stimulated the development of building technology, leading the modern trend towards better insulated buildings with less air leakage. In contrast with earlier buildings, the result of tightly sealing the building envelope and reducing the inflow of fresh air was that the indoor environment could be aggravated by the build-up of outgases from modern building materials, furniture and cleaning products. This trend led to the indoor environment of buildings becoming more and more dependent on the air distribution system than ever before. In the last two decades, the air distribution system was developed quickly to balance the controversial relationship between indoor air quality, thermal comfort and energy efficiency (Liddament 2000; Ballestini et al. 2005 and Seppänen 2008). Moreover, people spend more than 90% of their time in the artificial environments of modern society. The deterioration of indoor air quality has been experienced especially by people living or working in air-conditioned buildings manifesting the common SBS.

Generally, the role of the air distribution is to bring clean air intentionally to a certain space and to remove the stale or polluted air. Beyond that, the fresh air may also be heated or cooled, i.e. conditioned. In other words, the purpose of the air distribution system is to provide an acceptable microclimate in the space. The distributed airflow may either be blended with the existing room air (mixing principle) to dilute the pollutants uniformly, or be introduced without mixing (displacement principle) so that the breathing zone for the occupants becomes separated from the polluting sources. On the other hand, the presence of the occupant might also have an influence on the indoor air distribution (Cao et al. 2008). Modern air distribution strategies frequently aspire to the displacement approach, but this requires careful design and, very often, separate measures to provide an air-conditioned space (Liddament 2000). However, the fulfilment of the air distribution role is impeded by the fact that the thermal comfort conditions within a building enclosure for a typical person are limited to a narrow range (Fanger 1970).

## 1.2 General thermal comfort in rooms

Besides obtaining good indoor air quality, achieving acceptable thermal comfort would be another important goal of the air conditioning and ventilation system supplying fresh

air to rooms. Generally speaking, thermal comfort is the combined sensation of a complex interaction of different factors - the air temperature, the mean radiant temperature, the air velocity, the humidity and the human body. ISO 7730: 2005 specifies the methodology for predicting general thermal sensation and degree of discomfort experienced by people exposed to a moderate thermal environment. The index used in the method includes the predicted mean vote (PMV), the predicted percentage of dissatisfied (PPD) and a few local thermal discomfort factors, such as draught, vertical air temperature difference, warm and cool floors, and radiant asymmetry. In addition, ASHRAE 55.2004 presents guidelines for the thermal environmental conditions for occupants.

To achieve a satisfactory thermal environment, it is necessary to be able to predict what the effect of a particular combination of thermal conditions will be on the occupants. To obtain conditions of general thermal comfort, the modern indoor environment design methods are developed on the basis of the heat exchange conditions of the human body. The heat exchange can be calculated by the so-called heat balance equation, as studies have proved that the subjective thermal sensation is pleasant if the heat generated within the human body (metabolism) and the heat dissipated in various ways are in balance (Fanger 1970). Other human thermal models are based on transient heat transfer or the second law of thermodynamics, as every energy transfer and conversion is accompanied by an exergy transfer and conversion (Prek 2006). The main feature shared by most of the models is the application of energy balance to a person and the use of energy exchange mechanisms to predict the thermal sensation.

In many cases, the prediction of indoor thermal comfort is more complicated than the thermal model itself. Thermal comfort depends not only on environment factors, but also on personal factors such as human activities and clothing effects. Taking the uncomfortable conditions as an example, the three most common conditions are: asymmetrical thermal radiation, vertical air temperature gradient and draught (Awbi 1991). Non-uniform or asymmetrical thermal radiation in a space may be caused by cold/hot windows, walls, ceilings and heating panels. In offices and residential buildings, asymmetric radiation is mainly due to cold windows and heated ceilings, whereas in factory buildings it can be due to infrared heaters, hot or cold equipments, etc. The sensation of a draught is mainly caused by improper air supply and may be formulated as a function of air temperature, air velocity, and turbulence intensity.

### **1.3 Air distribution and local thermal discomfort - draught**

At present, internal heat gains and solar radiation may result in a large cooling load in a modern office building environment. Different air distribution systems have been developed and applied due to the different requirements of the temperature, gas, particle, humidity distributions and airflow patterns within a room (Hagström et al. 2000). Nielsen (2007) analyzed five different air distribution systems and found that the draught risk is low with a mixing ventilation system of optimal design and restricted heat load. Seppänen (2008) presented several strategies for air distribution and showed that selecting an appropriate strategy may maintain and improve the indoor air quality while reducing energy consumption. However, a draught risk may occur in air-conditioned rooms and becomes the most common indoor environment complaint in (V

and VIII). Griefahn et al. (2001 and 2002) reported the impact of air temperature, air velocity and workload on the indoor draught assessment. Generally, with regard to the thermal comfort of the indoor environment, the aim is to keep more than 80% of the occupants satisfied with the thermal conditions. An acceptable thermal condition is taken as being one in which no more than 6, 10 and 15%, representing the A, B and C category, of the occupants would be dissatisfied as a result of their overall thermal sensation. As for local thermal discomfort, no more than 10, 20 and 30% of the occupants should be dissatisfied owing to draught (ISO 7730. 2005). The ASHRAE 55.2004 standard requires a typical maximum permissible dissatisfaction rate of 20% in the case of draught, which is equivalent as the B category in ISO 7730.

A draught is defined as an unwanted local cooling of the body caused by air movement. In fact, a sensation of draught is determined by many factors, including the effect of the ambient environment, the occupant's metabolic rate, the air flow direction and personal sensitivity (Fanger et al. 1988; Toftum and Nielsen 1996a and 1996b; Toftum 2002 and Toftum and Melikov 2003). In earlier studies, subjects were exposed to a stable airflow at the level of their neck and ankles or in the head region (Fanger et al. 1986 and 1988). With respect to the model validation, the draught model was validated by turbulent airflow behind the subject at heights of 0.1 to 1.1 m from the floor. In ventilated spaces, however, the airflow is turbulent in the occupied zone. In Fanger's studies, the subjects expressed a greater degree of discomfort and sensitivity to draught than in the studies of Houghten (1938) presented in (Fanger and Christensen 1986). The main reason for the difference is that Houghten (1938) used a non-fluctuating airflow in the experiment. In other studies, the intensity of turbulence does play an important role in affecting the percentage of dissatisfied.

Earlier studies showed that the airflow direction, temperature elevation and the location of the draught assessment also have a significant effect on the evaluation and the prediction of draught. It is shown in (V) and (VIII) that the airflow direction may affect the sensation of a draught, especially when airflows from behind the neck and towards the face at the same temperature are compared. Mayer and Schwab (1988) discovered that subjects were more sensitive to a horizontal air flow from the back (neck) than to a horizontal airflow from the front (face). The airflow velocities from the front that caused the same sensation as a flow from the back were about 1.5 times higher (V). In the case of temperature elevation, Toftum et al. (1997) found that most experiences of a sensation of discomfort as a result of draught happen when people are exposed to air movements from below at 20 °C and 23 °C, but not at 26 °C and above. Considering the effect of the draught location, the literature review showed that about 1.5 times higher velocities at ankle level will cause the same draft sensations compared to neck level (VIII). Thus, if 0.2 m/s might be acceptable at neck level, 0.3 m/s could be accepted at ankle level.

In addition to the parameters determining the draught in present standards, air temperature, mean velocity and turbulence intensity, the impact of the frequency of velocity fluctuations on human thermal sensation have been reported (Zhou et al. 2002a, b). The equivalent frequency is defined as an integral measure for the frequency of the velocity fluctuations of a turbulent flow. Zhou and Melikov (2002a) have identified that the equivalent frequency of airflow in rooms in practice may vary from less than 0.1 Hz

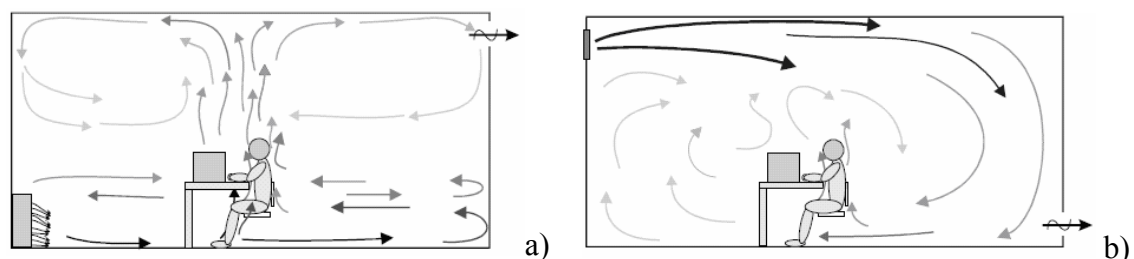
to 1.0 Hz. The subjects in their studies were most sensitive to draught at equivalent frequencies between 0.2 and 0.6 Hz.

#### 1.4 Different air distribution systems and air diffusers

Studies have shown that indoor air quality, thermal comfort, contaminant distributions and even occupant productivity depend strongly on indoor airflow characteristics and indoor airflow distribution from supply air diffusers (Sandberg et al. 1992; Awbi and Hatton 2000; Srebric et al. 2000; Seppänen et al. 2002 and Seppänen et al. 2004). Considering the mechanism of diluting pollutant and the corresponding airflow configuration, the air distribution system may be divided into a few classes, including local exhaust ventilation (LEV), piston ventilation (PisV), displacement ventilation (DV), mixing ventilation (MV) and task conditioning ventilation (TCV). Here, these systems would only represent the different air distribution patterns and different principles of indoor airflow configuration in rooms.

In this section, only the most common air distribution systems, DV and MV, are introduced to display the operational mechanism and corresponding air diffusers. The airflows pattern of DV and MV are presented in Figure 1.1 and show the displacement and mixing process in the indoor environment. DV aims at displacing air already present in a space, rather than mixing with it. With DV for cooling purposes, the supply air should be between 2-3 °C lower than the ambient room air temperature and emitted at a low level with a horizontal velocity, typically 0.1-0.3 m/s. This ensures airflow within the occupant breathing zone driven by a buoyancy rise to ceiling-mounted extract points (Liddament 2000). However, the supplied airflow reaching the breathing zone may also transport pollutants from the floor covering or from other mainly unheated pollution sources. This will decrease the quality of the air inhaled by the occupant (Melikov et al. 2005).

Unlike DV, the mechanism of MV involves mixing the supplied fresh air uniformly into a space and keeping the indoor air quality at an acceptable level. With MV, the air is mostly introduced at a relatively high velocity, for example higher than 1 m/s. Therefore the mixing of the supplied air with the room air through the entrainment process should take place before the air enters the occupied zone. As a result, the MV principle is characterized by the absence of significant room temperature and contaminant gradients (Loomans 1998). MV is still the most widely used method for the air-conditioning systems. A properly designed MV system can be used for heating and cooling as well as for ventilation in different indoor situations.






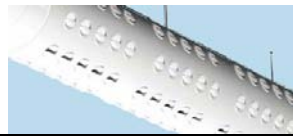



**Figure 1.1** Schematized airflow pattern by the displacement and the mixing ventilation principle. a) Displacement ventilation. b) Mixing ventilation. (Loomans 1998).



A more recent air distribution principle for office environments is the TCV principle, which like DV also originates from industrial application. If it were used directly for an occupant, it could be also called personalized ventilation (Faulkner et al. 1999, Melikov et al. 2005). TCV with a temperature below that of the room air temperature was able to bring ‘a cool head’ and increased the thermal comfort in comparison with the MV (Niu et al. 2007). In air distribution applications, different air distribution systems and air diffusers have been extensively studied (Sandberg 1987; Melikov et al. 1990, 2005 and 2007; Melikov 2004; Awbi 1991; Awbi and Hatton 2000; Nielsen 1991 and 2007). Table 1.1 shows the applications of different air diffusers in MV and DV air distribution systems.

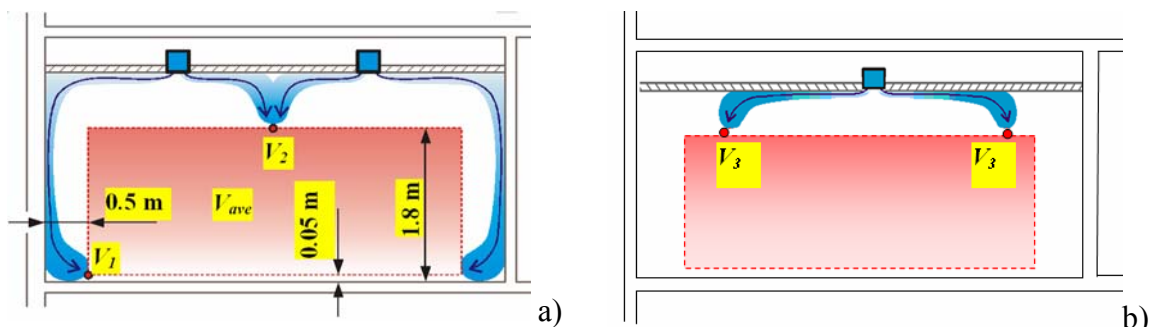
**Table 1.1** Different air diffusers in different air distribution systems.

Air diffusers	Supply pattern	Return pattern	Air distribution System
Linear slot diffuser 	Ceiling and end wall-mounted	End wall-mounted below ceiling	Mixing ventilation
Wall grille 	End wall-mounted	Return opening below or beside supply terminal	Mixing ventilation
Perforated diffuser  <i>Round Square</i>	Below ceiling mounted	End wall-mounted below ceiling	Mixing ventilation
Swirl diffuser  <i>Round Square</i>	Below ceiling mounted	End wall-mounted below ceiling	Mixing ventilation
Chilled beams 	Below ceiling mounted	End wall-mounted at floor level	Mixing ventilation
Duct diffuser 	Individually suspended installation	End wall-mounted	Mixing ventilation
Low speed air diffuser  <i>Semicircular Flat Circular</i>	End wall-mounted and ground-mounted in the middle of the space	End wall-mounted below ceiling	Displacement ventilation

### 1.5 The attached plane jet application

Ceiling-mounted attached jet systems have proven to be good complements to traditional air distribution systems such as DV and MV (Alamdari et al. 1998; Riffat et al. 2004). Nowadays, chilled beams are widely used in commercial and public buildings owing to providing good energy performance, excellent thermal comfort and silent operation (Alamdari et al. 1998; Kosonen et al. 2000; Fredriksson et al. 2001; Riffat et al. 2004; Kosonen and Tan 2005 and Kosonen and Virta 2007a). The active chilled beam is one of the ceiling-mounted attached plane jet diffusers. The active chilled beam can operate as a high-temperature cooling device, with a water flow temperature of 14–18 °C (Costelloe and Finn 2003). To calculate the induced air flow rate by the chilled beam, a novel method for measuring the jet induction rates was proposed by Ruponen and Tinker (2007).

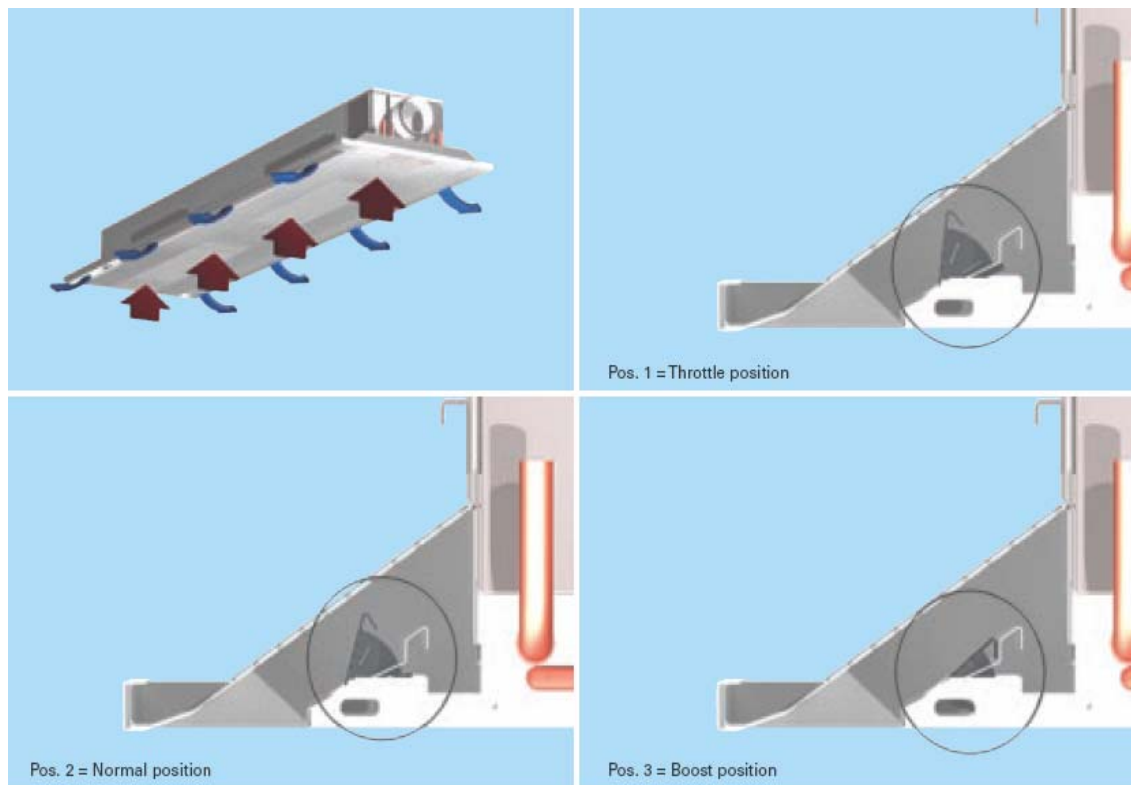
The probable airflow pattern of the attached plane jet is presented in Figure 1.2 and shows the critical controlled point with respect to the draught problem using the active chilled beam. It is very important that air jets are attached to the ceiling; and the dimensioning should ensure that the separation from the ceiling will not occur in the occupied zone, which is defined as the area 0.3 and 0.5 m from the internal and the external wall, respectively, and 1.8 m from the floor (ASHRAE 55.2004 and EN 13779:2007). It is in this area that people perform most of their ordinary daily activities. In particular, high-cooling power airflows along the wall down to the floor or from the upper boundary of the occupied zone may cause a draught when it discharges into the occupied zone (velocity  $V_1$ ,  $V_2$  and  $V_3$  in Figure 1.2). Thus, to avoid a draught the velocities  $V_1$ ,  $V_2$  and  $V_3$  should be precisely predicted in the designing process (EN 13182:2002). Earlier studies have shown that the most critical zone regarding the sensation of a draught is located near the floor region (V and VIII). In the non-isothermal attached jet application, the Archimedes number could be used to evaluate the jet separation distance from the attached surface. The Archimedes numbers below which a jet can be considered unaffected by buoyancy forces (a moderate non-isothermal jet) were:  $\leq 0.1$  for a compact jet;  $\leq 0.15$  for a linear jet;  $\leq 0.25$  for the vertical non-isothermal jets (Hagström et al. 1999). In this thesis the focus was put on the modelling of the jet along the wall and floor which will determine  $V_1$  velocity.



**Figure 1.2** Probable airflow patterns by the active chilled beam. a) Two diffusers used in the same room. b) One diffuser mounted in the middle of the room.

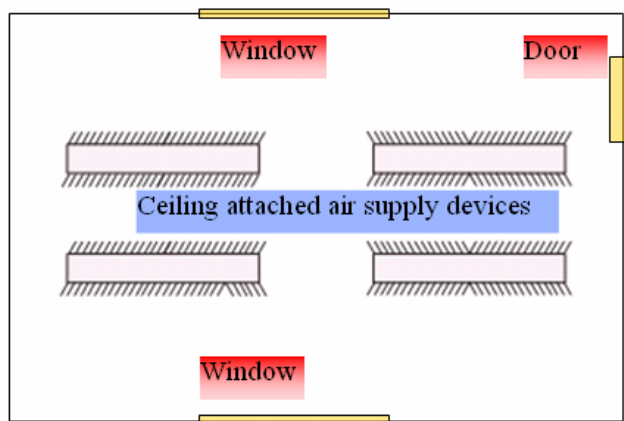
To control the critical velocity of the jets,  $V_1$ ,  $V_2$  and  $V_3$ , the manufacturers normally use two strategies: jet induction rate control and jet direction control. The adjustment process is presented in Figure 1.3 and shows the manual velocity adjustment with three

settings of the embedded damper. Here, the three settings (throttle position, normal position and boost position) could be applied by changing the damper position to enable the adjustment of conditions in different parts of the occupied zone. The adjustment has an impact on the induced room air-flow through the heat exchanger, and therefore it could increase or decrease both the air flow rate and the cooling/heating capacity of the chilled beam. It was reported that altering the geometry of a supply air slot may also affect the operation of the active chilled beam by changing the jet induction rate (Ruponen et al. 2005). In addition, the arrangement of the chilled beams and the layout of the work places may also have an effect on the indoor air distribution with linear slot diffusers (Zboril et al. 2007).

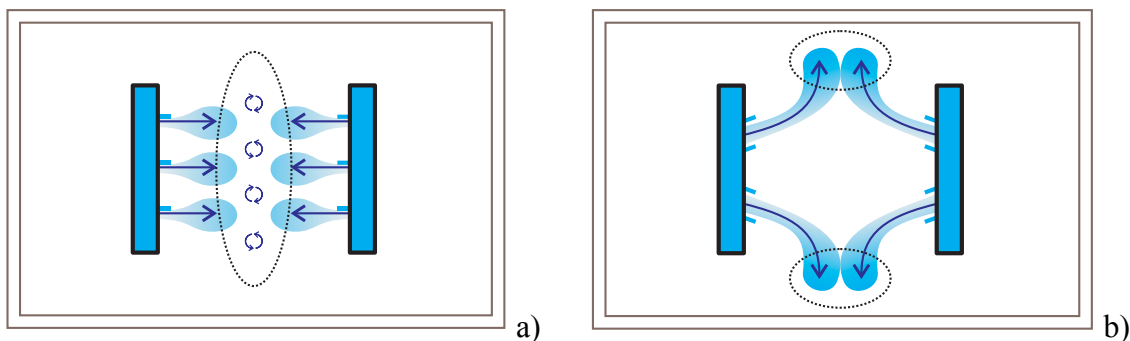


**Figure 1.3** Adjustment of airflow rate by changing the position of the throttle.

The control of the jet direction is presented in Figure 1.4 and Figure 1.5, and shows the effect of airflow direction control on the airflow pattern in rooms. These adjustments allow the position of the vertical airflow  $V_2$  between the air supply diffusers to be changed. If in normal conditions the highest velocities are on the centreline between the beams, the direction control allows the jets to be led to one or another end of the diffuser.



**Figure 1.4** Probable airflow direction adjustments.



**Figure 1.5** The effect of airflow direction control on the airflow pattern. a) No control. b) V-type distribution.

## 1.6 Objectives and contents of this thesis

The objective of this thesis is to give a basis for improving the existing modelling and calculation method applied to predict the jet velocity in both ventilated and air-conditioned rooms using attached plane jet diffusers to avoid the draught problem.

The sub-objectives of this study are:

- to specify the application conditions of the draught model and to determine the critical regions with the attached plane jet in a room, considering the draught sensations (V and VIII);
- to set up the near-wall region jet model under non-isothermal conditions at low Reynolds numbers in a room (I, VI and VII);
- to build the returning-air-jet model for the prediction of the jet velocity distribution after impinging the corner in a room (II);
- to distinguish and clarify the differences between the jet characteristics at low Reynolds numbers and at high Reynolds numbers (III and IV);
- to develop efficient and practical models to predict the maximum jet velocity decay in the transitional region and the fully developed region (III and IV);
- to obtain comprehensive measured data on the attached plane jet at low Reynolds numbers in both isothermal and non-isothermal conditions (I-IV).

The novelty values of this work are the validated models and the detailed data on the jet flow characteristics obtained by full-scale experimental measurements. The thesis consists of eight papers. The first four papers are journal papers and the other four are international conference papers. Here, full-scale experimental works provide the fundamental data for the studies on attached plane jet mean flow characteristics in two full-scale test chambers. Except (V) and (VIII), which specified the relationship between the draught risk and the airflow velocity by means of literature review, the other six papers were all based on experimental results in both isothermal cases (II and III) and non-isothermal cases (I, IV, VI and VII). Full-scale experiments were comprehensively designed and carried out in each study stage. In addition, different jet models were constructed and validated to predict the jet velocity distribution in different jet regions, including the corner region (II), the near-wall region after the impingement (I, VI and VII), the transition region before the impingement (III) and the buoyant region (IV).

As a preliminary study, the relationship between the jet velocity and the draught risk was specified and analyzed in (V) and (VIII). The literature review in (V) and (VIII) showed that complaints about the draught sensation rank extremely highly among complaints in air-conditioned rooms. In addition, the critical jet regions were distinguished by draught assessments where require accurate air flow design to avoid the draught sensation.

In (I), the air distribution in the near-wall region after impingement was measured and modelled in the first test chamber under typical office conditions, including both isothermal and non-isothermal conditions. The free convection model was set up for prediction of the vertical downward jet velocity. The superimposing methodology created in (I) was extended in (IV) to resolve the buoyant force effect on the jet behaviour. As the extension of (I), the jet dynamic characteristic coefficients were studied in (VII) as well.

The jet impingement in the corners was studied before the jet entering the occupied zone in (II). The separation and reattachment processes of the attached jet were investigated experimentally and theoretically. Paper (II) discovered that the turning jet flow reattached to the floor surface with entrained ambient air after the separation from the wall surface; at the same time, the rest air at low speed in the ventilated room did enforce the free shear at the free boundary of the attached jet. The returning-air-jet model was constructed by resolving the corner jet impinging process. The measured data was used to validate the model for calculation of the jet velocity in the corner regions.

Paper (III) focused on the jet behaviour in the transition region before entering the fully developed region. In (III) the behaviour of the turbulent attached plane jet undergoing the transition process was measured and modelled. The similarity model was set up to predict the maximum velocity decay in the jet transition region and fully developed region. It was revealed that the jet spreading mechanism directly determines the maximum jet velocity decay in the transition region after leaving the jet slot.

As an extension of the studies in (I, III and VII), the paper (IV) focused on the cooling attached plane jet characteristics, including the mean flow field behaviours, the jet development regions and the maximum velocity decay. To obtain detailed information on the whole flow field, comprehensive experimental work was carried out through different jet regions. Besides experimental measurement, a new superimposing model was derived and validated to predict the maximum velocity decay of the cooling jets in a room.

The acquired knowledge discussed in this thesis relates to:

- modelling of the attached plane jet at low Reynolds numbers in a room in order to solve the draught-problem;
- transitional characteristics of the buoyant attached plane jet at low Reynolds numbers in a room;
- free convection jet model set-up for velocity prediction in the near-wall regions;
- returning-air-jet model for calculation of the jet velocity in the corner region;
- superimposing model set-up by resolving the buoyancy force in the attached jet flow fields;
- comprehensive experimental data in both isothermal and non-isothermal conditions in a room.

## **2 TURBULENT ATTACHED PLANE JET FLOW**

### **2.1 Literature review**

The characteristics of the turbulent wall jet have been extensively studied for many decades (Glauert 1956; Schwarz and Cosart 1961; Bajura and Szewczyk 1970; Sato et al. 1981; Karimipناه 1996 and Abrahamsson 1997). The earlier theoretical investigation of the incompressible isothermal laminar attached plane jet, also called the wall jet, was carried out by Tetervin (1948) presented by Quintana et al. (1997). Tetervin predicted that the boundary layer thickness of the wall jet grew and the local maximum velocity decayed with the downstream distance as  $x^{3/4}$  and  $x^{-1/2}$ , respectively ( $x$  is the distance downstream from the jet nozzle). Glauert (1956) achieved the similarity solution for the laminar and turbulent radial and plane wall jet. Later, Bajura and Szewczyk (1970) carried out an experimental investigation of the laminar wall jets and obtained a good agreement with Glauert's similarity solution in a laminar situation. The results indicated that the differences between the experimental and theoretical velocity profile were that the experimental values were up to 3% above the theoretical curve in the velocity range  $0.9 \geq u/U_m \geq 0.6$  and then fell below the theoretical curve for  $u/U_m \leq 0.3$ .

In 1956, Glauert solved the boundary layer equations in relation to both the laminar flow and the turbulent flow and obtained a similarity solution for the laminar wall jet. He also found that complete similarity was not attainable in a turbulent flow. Hiroshi and Fujihiko (1964) carried out an experimental investigation of the instability of a two-dimensional jet at low Reynolds numbers. Poreh et al. (1967) obtained the mean velocity expression of an impinging wall jet by means of the maximum velocity and jet thickness at each station. Sychev (1972) studied the laminar separation of an

incompressible liquid on the smooth surface of a solid. Subba and Gorla (1976) studied the combined natural and forced convection in a laminar wall jet along a vertical plate. Mojola (1976) carried out an analysis of the steady flow separation along a straight streamwise corner. Karimipannah (1999) measured the pressure along the perimeter of slot-ventilated room and described the wall-jet deflection by pressure distribution. Awbi and Hatton (1999) measured the local and surface mean convective heat transfer and investigated the mixed convection situation by a jet flowing over the heated ceiling.

Considering the jet development, the most interesting region for a room is the fully developed velocity profile, which occurs after the potential core zone and the transition zone. In the developed region, the jet velocity profile performs the self-similarity characteristics in the far downstream position from the slot. The earliest known work on the attached plane jet was completed by Förthmann (1934) and described and quoted by Schwarz and Cosart (1961) and Rajaratnam (1976). Förthmann studied the self-preserving nature of the attached jet, and observed that the boundary layer thickness varied linearly with  $x$ , and the maximum velocity varied inversely as the half power of  $x$ . Beyond that, he discovered from the data that the velocity in the inner layer varied as the one-seventh power of the distance from the wall. When the jet approaches a vertical wall or other surface perpendicular to the jet flow, the fully developed jet flow might separate from the surface somewhere in a corner region.

A number of methods have been proposed for predicting and calculating the maximum velocity decay of a turbulent buoyant jet in some practically important cases, ranging from simple empirical formulae to complex models involving partial differential equations (Rajaratnam 1976; Sandberg 1987; Awbi 1991 and Yu et al. 2003 and 2007). Albright and Scott (1974) studied experimentally a cold, attached plane jet discharging vertically along a surface and derived both the temperature and the velocity expressions from the experimental data for  $1050 < Re < 8055$  in the fully developed region. Abdulhadi and Pedersen (1971) investigated experimentally the behaviour of a downward-directed heated attached jet and compared the influence of Archimedes number on the jet discharging with an outlet velocity of 1.0 to 6.0 m/s. By taking Archimedes number into account, Grititlin (1970), Lilja (1980) and Regenscheit (1975) derived different correlations for the non-isothermal free jet presented in (Klobut and Palonen 1992). The models could be applied for both buoyancy and negative buoyancy jets. Moog (1978) presented a correlation for the negative buoyancy wall jet. Sato et al. (1981) studied the maximum penetration distance of a vertical buoyant jet and derived the corresponding correlation equations.

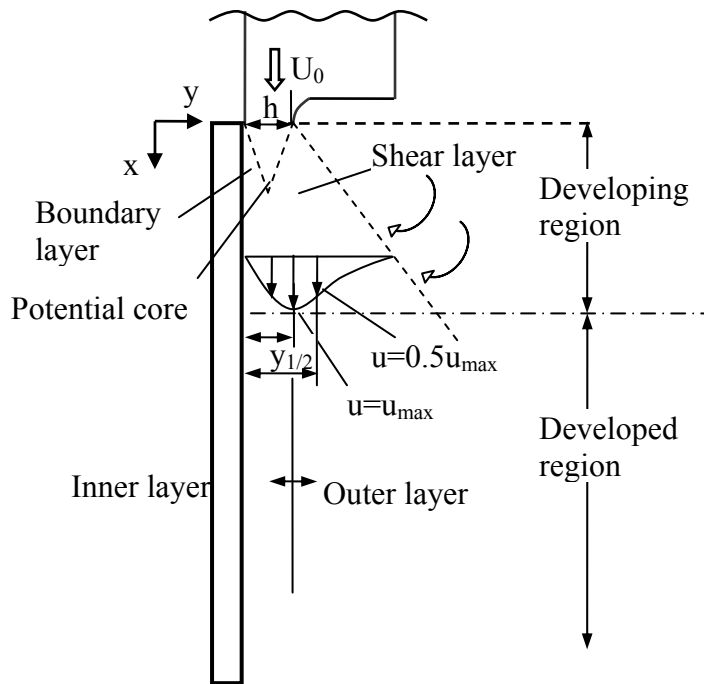
In engineering applications, attached jet discharging is one of the applications commonly used for the ventilated or the air-conditioned room (Nielsen and Möller 1987; Sandberg 1987 and Sandberg et al. 1992). The jet flow should attach to the ceiling so that the high-velocity region is restricted to the ceiling to free the lower space from draught. In the attached plane jet application, the earlier studies showed that the most critical zone regarding draught is located near the floor region (VI and VIII). In addition, natural convection plumes generated by indoor heat loads could change considerably the distribution of the airflows in non-isothermal conditions (Kosonen et al. 2007b; Melikov et al. 2007). On the basis of the measurement results, the conventional non-isothermal model presented by Regenscheit (1975) as well by Hagström (1999) may not

predict the cooling jet velocity distribution correctly with the active chilled beam (VI). The non-isothermal air jet models always predicted a higher air velocity than the measured one in the near-wall region. Predicted velocities increased slightly towards the floor, while the measured velocity decreased significantly along the wall in (VI and VII).

## 2.2 The structure of the attached plane jet

### 2.2.1 Isothermal attached plane jet

In (II) and (III), the turbulent attached plane jet under isothermal conditions was studied experimentally and theoretically. The structure of the attached plane jet is generally divided into two distinct flow regions: an inner region, where the flow resembles that of the conventional boundary layer flow, and an outer region, where the flow is similar to that of a free shear layer flow (Gogineni and Shih 1997; Hsiao and Sheu 1996). In the downstream jet flow field, the jet flow field has different divisions under isothermal and non-isothermal conditions (see Figure 2.1 and Figure 2.2).



**Figure 2.1** Schematic view of a vertical isothermal jet structure.

The flow field of the isothermal attached plane jet is presented in Figure 2.1, which schematically shows the jet flow structure downstream of the jet slot and defines the coordinate system used in this study. Conventionally, the inner region and outer region have been studied and modelled by assuming the same similarity in both regions. However, the similarity might be affected by the background condition in the outer region and inner region. The factors could be the acoustic environment, rough wall surface and higher turbulent intensity level at the jet exit.

A later study carried out by Barenblatt et al. (2005) demonstrates a triple-layered structure and incomplete similarity in the turbulent attached jet. It was found that attached jet flows consisted of two self-similar layers: a top layer and a wall layer,



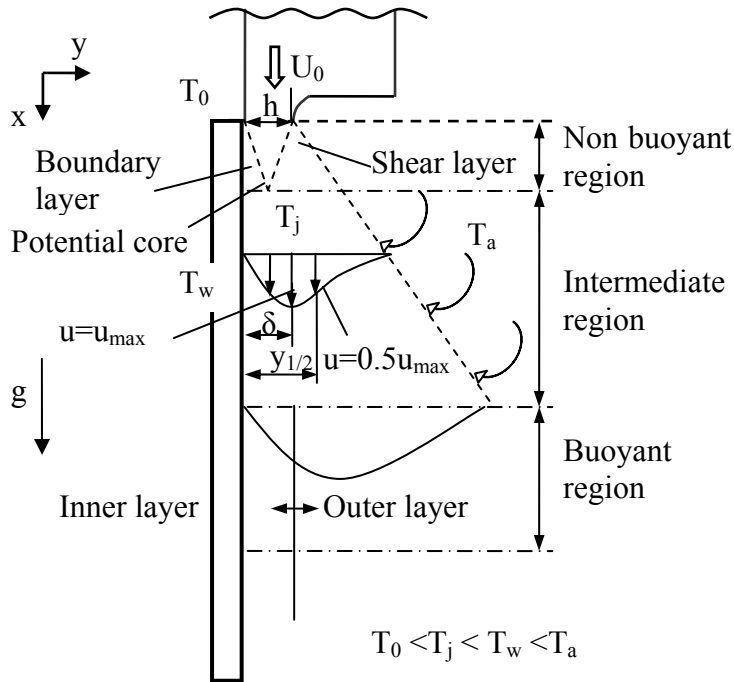
separated by a mixing layer where the velocity was close to the maximum jet velocity. Differing from the earlier studies, it was reported that the scaling laws in the top and wall layers are different. Both exhibit an incomplete similarity arising from the strong influence of the slot width, which had previously been overlooked.

In addition, following the streamwise direction of the jet flow, Figure 2.1 displays the two-region division of the jet flow field: the developing region and the developed region. The first region, the developing region, includes the probable potential core and the transition region. The developed region, which represents the self similarity of the jet, includes both the inner and the outer region. Gogineni and Shih (1997) used laser-sheet smoke-flow visualizations to demonstrate clearly the attached plane jet flow separation process at a low exit Reynolds number. The results revealed that under the influence of the free-shear-layer vortex, the local boundary layer becomes detached from the surface and inviscidly unstable, and a vortex was formed in the inner region. Once this vortex was formed, the free-shear-layer vortex and the inner-region vortex form a vortex couple and convect downstream. The mutual interactions between these inner- and outer-region vortical structures dominated the jet transition process. Further downstream, the emergence of the three-dimensional structure in the free shear layer initiates the complete breakdown of the flow.

#### 2.2.2 Non-isothermal attached plane jet

In (I, IV, VI and VII), the behaviour and characteristics of the jet were studied in non-isothermal conditions. Generally, if the jet temperature differs from the ambient air temperature, the jet is called a non-isothermal jet.

The jet flow field of the non-isothermal jet is presented in Figure 2.2 and shows the three-region division of the buoyant jet structure. Unlike the isothermal jet, especially in some practical situations, the buoyant jet refers to a jet where the buoyancy force acts in the direction of the jet velocity at the origin. When the buoyancy force acts in the opposite direction of the airflow, the flow is called a negative buoyant jet (Chen and Rodi 1980). In addition the flow in a buoyant attached jet is dependent upon the relationship between the inertia, the buoyancy and the viscous forces acting on the jet. The jets in a quiescent ambient can be classified according to the relative importance of the initial momentum,  $M$ , and the initial buoyancy flux,  $B$ . The jet is a steady plume when  $M$  is small compared to  $B$ , while it is a pure jet when  $B$  is negligible compared to  $M$ . It is a buoyant jet when the two parameters are of comparable importance (So and Aksoy 1993). The structure of an attached plane jet was characterized by Sigalla (1958), Abdulhadi and Pedersen (1971) and Launder and Rodi (1981) as having three flow regions, a non-buoyant region, an intermediate region and a buoyant region.



**Figure 2.2** Schematic view of a vertical buoyant jet structure.

The non-buoyant region is the region close to the jet exit where the maximum velocity has not yet begun to decay. In isothermal jet studies a potential core was used to describe the non-decay region by Rajaratnam (1976). As in the non-isothermal jet studies, namely the buoyant jet, the non-buoyancy region refers to the same region as well (Chen and Rodi 1980). The inner region of the buoyant jet is bounded by the wall and the point of maximum velocity. The behaviour of this layer is assumed to be similar to an ordinary turbulent boundary flow over a flat plate. The outer layer is the region beyond the point of maximum velocity and is assumed to behave like a free jet.

At present, most of the empirical and theoretical models have been constructed and validated by assuming that the major heat transfer exists between the wall and the jet (Yang and Patel 1973; Albright and Scott 1974 and Subba and Gorla 1976). However, a well-insulated surface is often applied instead of an ideal isothermal wall, differing from other literature (Abdulhadi and Pedersen 1971).

### 2.3 Attached plane jet mean flow equations

The jet considered in this thesis is the turbulent air jet issuing from a slot in both isothermal and non-isothermal conditions. The variations of properties like the viscosity and the thermal conductivity of the air with temperatures are negligible. The fluid is assumed to be incompressible, and the density varies linearly with temperature only in the buoyancy term. These are the Boussinesq approximations applied in the following equation derivatives and only mean flow quantities in two dimensions are discussed in this study.

Basically, a non-slip condition is applied on the surface by which the jet flow is bounded. The following boundary conditions are used in the jet flow field:

$$\bar{u} = \bar{v} = 0 \quad \text{at} \quad y = 0$$

and

$$\bar{u} = \bar{v} = 0 \quad \text{at} \quad x = \infty, y = \infty$$

In the cooling jet case over the insulated surface, the heat flux between the wall and the jet was assumed to be negligible. Thus:

$$q_w = 0 \quad \text{at} \quad y = 0$$

$$T_w = T_{jet} \quad \text{at} \quad y = 0$$

The above thermal boundary conditions were presented also by Abdulhadi and Pedersen (1971). Therefore, the analytical treatment was limited to the well-insulated wall condition in the superimposing models presented in (I) and (IV).

To determine the variation of the maximum velocity and the boundary layer thickness beyond the non-buoyancy region, with the usual boundary layer approximations, the equations (continuity, momentum and energy equations) governing the two-dimensional mean flow in the vertical buoyant jet, where the gravity vector is along the  $x$  coordinate are expressed as:

Continuity:

$$\frac{\partial \rho \bar{u}}{\partial x} + \frac{\partial \rho \bar{v}}{\partial y} = 0 \quad (1)$$

Momentum ( $x$  direction, the same as the gravity vector):

$$\rho \left( u \frac{\partial \bar{u}}{\partial x} + v \frac{\partial \bar{v}}{\partial y} \right) = \rho g - \frac{\partial \bar{P}}{\partial x} + \frac{\partial}{\partial y} \left( \mu \frac{\partial \bar{u}}{\partial y} - \overline{\rho u' v'} \right) \quad (2)$$

Energy:

$$\rho c_p \left( u \frac{\partial \bar{T}}{\partial x} + v \frac{\partial \bar{T}}{\partial y} \right) = \frac{\partial}{\partial y} (-q) + \bar{\Phi} \quad (3)$$

In Equation 2, the term of  $-\overline{\rho u' v'}$  represents the turbulent shear or Reynolds shear. In addition, the Boussinesq approximation states that the density difference is sufficiently small to be neglected, except where it appears in the term multiplied by  $g$ , the acceleration due to gravity. The essence of the Boussinesq approximation is that the difference in inertia is negligible, but gravity is sufficiently strong to make the difference appreciable.

Therefore,

$$\frac{\partial \bar{P}}{\partial x} = -\rho_\infty g \quad (4)$$

$$\frac{\partial \bar{P}}{\partial x} - \rho g = -\rho_\infty g - \rho g \quad (5)$$

Then

$$\frac{\partial \bar{P}}{\partial x} - \rho g = -g(\rho_\infty - \rho) \quad (6)$$

By introducing an expansion ratio, the expression takes the form as below:

$$\beta = -\frac{1}{\rho} \left( \frac{\partial \rho}{\partial T} \right)_p \quad (7)$$

Thus an approximation of the density difference between the jet and the ambient air is obtained as:

$$(\rho_\infty - \rho) \approx -\rho \beta (T_\infty - T) \quad (8)$$

Substituting Equation 6 and 8 into Equation 2, the momentum equation becomes:

$$\rho \left( \bar{u} \frac{\partial \bar{u}}{\partial x} + \bar{v} \frac{\partial \bar{v}}{\partial y} \right) = \underbrace{\rho g \beta (T_\infty - T)}_{\text{Buoyant term}} + \underbrace{\mu \frac{\partial^2 \bar{u}}{\partial y^2}}_{\text{Molecular term}} + \underbrace{\frac{\partial}{\partial y} (-\rho \overline{u'v'})}_{\text{Turbulent term}} \quad (9)$$

In Equation 3, the total-heat-flux vector  $q$ , which includes molecular flux and the turbulent flux  $\rho c_p \overline{v'T'}$ , has the form of:

$$q = -k \frac{\partial \bar{T}}{\partial y} + \rho c_p \overline{v'T'} \quad (10)$$

The total dissipation term is obviously complex in the general case. In the two-dimensional turbulent-boundary layer flows, the dissipation term reduces approximately to:

$$\bar{\Phi} \approx \frac{\partial \bar{u}}{\partial y} \left( \mu \frac{\partial \bar{u}}{\partial y} - \rho \overline{u'v'} \right) \quad (11)$$

After substituting Equation 10 and 11 into Equation 3, the new energy equation is obtained as:

$$\rho c_p \left( \bar{u} \frac{\partial \bar{T}}{\partial x} + \bar{v} \frac{\partial \bar{T}}{\partial y} \right) = \frac{\partial}{\partial y} \left( k \frac{\partial \bar{T}}{\partial y} - \rho c_p \overline{v'T'} \right) + \frac{\partial \bar{u}}{\partial y} \left( \mu \frac{\partial \bar{u}}{\partial y} - \rho \overline{u'v'} \right) \quad (12)$$

Rewrite Equation 12 as:

$$\rho c_p \left( \bar{u} \frac{\partial \bar{T}}{\partial x} + \bar{v} \frac{\partial \bar{T}}{\partial y} \right) = \underbrace{k \frac{\partial^2 \bar{T}}{\partial y^2}}_{\text{Laminar term}} - \underbrace{\frac{\partial}{\partial y} (\rho c_p \overline{v'T'})}_{\text{Turbulent term}} + \underbrace{\frac{\partial \bar{u}}{\partial y} \left( \mu \frac{\partial \bar{u}}{\partial y} - \rho \overline{u'v'} \right)}_{\text{Dissipation term}} \quad (13)$$

Now, Equations 1, 9 and 13 are the Reynolds-averaged basic differential equations for the two-dimensional turbulent mean flow.

The introduction of eddy diffusivity and subsequently the turbulent Prandtl number acts as a way to define a simple relationship between the extra shear stress and heat flux that is present in the turbulent mean flow equation. In Equation 13, if the turbulent term and the thermal eddy diffusivities are zero, the turbulent flow equation reduces to the laminar equation. The definition of the eddy diffusivities for momentum transfer  $\varepsilon_M$  and heat transfer  $\varepsilon_H$  is presented as:

$$\rho \varepsilon_M \frac{\partial \bar{u}}{\partial y} \equiv -\overline{\rho u' v'} \quad (14)$$

$$\varepsilon_H \frac{\partial \bar{T}}{\partial y} \equiv -\overline{v' T'} \quad (15)$$

Substituting Equation 14 into Equation 9 yields:

$$\bar{u} \frac{\partial \bar{u}}{\partial x} + \bar{v} \frac{\partial \bar{v}}{\partial y} = g\beta(T_\infty - T) + (\nu + \varepsilon_M) \frac{\partial^2 \bar{u}}{\partial y^2} \quad (16)$$

Substituting Equation 15 into Equation 13 yields:

$$\rho c_p \left( \bar{u} \frac{\partial \bar{T}}{\partial x} + \bar{v} \frac{\partial \bar{T}}{\partial y} \right) = k \frac{\partial^2 \bar{T}}{\partial y^2} + \frac{\partial}{\partial y} \left( \rho c_p \varepsilon_H \frac{\partial \bar{T}}{\partial y} \right) + \frac{\partial \bar{u}}{\partial y} \left( \mu \frac{\partial \bar{u}}{\partial y} + \rho \varepsilon_M \frac{\partial \bar{u}}{\partial y} \right) \quad (17)$$

$$\alpha = \frac{k}{\rho c_p} \quad (18)$$

$$\bar{u} \frac{\partial \bar{T}}{\partial x} + \bar{v} \frac{\partial \bar{T}}{\partial y} = (\alpha + \varepsilon_H) \frac{\partial^2 \bar{T}}{\partial y^2} + \frac{1}{c_p} \left( \nu \frac{\partial \bar{u}}{\partial y} + \varepsilon_M \frac{\partial \bar{T}}{\partial y} \right) \frac{\partial \bar{u}}{\partial y} \quad (19)$$

If the turbulent Prandtl number is defined as:

$$\text{Pr}_t = \frac{\varepsilon_M}{\varepsilon_H} \quad (20)$$

The eddy diffusivity for heat transfer,  $\varepsilon_H$ , is obtained by measurement as 0.00063 m<sup>2</sup>/s and varies in a narrow range (Kulkarni and Joshi 2005). As for the turbulent viscosity or eddy diffusivity, the most appreciated turbulent viscosity model may be the  $k$ - $\varepsilon$  model, which employs the turbulent kinetic energy,  $k$ , and the energy dissipation rate,  $\varepsilon$ , and is expressed as:

$$\nu_t = C_\mu \frac{k^2}{\varepsilon} \quad (21)$$

By the Boussinesq approximation, the new set of the two-dimensional mean flow field equation for the turbulent non-isothermal plane jet becomes:

Continuity:

$$\frac{\partial \bar{u}}{\partial x} + \frac{\partial \bar{v}}{\partial y} = 0 \quad (22)$$

Momentum ( $x$  direction, the same as the gravity vector):

$$u \frac{\partial \bar{u}}{\partial x} + v \frac{\partial \bar{v}}{\partial y} = g\beta(T - T_\infty) + \nu_M \frac{\partial^2 \bar{u}}{\partial y^2} \quad (23)$$

$$\nu_M = \nu + \varepsilon_M \quad (24)$$

Energy:

$$u \frac{\partial \bar{T}}{\partial x} + v \frac{\partial \bar{T}}{\partial y} = \alpha_H \frac{\partial^2 \bar{T}}{\partial y^2} + \frac{1}{c_p} \left( v \frac{\partial \bar{u}}{\partial y} + \varepsilon_M \frac{\partial \bar{T}}{\partial y} \right) \frac{\partial \bar{u}}{\partial y} \quad (25)$$

$$\alpha_H = \alpha + \varepsilon_H \quad (26)$$

where  $\varepsilon_M$  is the eddy diffusivities for momentum transfer and  $\alpha_H$  is the eddy diffusivities for heat transfer. The momentum Equation 23 and energy Equation 25 derived here differ from the jet equations of the mean flow field jet studies in Chen and Rodi (1980).

### 3 EXPERIMENTAL SETUP

The flow field of the attached plane jet is investigated by means of experiment and mathematical modelling in both isothermal and non-isothermal conditions. The experiments presented in (I-IV) and (VI-VII) covered the whole jet flow region from the starting region to the developed region. In the modelling part, the whole jet flow field downstream of the jet slot is modelled by a set of jet velocity models. The experimental set up in this study will be described in detail in this section.

#### 3.1 The test chambers and the air supply devices

##### 3.1.1 The test chambers

During the measurement period, two test chambers were built and used to carry out the measurements yielding detailed information on the jet flow field. The photographs and layout of the two test chambers are presented in Figures 3.1 to 3.4 and show the arrangement of the heat sources in two rooms.

In the first chamber shown in Figure 3.1, the measured wall region is located on the opposite side to the door. The wall was insulated so that there was no significant temperature difference between the wall surface and the attached air jet. The second test chamber consisted of a well-insulated wall and a two-meter-long jet supply device mounted on the top of the wall. Besides the air supply device, two transparent side walls

were built to allow photographic studies of the jet behaviour by smoke injection and to permit the observation of measuring sensors without entering the chamber and disturbing the flow. There was no significant temperature difference between the wall surface and the air jet attached to the wall.

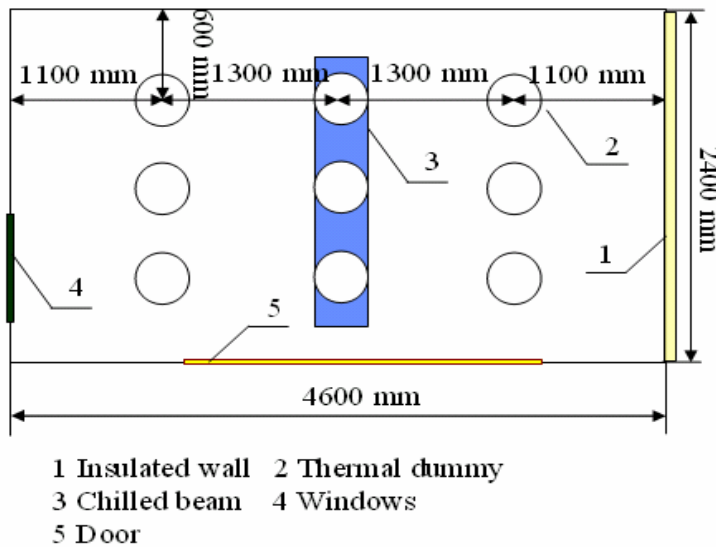
Nine simplified cylindrical dummies specified in DIN4715-1 were used as heat sources for the cooling jet measurement. Each of these dummies has a power of 120 W (3 x 40 W lamps with 40 W of power). The total output power of the nine dummies was monitored with a PM 300 energy meter. In different cases, the total output power was changed by adjusting the electric current regulator from zero to the maximum value. In the cooling jet cases, the power of the dummies was set according to the cooling load of the air. The preliminary smoke tracer test showed that the plumes produced by these dummies did not disturb the air jet in any of the three buoyant jet regions. Therefore, the measurement conditions could be regarded as undisturbed conditions.



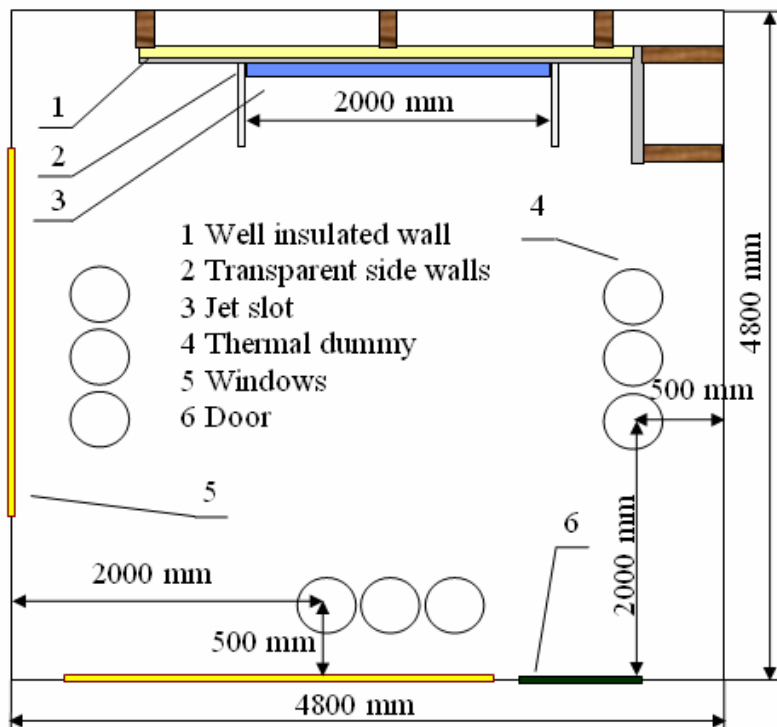
**Figure 3.1** Photograph of the first test chamber with nine simplified cylindrical dummies.



**Figure 3.2** Photograph of the second test chamber with nine simplified cylindrical dummies.



**Figure 3.3** The layout of the first test chamber.



**Figure 3.4** The layout of the second test chamber.

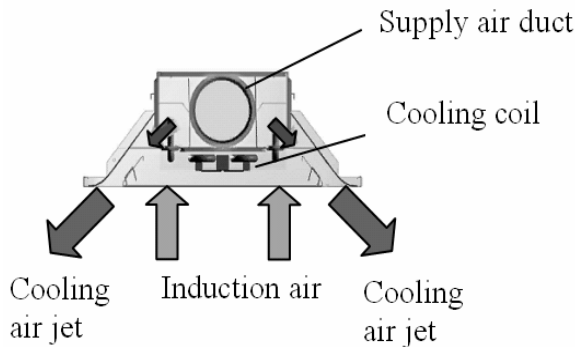
### 3.1.2 Air diffusers for discharging jet flow

In the experimental works through (I-IV) and (VI and VII), two types of air supply diffuser were applied to produce the air jet needed for both isothermal and non-isothermal studies. In the two chambers, one chilled beam and one two-meter-long slot device were applied to generate the attached plane jet.

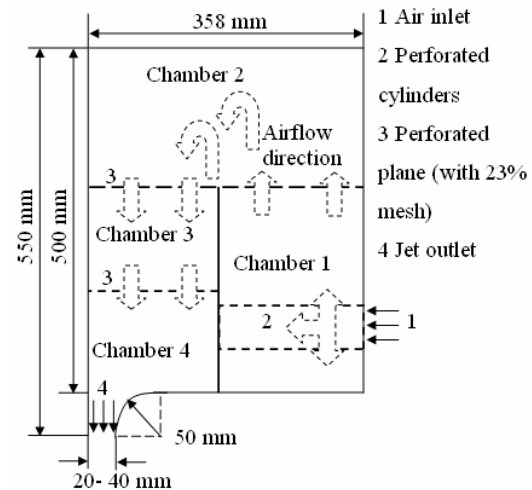
Figure 3.5 shows the cross-section of the chilled beam used in the first chamber. The supply air was ducted to the beam and discharged from the slot, inducing ambient air through cooling coil. The ratio of supply air and total airflow through the chilled beam was in the range of 3.8-4.3. Two supply airflow rates, 20 and 28 L/s, were used to produce the attached plane jet in the first chamber.

The jet supply device used in the second chamber is presented in Figure 3.6 and shows the cross-section of the air supply device. The jet supply device was made of sheet metal with a two-meter-long adjustable slot. The inner space of the device was divided into four chambers using two perforated cylinders and two perforated plates. The air supplied to the jet was generated by a variable-speed frequency-controlled centrifugal fan. A different jet exit velocity, from 0.50 to 2.00 m/s, could be obtained by regulating the outflow restriction from 30 to 120 L/s. The slot height from which the airflow could discharge could be adjusted from 20 mm to 40 mm, producing an attached plane jet. The turbulence intensity at the nozzle exit centre is about 0.95%.





**Figure 3.5** Cross-sectional view of the chilled beam used in the first chamber.



**Figure 3.6** Cross-sectional view of the air supply device used in the second chamber.

### 3.2 Measurement conditions

In the first chamber, six different conditions were measured: isothermal cases, Case 3 and Case 6, and non-isothermal, Case 1, 2, 4 and 5. During the measurement, the room temperature was set as 24.0 °C. The six experimental conditions carried out in the first test chamber are presented in Table 3.1. Table 3.2 shows the measurement conditions in the second test chamber including isothermal cases and non-isothermal situations.

**Table 3.1** Six experimental conditions in the first test chamber.

	$q_{vs}$ [L/s]	$T_S$ [°C]	$P_c$ [W]	$P-c/A$ [W/ m <sup>2</sup> ]
Case 1	20	20	- 879	- 80
Case 2	20	24	-446	-40
Case 3	20	24	0	0
Case 4	28	17.5	-1107	-100
Case 5	28	24	-668	-61
Case 6	28	24	0	0

$q_{vs}$  supply airflow rate

$T_S$  supply air temperature

$P_c$  total cooling power

$P-c/A$  cooling power per square meter

**Table 3.2** Twenty-one experimental conditions in the second test chamber.

Slot height	Slot $V(m/s)$	$q_{vs}$ [L/s]	$\Delta T$	$T_S$ [°C]	$T_R$ [°C]	$P_c$ [W]	$P_h$ [W]	$Re_{slot}$	$Ar_{slot}$
20 mm	0.5	20	0	23.4±0.3°C	23.4±0.3°C	0	0	667	0
	1	40	0	22.3±0.3°C	22.3±0.3°C	0	0	1333	0
	2	80	0	22.1±0.3°C	22.1±0.3°C	0	0	2667	0
	0.5	20	-3	20.0±0.1°C	23.0±0.2°C	-72	72	667	0.00795
	1	40	-3	20.5±0.2°C	23.5±0.2°C	-144	144	1333	0.00199
	2	80	-3	20.0±0.2°C	23.0±0.2°C	-288	288	2667	0.00050
	1	40	-6	16.5±0.2°C	22.5±0.2°C	-288	288	1333	0.00398
	2	80	-6	16.5±0.2°C	22.5±0.2°C	-576	576	2667	0.0010
	1	40	-8	13.0±0.2°C	21.5±0.2°C	-384	384	1333	0.00533
Slot height	Slot $V(m/s)$	$q_{vs}$ [L/s]	$\Delta T$	$T_S$ [°C]	$T_R$ [°C]	$P_c$ [W]	$P_h$ [W]	$Re_{slot}$	$Ar_{slot}$
30 mm	0.5	30	0	22.8±0.3°C	22.8±0.3°C	0	0	1000	0
	1	60	0	21.8±0.3°C	21.8±0.3°C	0	0	2000	0
	2	120	0	22.5±0.3°C	22.5±0.3°C	0	0	4000	0
	0.5	30	-3	19.0±0.1°C	22.0±0.2°C	-108	108	1000	0.00366
	1	60	-3	18.6±0.1°C	21.6±0.2°C	-216	216	2000	0.00092
	2	120	-3	18.9±0.2°C	21.9±0.3°C	-432	432	4000	0.00023
	1	60	-6	15.8±0.2°C	21.8±0.3°C	-432	432	2000	0.00183
	2	120	-6	16.2±0.2°C	22.2±0.3°C	-864	864	4000	0.00046
	2	120	-8	13.8±0.2°C	21.8±0.3°C	-1152	1152	4000	0.00061
	0.5	30	+3	22.0±0.2°C	19.0±0.2°C	108	-108	1000	-0.0037
	1	60	+3	23.2±0.2°C	20.2±0.3°C	216	-216	2000	-0.0009
	2	120	+3	22.8±0.2°C	19.8±0.2°C	432	-432	4000	-0.0002

$\Delta T$  temperature difference between the jet and the room air

$T_R$  room air temperature

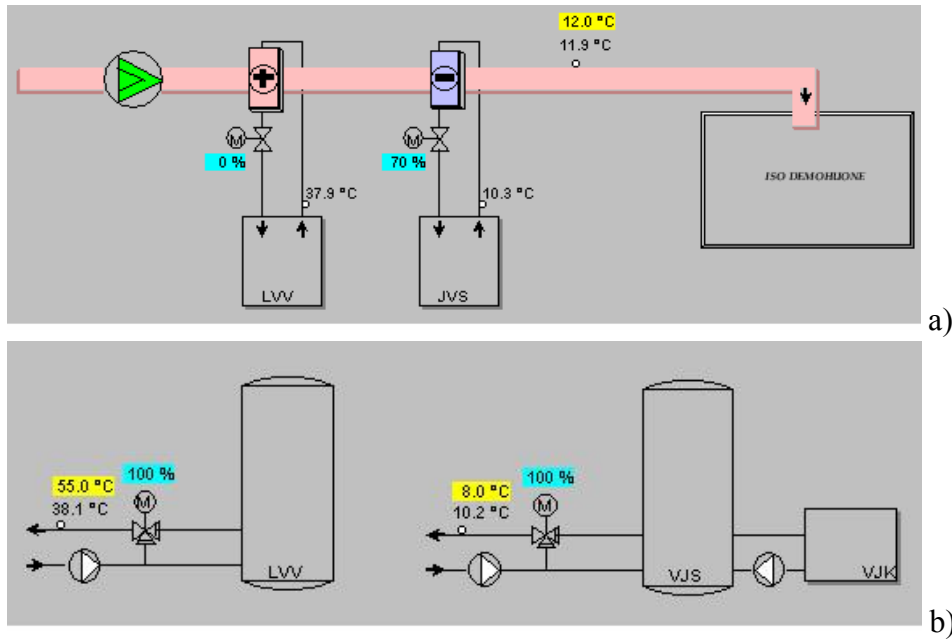
$P_h$  heat load power of thermal dummies

$Re_{slot}$  slot Reynolds number

$Ar_{slot}$  slot Archimedes number

### 3.3 The supply air duct system and the cooling & heating source

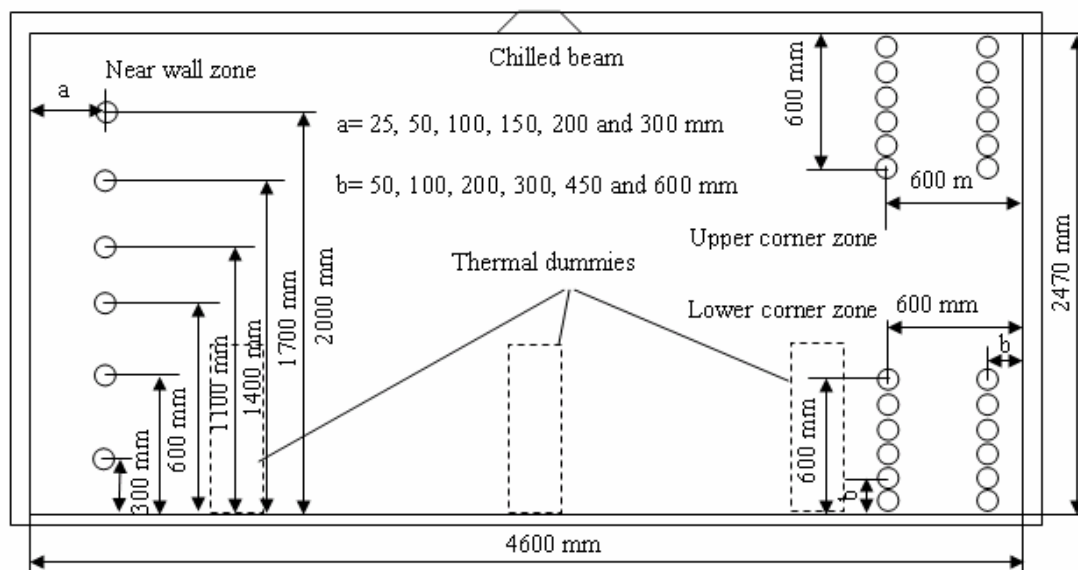
In the measurements, different airflow rates could be obtained by regulating the outflow restriction from 20 to 120 L/s through the insulated duct system in the two test chambers. Figure 3.7 shows the supply air duct system and cooling/heating source used in the two test chambers. In the duct system, two fan coils, independently controlled by a computer, were used to heat or cool down the supply air. The temperature accuracy of the controlled supply air was  $\pm 0.5^\circ\text{C}$  by measuring the duct air temperature. The accuracy of the supply airflow rate was  $\pm 3\%$  of the total supply airflow.



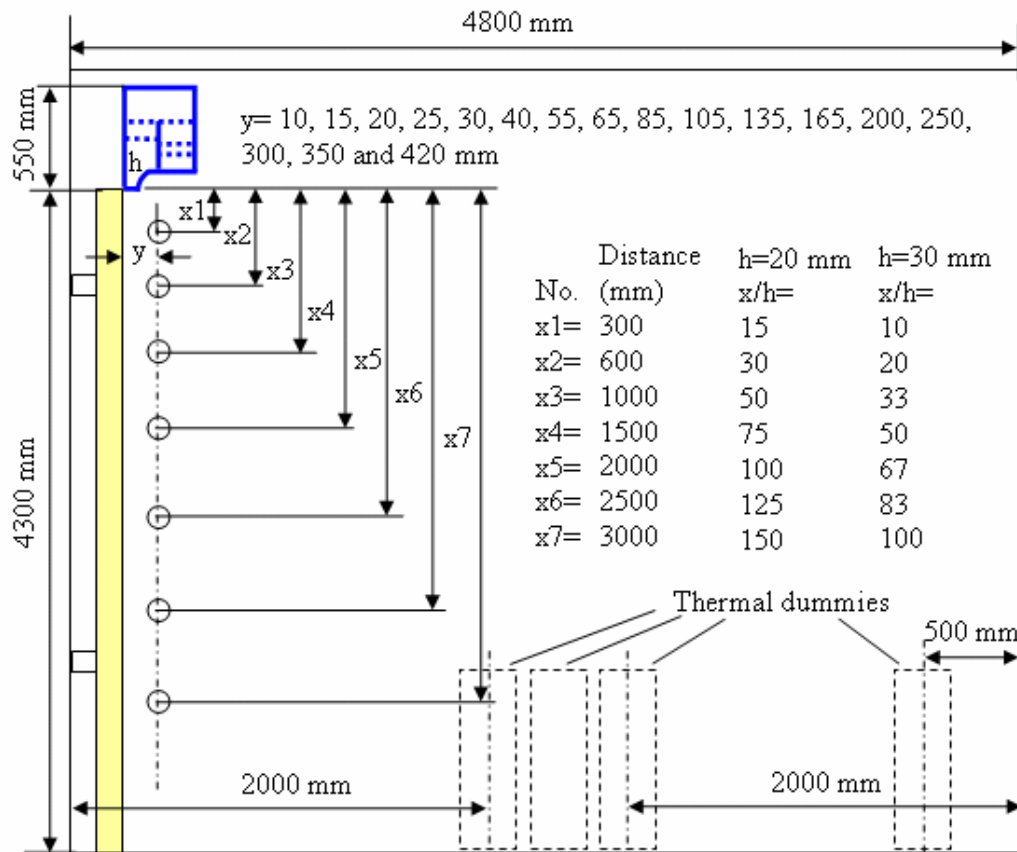
**Figure 3.7** The supply air duct system and the cooling/heating source. a) Air duct system used to produce the air jet in the first and second test chambers. b) Cooling and heating source used to provide cold and hot water for the chilled beam.

### 3.4 The measurement points distribution

In the two test chambers, the measurement points were distributed throughout the jet flow field downstream of the jet slot. In the first chamber, the jet velocity, temperature and turbulent intensity were measured in both the near-wall region at six different heights and the corner region under undisturbed conditions. In the second chamber, only the straight downstream direction flow field was measured. Figure 3.8 and Figure 3.9 display the measurement point distributions in the two chambers.



**Figure 3.8** Distribution of measurement points in the first chamber.

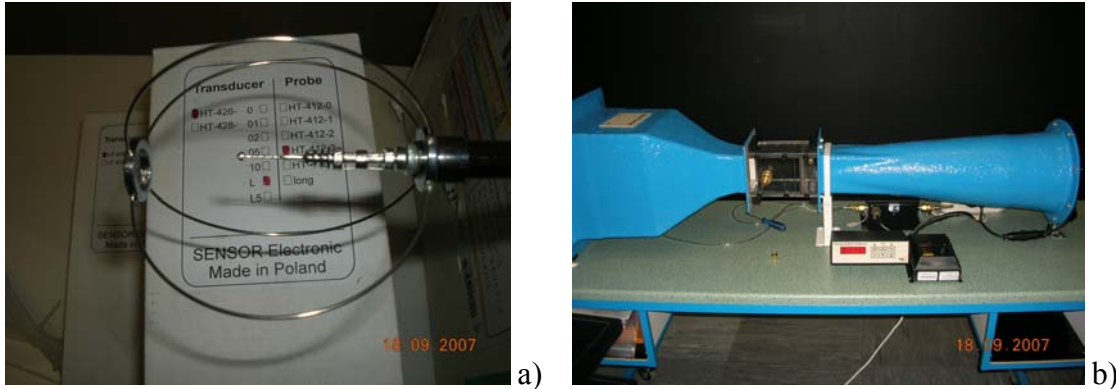


**Figure 3.9** Distribution of measurement points in the second chamber.

### 3.5 Measuring instruments and accuracy

#### 3.5.1 Anemometer and calibration

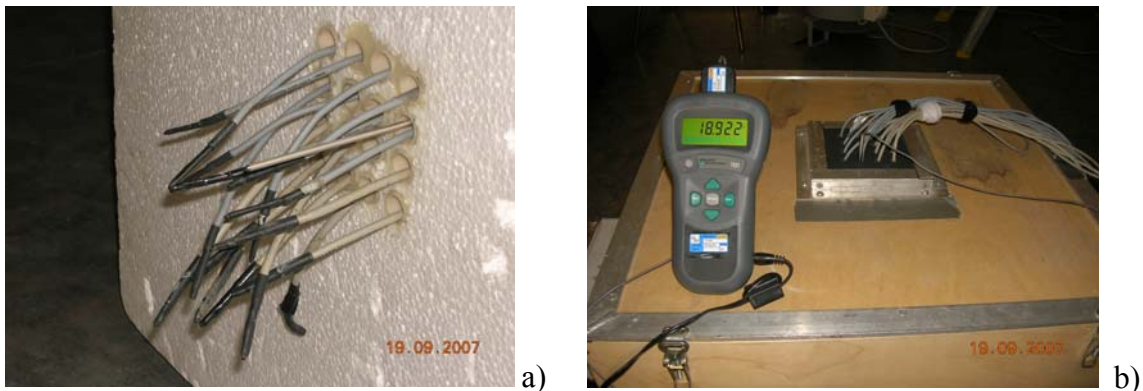
The streamwise velocity was measured using seven omni-directional spherical anemometers. The probe of the omni-directional spherical anemometer has a 2 mm diameter with the measurement range of 0.05 to 1.0 m/s. The digital HT400 recording system collects signals from the anemometer and thermometer with frequency 5 Hz. The output of the velocity, temperature and mean values were calculated every second. The anemometers have an upper frequency 0.5 Hz, which means that it can properly follow velocity changes slower than 0.5 Hz. More information about the definition of the upper frequency was given by Melikov et al. (1998) and Stannov and Melikov (1998). Before the measurement, all these anemometers were calibrated with the TSI Model 8392 Certifier Air Velocity Calibrator. During the calibration and the measurements, the velocity probes were positioned perpendicular to the airflow. The calibrator enables us to calibrate the probed air velocity meters or transducers at a velocity as low as 0.15 m/s. Figure 3.10 shows the anemometer and the calibrator used in the experiment.



**Figure 3.10** Air velocity measuring instrument and calibration equipment. a) Omni-directional spherical anemometer. B) The wind tunnel used for anemometer calibration.

### 3.5.2 Temperature sensor

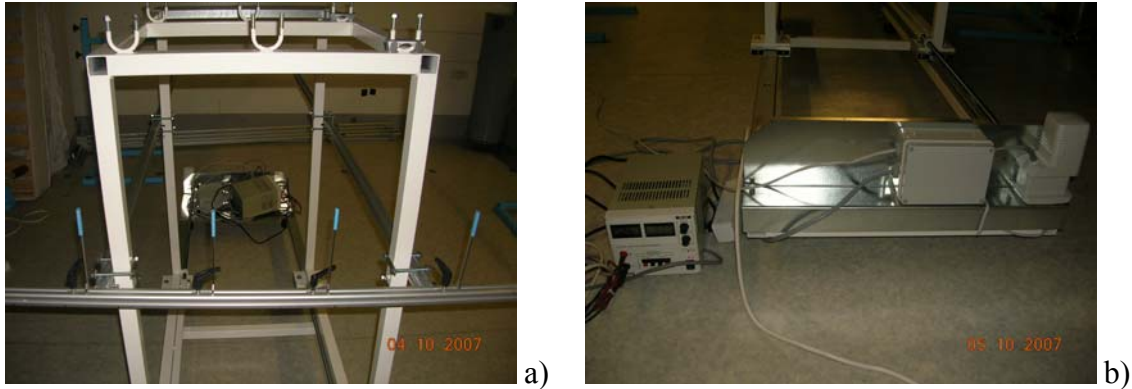
In the experiments carried out in the first test chamber, the PT 100 class A temperature sensor was used for temperature measurement. In the second test chamber, Thermistors temperature sensors and the SQUIRREL 1000 Series logger were used to measure and record the temperature of room air and supply air. The temperature sensors were calibrated in an ambient environment-controlled test chamber by changing the supply air temperature. When the room temperature reached the setting point, all the temperature sensors were put into a well-insulated test box with the temperature calibration sensor. Figure 3.11 showed the temperature sensors, the temperature calibrator and the calibration test chamber. The calibration error of the sixteen sensors was calculated by averaging the ten-minute measured error between the calibrator and the temperature sensors. The response time of the temperature sensor was 2 second.



**Figure 3.11** Temperature measuring instrument and calibration equipment. a) Temperature sensors. b) Temperature calibration chamber.

### 3.5.3 Traversing device

One traversing device was designed to carry all the temperature sensors and the anemometers during the measurement. The device can move forward and backward on two parallel rails by a digital motor which can control the travelling distance. A length step of 5 or 10 mm was used in the isothermal and non-isothermal jet measurements. The accuracy of the traversing device was approximately  $\pm 1$  mm/ position and the mislocation error was corrected in each 10 steps. Figure 3.12 shows photographs of the traversing device and the control motor fitted to the device.



**Figure 3.12** Traversing device for the measuring instruments. a) Frame of the traversing device. b) Micro-motor for control of the moving distance.

### 3.5.4 Estimation of measurement accuracy

In the experiment, the supply air was ducted by a variable speed centrifugal fan using a frequency controller. The airflow rate could be measured by monitoring the pressure drop before and after an orifice in the duct. Before the measurement, the orifice was calibrated to determine the airflow rate parameter. The airflow rate was calculated by Equation 27:

$$q_v = k_p \cdot \sqrt{\Delta P} \quad (27)$$

where  $q_v$  is the calculated airflow rate,  $k_p$  is the parameter obtained by test,  $\Delta P$  is the measured pressure drop in the duct system.  $k_p$  is determined by using the measured pressure drop with a manometer and adjustment module. In the experiment, the airflow rate was measured by using the measured pressure drop and the given  $k_p$ .

To estimate the overall measurement accuracy, Table 3.3 presents a summary of the measuring instrument accuracy.

**Table 3.3** Accuracy of the measuring instruments.

Velocity Range(m/s)	Accuracy			
	Anemometer	Temperature sensor	Air flow	Traversing device
1.25-7.5	2.0% of reading ±0.025 m/s	±0.1°C	±3.6 L/s (3.0% of supply air)	± 1 mm
0.15-1.25	2.0% of reading ±0.01 m/s	±0.1°C	±1.8 L/s(3.0% of supply air)	± 1 mm

Besides the uncertainty mentioned in Table 3.3, the measurement error sources also include the directional sensitivity of the velocity sensor, the natural convection flow generated by the heated velocity sensor, the dynamic response of the anemometer, and velocity and temperature gradients in the airflow. Popiolek et al. (1998) studied the effect of natural convection on the accuracy of low-velocity measurements by means of thermal anemometers with an omni-directional sensor. Melikov et al. (2007) studied the accuracy limitation of a low-speed indoor airflow. It was pointed out that the different error sources from the measurement of airflow rate, mean speed, standard deviation of

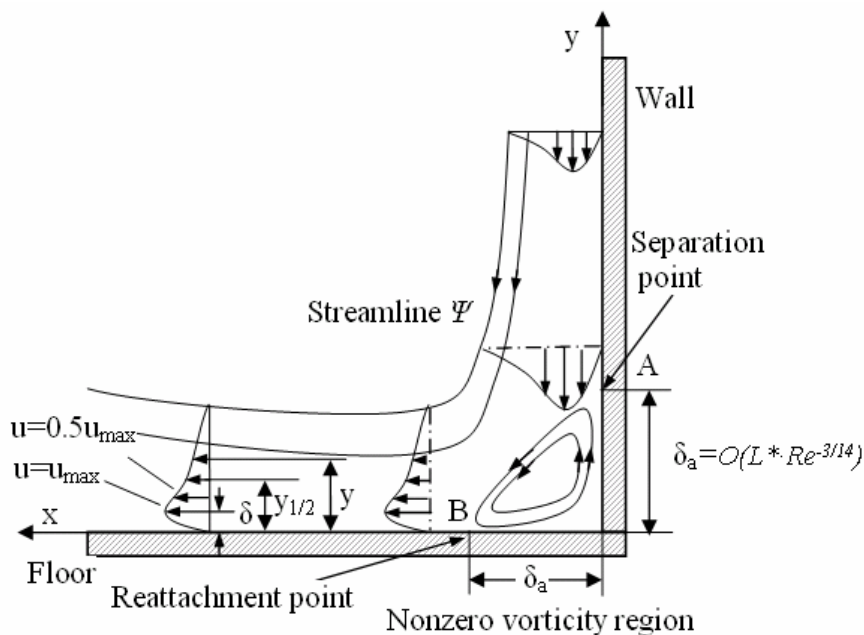
speed, turbulence intensity may result in a combined impact on the overall measurement accuracy.

## 4 ISOTHERMAL AND NON-ISOTHERMAL JET VELOCITY MODELLING

### 4.1 Corner region modelling

In the jet flow field, the corner contains a non-zero vorticity region; this occurs similarly in a stagnation-point flow (White 2006). The boundary layer of the downward air jet separates from the wall at a certain height in the lower wall-floor corner, as illustrated in Figure 4.1, and then reattaches to the floor by passing smoothly through the non-zero vorticity region (II).

Figure 4.1 shows the probable jet separation and reattachment points in the non-zero vorticity region. The probable separation point and reattachment point are marked in Figure 4.1; the height  $\delta_a$  and width  $\delta_a$  are shown to specify the non-zero vorticity region. Smith and Duck (1977) studied the nature of the separation and subsequent return flow occurring when a jet-like boundary layer on a wall encounters a concave corner of finite angle  $\alpha$  ( $0^\circ < \alpha < 90^\circ$ ) or collides with an opposing jet. Based on Smith's study, it can be said that the upstream pressure rising at the attached surface may be sustained by the inviscid displacement of the jet, because the inviscid displacement generates an adverse pressure gradient across the attached jet. Throughout most of the jet flow, the induced pressure would be proportional to the curvature of the jet displacement. In addition the separation point can be predicted to occur at a distance  $O(L \cdot Re^{-3/14})$  from the jet flow corner. The results apply to some well-known jet situations in rotating fluids, oscillatory motions and free convection boundary layers.



**Figure 4.1** Non-zero vorticity region in the corner airflow.

By assuming  $L^*$  is the geometry characteristic of the room by the active chilled beam,  $L^*$  is defined as:

$$L^* = W \text{ (in ceiling-wall corner)} \quad \text{and} \quad L^* = H \text{ (in wall-floor corner)} \quad (28)$$

where  $W$  is the width and  $H$  is the height of the room. Then the non-zero vorticity region in the wall-floor corner airflow is defined as:

$$\delta_a = H^* \text{Re}^{-3/14} \quad (29)$$

$$H^* = H - \delta_a^1 \quad (30)$$

$\delta_a^1$  is the separation distance of the first upper ceiling-wall corner,  $H^*$  is the distance between the slot and separation point in the upper ceiling-wall corner, and also refers the distance between the ceiling and separation point in the lower wall-floor corner.

The decay of the maximum jet velocity can be expressed by the assumption equation below derived from the experimental data in (II):

$$\frac{U_m}{U_0} = 0.82 \left( \frac{|x - 2\delta_a|}{\delta_a} \right)^{-0.11} \quad (31)$$

The returning air velocity profile could be obtained as:

$$u_y = U_m \cdot \exp(-0.937(\eta - 0.14)^2) \quad (32)$$

The two corner returning-air-jet models consisting of Equations 28 to 32 could be applied by using the following assumptions:

- the air entrained by the jet is at room air temperature;
- the only force opposing the downward airflow is the wall shear stress and free shear stress of the room air;
- the downward air jet along the wall, which flows with a thin boundary layer compared with the occupied region geometry, contains an air-jet structure characteristic similar to that of an impinging jet;
- the returning airflow passes the non-zero vorticity region smoothly without losing momentum and jet core velocity;
- the model could be validated only outside the non-zero vorticity region.

## 4.2 Non-corner region modelling

### 4.2.1 Isothermal model

Two isothermal jet models were constructed to predict the maximum velocity decay of the low Reynolds number ( $\text{Re}=1000, 2000$  and  $4000$ ) attached plane jet in the transitional process in a room in (III). The two models were validated at a distance of 10-37 slot heights downstream from the jet slot. The distance validated by the measurement covers the jet transition region and the beginning of the fully developed region. Therefore, the same assumption used for the transitional jet modelling is suitable for the fully developed jet modelling.

### Model 1: Conventional jet model



In the isothermal jet studies, if the jet momentum from the slot could be considered to be approximately preserved, the effect of viscosity would then be neglected when modelling the maximum velocity decay. The main parameter influencing the jet behaviour will be the initial momentum flux  $M_0$  from the jet slot, so the maximum velocity could be written:

$$u_m(x) = f_1(M_0, \rho, x)^{0.5} \quad (33)$$

where  $M_0$  is the initial momentum flux,  $\rho$  is the air density,  $x$  is the distance downstream of the jet slot presented (Rajaratnam 1976).

For a compact jet, the centreline jet velocity in the fully developed region could be calculated from the equation based on the principle of initial momentum conservation along the jet (Abramovich 1948 and Loitzansky 1973; cited by Hagström et al. 1999):

$$M_0 = 2\pi\rho \int_0^\delta u_m^2 y dy \quad (34)$$

where  $M_0 = \rho u_m^2 A_c$  is the initial momentum flux  $M_0$ , where  $A_c$  is the jet slot area,  $\delta$  is the distance from the axis to the jet boundary.

By the application of the Gauss error-function equation for the jet velocity profile, the centreline velocity of the compact jet becomes:

$$u_m(x) = \frac{1}{\sqrt{\pi c_m}} \left( \frac{M_0}{\rho} \right)^{0.5} \frac{1}{x} \quad (35)$$

The finalized jet velocity model, as presented by Rajaratnam (1976), Awbi (1991) and Hagström et al. (1999), applied the diffuser jet dynamic characteristics parameter which describes the intensity of the jet velocity decay along the jet. Then the conventional jet model for a linear jet application derived from the above equation becomes:

$$\frac{u_m}{u_0} = K \sqrt{\frac{h}{x}} \quad (36)$$

where  $u_m$  is the maximum air velocity,  $u_0$  is the initial slot air velocity,  $K$  is the dynamic coefficient of the jet which will depend on the slot Reynolds number if the slot Reynolds number is less than  $10^4$ ,  $x$  is the jet horizontal travelling distance, and  $h$  is the jet slot height. For the compact jet,  $K$  varies from 5.7 to 7, as reported in Hagström et al. (1999). Rajaratnam (1976) and Awbi (1991) used a value of 3.5 for  $K$  to predict the attached plane jet velocity. In addition, for the application of linear diffusers,  $K \approx 2.5$  is presented by Hagström et al. (1999). Most recently,  $K = 2.6$  was used for the low Reynolds number jet proposed by Topp et al. (2000).

Basically, Equation 36 is for free jet velocity prediction and could still be used for the attached plane jet velocity due to the symmetry consideration by multiplying by the square root of two (I and VI). Rajaratnam (1976) and Awbi (1991) used the equation to calculate the maximum velocity of the attached plane jet:

$$\frac{u_m}{u_0} = 3.5 \sqrt{\frac{h}{x}} \quad (37)$$

## Model 2: Virtual origin model

If the virtual origin exists upstream of the jet exit, let the downstream distance measured from the jet exit be denoted by  $x$  and the distance from the exit to the virtual origin be denoted by  $x_0$ . Then the downstream coordinate  $x'$  is given by  $x+x_0$ . The value of  $x_0$  is taken as positive if the virtual origin lies within the jet slot. As a result of this assumption,  $x'$  is now an unknown quantity and depends on the value of  $x_0$ . Unlike the exponent for the jet velocity, -0.5, for the maximum jet velocity decay in the conventional jet model, experimental studies showed that the jet velocity could be expressed by different exponents and different bases. Schwarz and Cosart (1961) present a relationship between the local maximum velocity and downstream position as:

$$u_m(x) = K_1(x + x_0)^b \quad (38)$$

$K_1$  is the jet characteristics parameter, which could be determined by test data; and the exponent  $b$  in Equation 38 was given by the experimental results as -0.555 for turbulent jet flow and -0.5 for laminar jet flow by Schwarz and Cosart (1961). By experimental study, Bajura and Szewczyk (1970) obtained average values for the exponent of the maximum velocity and boundary layer, -0.48 and 0.74, respectively, for relative high Reynolds numbers. In addition, the virtual origin  $x_0=11.2$  slot heights upstream within the jet slot, was used in the study of Schwarz and Cosart (1961), in which the Reynolds number in the experiment varies from 13000 to 41000.

If the part of the slot velocity is extracted from the right-hand side of Equation 38, then the virtual origin jet equation could take the same base and exponent, but a different parameter is to be determined. By using the concept of the virtual origin and the exponent, the virtual origin model could be written as:

$$u_m(x) = U_s D_1 (x + x_0)^p \quad (39)$$

$$\delta(x) = D_2 (x + x_0)^q \quad (40)$$

where  $u_m(x)$  is the local maximum velocity,  $U_s$  is the slot mean velocity,  $\delta(x)$  is the local boundary layer thickness at which point the maximum jet velocity occurs,  $D_1$  and  $D_2$  are parameters that should be determined by test, and  $p$  and  $q$  represent the jet velocity exponents. In this study,  $p$  is given -0.55 due to the mild Reynolds number level of the supplied jet flow ( $1000 \leq Re \leq 4000$ ). In addition, the linear correlation of the virtual origin with the Reynolds number is obtained by using the slot height  $h$  to make the virtual origin non-dimensional (Bajura and Szewczyk, 1970):

$$\frac{x_0}{h} = D_3 + D_4 Re \quad (41)$$

The parameters in Equation 39 and 41 are determined by a few test cases; factor  $D_1$  is 0.75, factors  $D_3$  and  $D_4$  are 0.54 and 0.0021, respectively. Then Equation 41 becomes:

$$\frac{x_0}{h} = 0.54 + 0.0021 Re \quad (42)$$

The two isothermal jet models consisting of Equation 33 to 42 could be applied by using the following assumptions: 1) the air entrained by the jet is at room air temperature; 2) the only force opposing the downward airflow is the wall shear stress

and free shear stress of the room air; 3) the turbulent jet momentum in the mixing process is approximately preserved; 4) the attached plane jet with a low Reynolds number and a high turbulence level has a similarity exponent similar to that of the high Reynolds number jet.

#### 4.2.2 Free convection model

In non-isothermal conditions, the buoyancy is due to the combined presence of a fluid density gradient and a body force that is proportional to density. In the buoyant jet cases, the only body force is the gravity, which is implemented by applying the Boussinesq approximation. In the Boussinesq model, the local density variation is defined as:

$$\rho = \rho_0(1 - \beta(T - T_{ref})) \quad (43)$$

where  $T_{ref}$  is the buoyancy reference temperature,  $\rho_0$  is the fluid density, where  $\beta$  is the thermal expansion rate approximated as:

$$\beta \approx -\frac{1}{\rho} \frac{\rho_0 - \rho}{T_{ref} - T} \quad (44)$$

If the air jet issues from a slot of very large aspect ratio (i.e.  $b/h > 40$ ) where any lateral change in the flow properties occurs only in a plane normal to the slot length, the jet could be considered as an attached two-dimensional jet (Awbi 1991). In the study on chilled beams, the air jet issues from the chilled beam slot with large aspect ratio of 60, so we were dealing with a two-dimensional jet.

The conventional non-isothermal jet equation enabling the calculation of vertical air jet velocity was an empirical model given by Grititlin (1970) as:

$$\frac{v_x}{v_0} = K_1 \left[ \frac{h}{x} \right]^{0.5} \sqrt[3]{1 \pm 1.8 Ar_x} \quad (45)$$

$$\frac{\Delta t_x}{\Delta t_0} = K_2 \left[ \frac{h}{x} \right]^{0.5} \frac{1}{\sqrt[3]{1 \pm 1.8 Ar_x}} \quad (46)$$

$$Ar_x = \frac{K_2}{K_1^2} \cdot Ar_0 \cdot \left[ \frac{x}{h} \right]^{3/2} \quad (47)$$

where  $v_x$  is the vertical airflow velocity (m/s),  $v_0$  is the initial air jet velocity (m/s),  $K_1 \approx 2.6$  is the velocity coefficient for the rectangular jet at a distance of six slot widths downstream from the jet slot,  $K_2 \approx 2.4$  is the temperature coefficient under the same conditions as the velocity coefficient,  $h$  is air jet slot height (m),  $x$  is the vertical distance from the initial point (m),  $\Delta t_x$  is the centreline temperature difference of the air jet at a distance of  $x$  m downstream from the jet slot,  $\Delta t_0$  is the initial temperature difference of the air jet,  $Ar_x$  is the local Archimedes number, and  $Ar_0$  is the initial Archimedes number defined as:

$$Ar_0 = gd(T_s - T_\infty)/(T_h v_0^2) \quad (48)$$

where  $g$  is the acceleration owing to gravity ( $9.81 \text{ m/s}^2$ ),  $T_s$  is the supply air temperature ( $^\circ\text{C}$ ), and  $T_\infty$  is the ambient air temperature ( $^\circ\text{C}$ ).

In (VII), the Grimitlin model was tested by the near-wall measured velocities and it was found that the model failed to predict either the maximum vertical velocity of the air jet or the velocity profile with the given  $K_1$  and  $K_2$ . The impingement jet flow behaviours of the chilled beam may result in this failure. Thus, we assumed that the attached jet near the vertical wall surface could be treated as a combination of the isothermal downward air jet flow and the free convection flow. The equation for the isothermal jet velocity takes the form of Equation 36. When taking into account the distance from the slot to the impinged wall, Equation 36 is rewritten as:

$$\frac{u_m}{u_0} = K \left( \frac{h}{x+y} \right)^{0.5} \quad (49)$$

Equation 49 is applied as a linear jet equation for the maximum air velocity calculation in the linear diffuser jet described in (VI and VII).  $K$  is the characteristic factor obtained from experiment results. For linear diffusers, Knystautas and Miller gave  $K=2.43$  and, according to Shepelev, Görtler, Kraemer and Becher,  $K=2.62, 2.43, 2.51$  and  $2.55$ , respectively reported in Hagström et al. (1999). For the plane jet by active chilled beam, (I) reported that  $K=2.85$  ( $K^2=8.13$ ), which was obtained from an isothermal case and calculated from the average chilled beam slot air velocity. Under non-isothermal conditions,  $K=2.23$  and  $2.5$  were used to calculate the centre jet velocity decay by Grimitlin (1970) and Regenscheit (1970), respectively.

The free convection flow equation was presented in Miettinen and Aitta (1992) as:

$$u(x, y) = \frac{\nu}{L_x} \left( \frac{80}{3} \cdot \frac{Gr_x}{\left(\frac{20}{21} + Pr\right)} \right)^{0.5} \cdot \frac{y}{\delta} \cdot \left(1 - \frac{y}{\delta}\right)^2 \quad (50)$$

where  $u(x, y)$  is the velocity component,  $x$  and  $y$  are the coordinates along and normal to the plate measured from leading edge,  $\nu$  is the kinematic viscosity,  $L_x$  is the distance from the ceiling, and  $Gr_x$  is the Grashof number, which is defined as:

$$Gr_x = \frac{g\beta(T_s - T_\infty)L_x^3}{\nu^2} \quad (51)$$

where  $g$  is the acceleration due to gravity,  $T_s$  is the wall surface temperature,  $T_\infty$  is the ambient temperature,  $Pr$  is the Prandtl number,  $Re$  is the Reynolds number, and  $\delta$  is the boundary layer thickness, defined as:

$$\delta = \frac{5x}{\sqrt{Re}} \quad (52)$$

It is assumed that the non-isothermal jet along the ceiling and the wall surface can be calculated as the superposition of the laminar free convection air velocity and the isothermal jet velocity. For the horizontal ceiling part, only the isothermal jet velocity is applied as the jet is considered attached. Another assumption is that the free convection air flow is driven by the air temperature difference between the air jet and the ambient room air. The probable temperature difference between the jet and wall surface is small and may be neglected. Finally, the free convection model is expressed as:

$$u(x, y) = u_0 \cdot \left[ \frac{K \cdot h}{x + y} \right]^{0.5} + \frac{\nu}{L_x} \left( \frac{80}{3} \cdot \frac{Gr_x}{\left( \frac{20}{21} + Pr_x \right)} \right)^{0.5} \cdot \frac{y}{\delta} \cdot \left( 1 - \frac{y}{\delta} \right)^2 \quad (53)$$

When considering the physical background of Equation 53 one should note that it is adding velocities obtained by the empirical jet equation and the free convection equation. These parts of equations only apply to the respective flow phenomena in isolation. Strictly speaking, it is not physically correct to add the results, as both terms represent non-linear relationships. This means that Equation 53 should be considered as an empirical equation that is validated under the given conditions in this study.

On the basis of the non-isothermal jet modelling in (I), Equation 53 should be used with the following assumptions:

- the jet of cooled air is projected into an unbounded atmosphere of still air of uniform temperature;
- the only force opposing the downward flow of the heated air or upward flow of the cooled air is a buoyancy force;
- the air entrained by the jet is at room air temperature;
- the velocity profile and the temperature difference profile have shapes that can be approximated by an error function-type curve.

#### 4.2.3 Buoyancy superimposing model

When studying the non-isothermal attached jet in a high room without the corner effect, the free convection model could not obtain agreement with the preliminary measured turbulent jet velocity in the fully developed jet region (see Figure 5.10). Thus, the new model, the buoyancy superimposing model, was derived to predict the jet velocity decay in a high room.

On the basis of papers (VI) and (VII), the free convection model was derived and presented in (I) to predict the maximum velocity of the attached plane jet in the near wall region in non-isothermal conditions. It is assumed that the non-isothermal jet along the ceiling and the wall can be calculated as a superposition of the laminar free convection air velocity and the isothermal jet velocity. By the same modelling methodology, paper (IV) shows a new buoyant superimposing model set up to calculate the maximum jet velocity decay of the buoyant jet. The model consists of two parts: one is the isothermal part and the other is the buoyant part. The conception of the virtual origin is used to model the isothermal velocity component which solves the effect of wall shear stress in the boundary layer and free shear stress in outer region of air jet. The superimposed non-isothermal part is based on the hypothesis of the Boussinesq approximation. Therefore, the overall superimposing model could be considered as a semi-empirical jet model, in which the jet dynamic characteristics coefficient should be determined by experiments. The first part is the isothermal maximum jet velocity decay which can be expressed by the jet similarity Equation 39.

In the non-isothermal part, the buoyancy force acting vertically on a certain volume element of airflow,  $Q'$ , of an air jet of temperature  $T$  and density  $\rho$  which are different from those of the surrounding fluid  $T_0$  and  $\rho_0$ , is:

$$F_b = Q' g(\rho_0 - \rho) \quad (54)$$

The air density of the volume element of airflow could be inversely proportional to the air temperature as:  $\rho \propto 1/T$ . Then Equation 52 becomes:

$$F_b = Q' g\rho(T/T_0 - 1) \quad (55)$$

The force due to the temperature difference will produce a vertical acceleration  $a$  expressed as:

$$a = F_b / (Q' \rho) \quad (56)$$

Substituting for  $F_b$  yields:

$$a = g\Delta T / T_0 \quad (57)$$

where  $\Delta T = T - T_0$

If the vertical distance between this given volume element and a reference point is  $L$ , then the volume element of airflow will move vertically at a velocity,  $u_1$ , relative to the reference point such that:

$$u_1^2 = 2La \quad (58)$$

Substituting for  $a$  from Equation 58 yields:

$$u_1^2 = 2gL\Delta T / T_0 \quad (59)$$

Then:

$$u_1 = \left( \frac{2gL\Delta T}{T_0} \right)^{1/2} \quad (60)$$

Equation 60 presents the velocity component due to the buoyancy force acting vertically on a unit volume element of airflow with a different temperature from the surroundings. Here, the temperature decay coefficient,  $K^e$ , is introduced to calculate the velocity due to the buoyancy effect at a distance,  $x$ , downstream of the jet slot. With the temperature decay coefficient,  $K^e$ , Equation 60 is expressed as:

$$u_1 = \left( K^e \frac{gx\Delta T}{T_0} \right)^{1/2} \quad (61)$$

The non-isothermal attached jet velocity decay is dependent upon the relationship between the inertia, buoyancy and viscous forces acting on the jet. In a quiescent ambient, the behaviour of a buoyant jet depends mainly on the initial momentum and corresponding buoyancy.

Combining the initial velocity and the buoyancy velocity, the maximum velocity could be calculated by superimposing the isothermal part, Equation 39, and the buoyancy acceleration part, Equation 61. Finalizing the above equations yields the superimposing jet model as:

$$u_m = u_x + u_1 = U_0 D_l (x + x_0)^p + \left( K^e \frac{g x \Delta T}{T_0} \right)^{1/2} \quad (62)$$

where  $D_l$  is the slot characteristic parameter, 0.51 and 0.70 for 20 mm and 30 mm nozzle heights respectively,  $p$  is the similarity component -0.55, and  $K^e$  is the temperature decay coefficient, 0.53 is used in the calculation.

The models consisting of Equations 54 to 62 could be applied by using the following assumptions:

- the air entrained by the jet is at room air temperature;
- the only forces opposing the downward volume element of airflow are the wall shear stress, the free shear stress of the room air and the gravitational force;
- the turbulent jet momentum in the mixing process is approximately preserved;
- the attached-plane-jet at a low Reynolds number and a high turbulent level has a similarity exponent similar to that of the high Reynolds number jet.

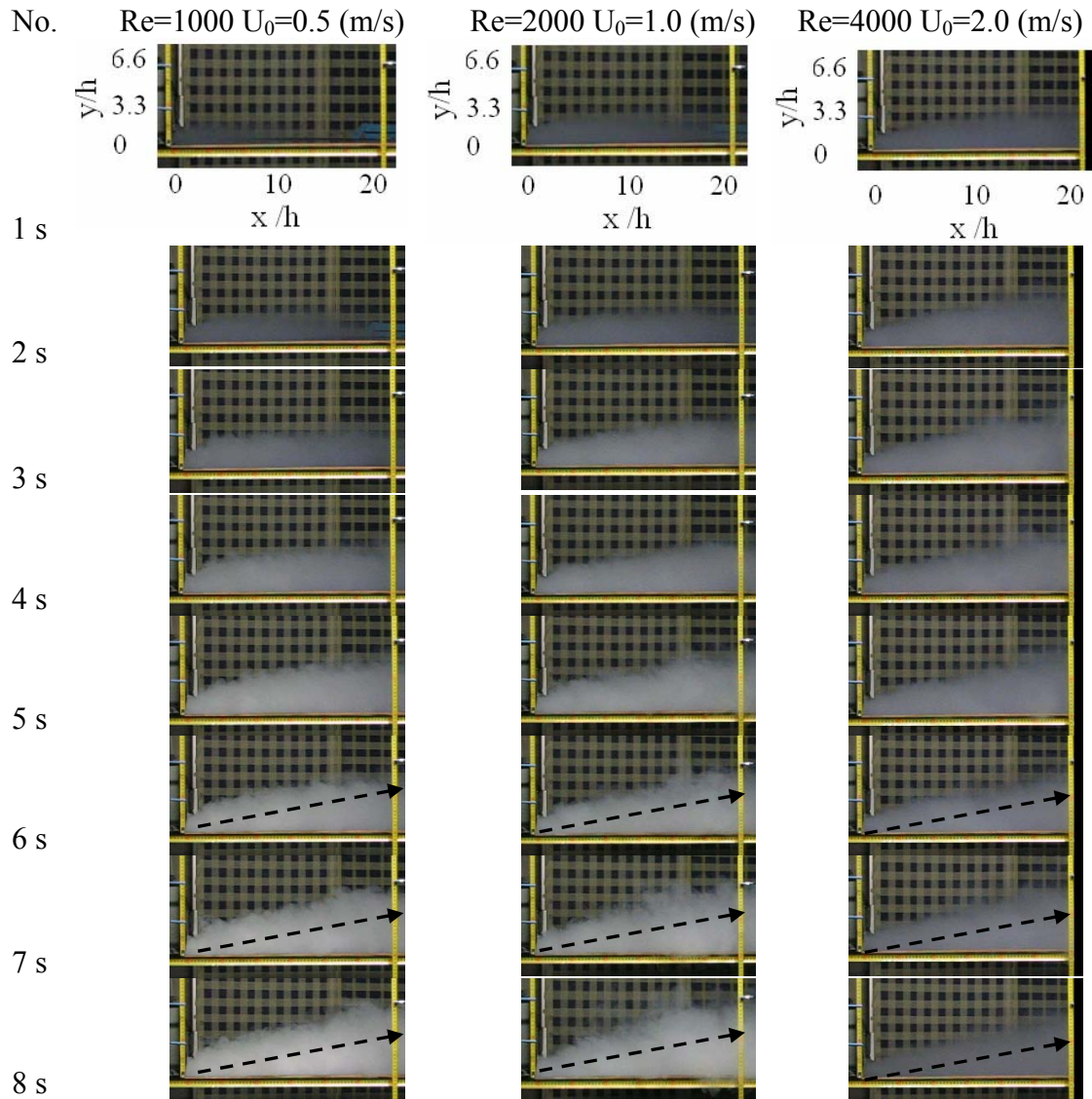
From a practical point of view, the buoyant superimposing model could be considered as a semi-empirical jet model by which the maximum velocity of the attached plane jet in a room can be calculated. For various jet supply devices, the jet dynamic characteristics coefficients should be determined by experiments in both isothermal and non-isothermal cases.

## 5 CALCULATION AND MEASUREMENT RESULTS

### 5.1 Jet flow field visualization

Firstly, the attached plane jet flow was studied by tracer gas visualization. Parts of the visualization results are reported in (III). Here, the visualization results in (III) are shown below. Three jet slot velocities were taken, 0.5, 1 and 2 m/s, over a range of distances downstream of the jet slot. In the visualization, the distance from the slot to 0.6 m downstream of the slot has been observed by smoke test.

The photographs of the jet flow visualization are presented in Figure 5.1 and show the jet development process over eight seconds. The attached plane jet displays unstable characteristics due to the probable double row pairing vortex structure. During the experiments using trace gas, it can be observed that after just a few seconds the jet becomes turbulent by inducing ambient air and the jet volume grows.



**Figure 5.1** Sequential digital camera photographs of the jet discharging process at one-second intervals over an eight-second period.

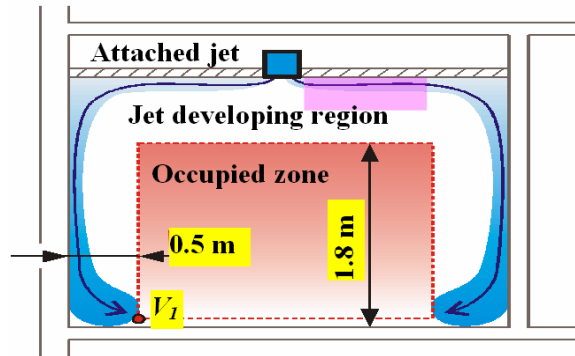
The turbulent shear stress has a strong influence on the induction mechanism in the jet growth processing. Obviously, one observable trend is that the jet grows faster at  $Re=1000$  than at  $Re=4000$ . The trend indicates a jet with a relatively low Reynolds number tends to induce more ambient air into the jet after the jet leaves the slot. At lower Reynolds numbers, where viscous forces are dominant, the shear stress in the outer layer and the boundary layer in the inner layer of the attached jet result in the growth of a thicker jet. Contrastingly, at higher Reynolds numbers the jet flow is dominated by inertial forces, which tend to produce random eddies, vortices and other flow fluctuations downstream of the jet slot. The driving forces of the jet flow, by inertial forces or viscous forces, cause significantly different jet spreading angles under room conditions. The spreading angles according to the visualisation results are approximately  $13^\circ$ ,  $13^\circ$  and  $11^\circ$  for Reynolds number 1000, 2000 and 4000, respectively.



## 5.2 Jet velocity distribution in the developing region

### 5.2.1 Measurement results

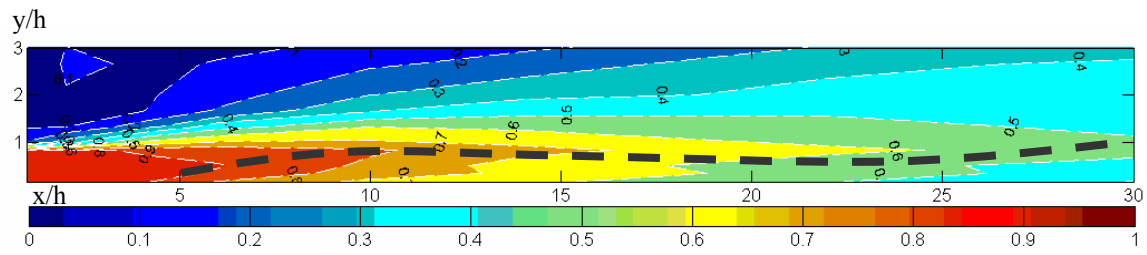
In the streamwise direction, the new two-zone jet divisions, the developing zone and the developed zone, have been presented in (III). The first zone includes the possible potential core and transition zone during the whole transition process. The developed zone, representing the region in which jet self similarity is displayed, includes both the inner and outer region. The first zone of the attached plane jet is presented in Figure 5.2 and displays the relative position of the jet developing region in a room.



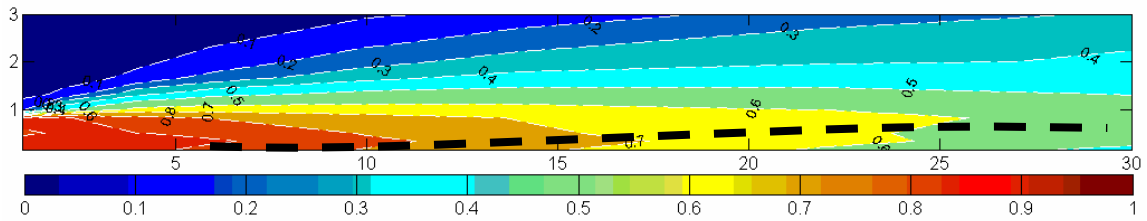
**Figure 5.2** The jet developing region in the jet flow field.

The measurement results are presented in Figure 5.3 and show the mean velocity contours where the jet transition process is displayed using the attached plane jet under the room conditions. The measured plane normal to the attached surface is extended to 3 slot heights downstream of the jet slot. Three-minute period was used as the averaging time period to calculate the mean velocity jet flow characteristics, e.g. jet velocity, jet temperature and turbulent intensity. The data sampling time was one second. In Figure 5.3, the black dashed line denotes the locations of local maximum streamwise velocity. The inner region and the outer layer region illustrated in Figure 2.1 could be observed below and above the dashed line, respectively. In addition, the potential core region, where the streamwise velocity is greater than 99% of the jet's average exit velocity, exists near the jet slot and extends to a downstream location of about 2, 3 and 6 slot heights for Reynolds numbers 1000, 2000 and 4000, respectively.

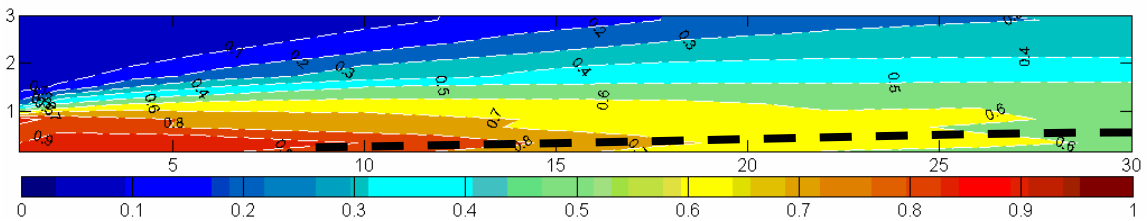
Due to the existence of the potential core region, the outer and inner layers are separated by an unperturbed region and may evolve independently in the initial stage of transition. The three-minute averaged flow velocity in the near field region from  $x=1$  to 30 slot heights represents the spreading speed of the inner layer region by different Reynolds numbers. The inner region becomes wider when  $x=7$ , 15 and 25 slot heights for Reynolds numbers 1000, 2000 and 4000. The spreading of the outer layer region indicates that the primary vortex initially forms at a point about 3 slot heights before the inner region becomes wider.



(a)  $Re=1000$  ( $U_0=0.50$  m/s)



(b)  $Re=2000$  ( $U_0=1.00$  m/s)

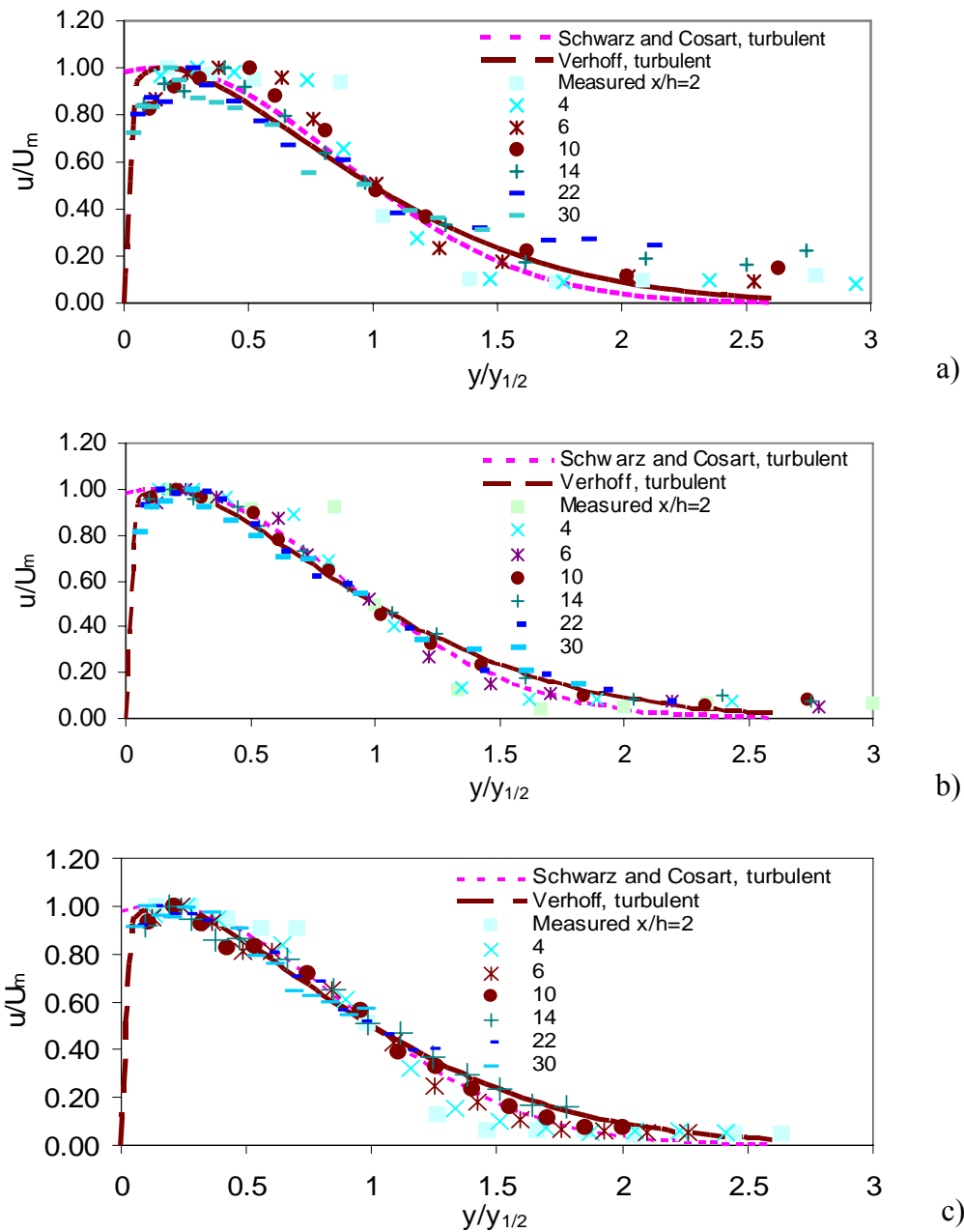


(c)  $Re=4000$  ( $U_0=2.00$  m/s)

**Figure 5.3** The measured jet velocity distribution  $u/U_m$  at different Reynolds numbers.

The jet similarity characteristics in the transition process have been studied in (III) as well. The velocity profiles in various regions of the jet flow are plotted non-dimensionally and compared with previous turbulence studies. The streamwise mean velocity distributions are presented in Figure 5.4, where the velocities are normalized by the local maximum velocity, and the jet discharging distance is normalized by the jet half-width distance, shown as  $u/U_m$  and  $y/y_{1/2}$ , respectively.

Figure 5.4 shows that the profiles express similarity to some extent in each case by Reynolds numbers from 1000 to 4000. Most of the data could fit the theoretical curve quite well, except very close to the jet slot. A high degree of similarity is found in the downstream region at a distance of more than 6 slot heights in the case of  $Re=1000$ . In the cases of  $Re=2000$  and 4000, when at a distance downstream of more than 4 slot heights, good agreement has been obtained with the turbulence profiles of Schwarz and Cosart (1961). Between the maximum velocity and half maximum velocity in the outer region,  $0.15 < y/y_{1/2} < 1$ , most of measured data could fit both turbulent attached plane jet velocity profiles very well.

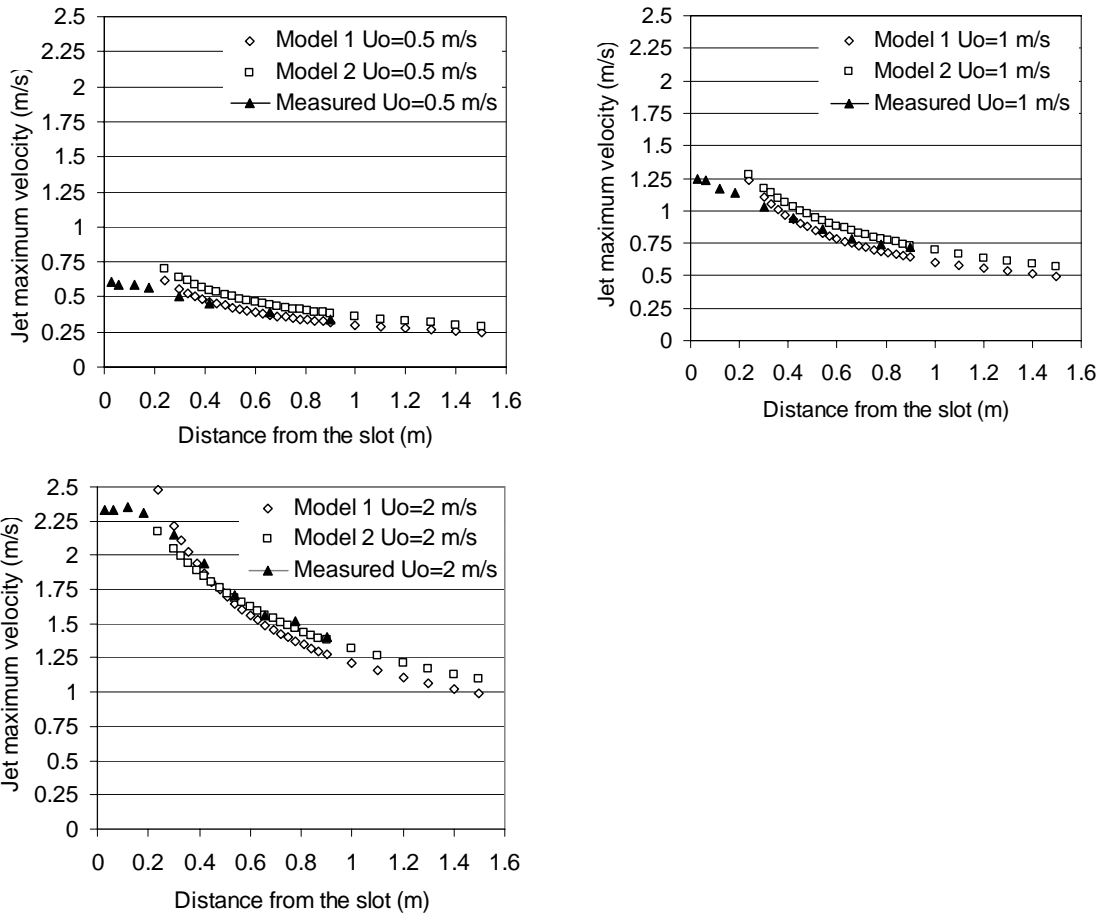


**Figure 5.4** The non-dimensional jet velocity profiles under three isothermal conditions. a)  $Re=1000$  ( $U_0=0.5$  m/s). b)  $Re=2000$  ( $U_0=1.0$  m/s). c)  $Re=4000$  ( $U_0=2.0$  m/s).

### 5.2.2 Calculation results

In (III) the calculated maximum jet velocity by Model 1 and Model 2 was compared with the measured data at Reynolds number 1000, 2000 and 4000. The calculated and measured results are presented in Figure 5.5 and show the performance of Model 1 and Model 2. The results indicate that the maximum velocity calculated by both models can obtain a certain agreement compared with measured ones at a distance of 0.3 to 0.9 m, the same as 10 to 30 slot heights, from the jet slot. At  $Re=1000$ , the calculated results by Model 1 fitted the measured data very well after a distance of 15 slot heights downstream of the slot. At  $Re=2000$ , Model 1 still predict better results than Model 2

between at a distance of 14 to 26 slot heights downstream of the jet slot. Beyond that distance, Model 2 starts to predict closer data than Model 1. At  $Re=4000$ , the two velocity curves obtained by the two models intersect at a distance of 15 slot heights; after that Model 2 predicts a higher jet velocity than Model 1. The maximum air velocity calculated by Model 2 beyond a distance of 14 slot heights obtain better agreement than the data calculated by Model 1 at  $Re=4000$ .

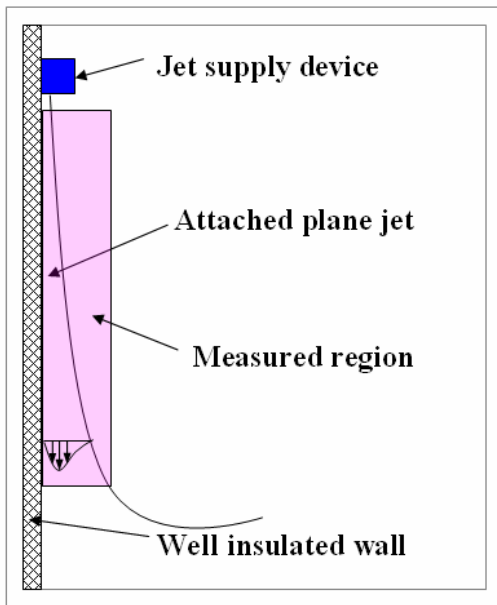


**Figure 5.5** Comparison of calculated and measured maximum jet velocity decay.

### 5.3 Jet velocity distribution in the developed region

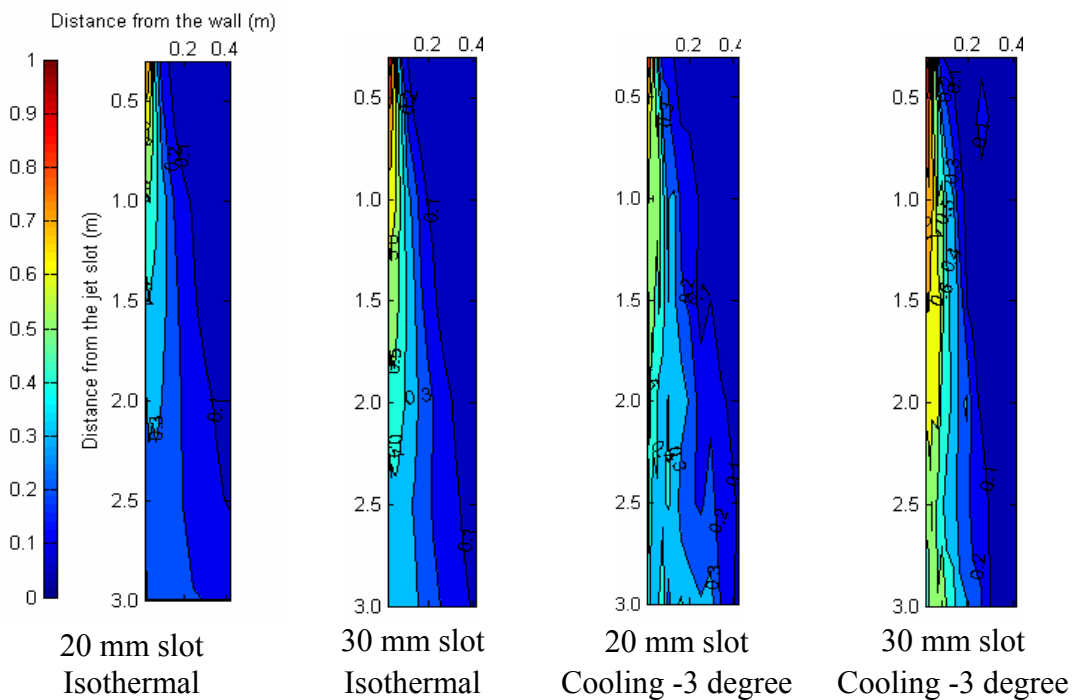
#### 5.3.1 Measurement results

The jet velocity in the whole flow field is measured and modelled in (IV). The measurements are made in the second test chamber by supplying cooling air at 3.0, 6.0 and 8.0 °C lower than the room air temperature over the insulated wall. Three average jet slot velocities were taken, 0.50, 1.00 and 2.00 m/s, over a range of distances downstream of the slot. The jet velocity was measured at distances between 300 to 3000 mm from the diffuser slot. During the measurement, the velocity was recorded every second and the average velocity was obtained over each three-minute period. The mean velocities are plotted in the contour figures by MATLAB R2006B to show the whole structure of the jet in both isothermal and non-isothermal conditions. Figure 5.6 shows the measured jet region in the second test chamber.



**Figure 5.6** The measured developed region of the jet in the second test chamber.

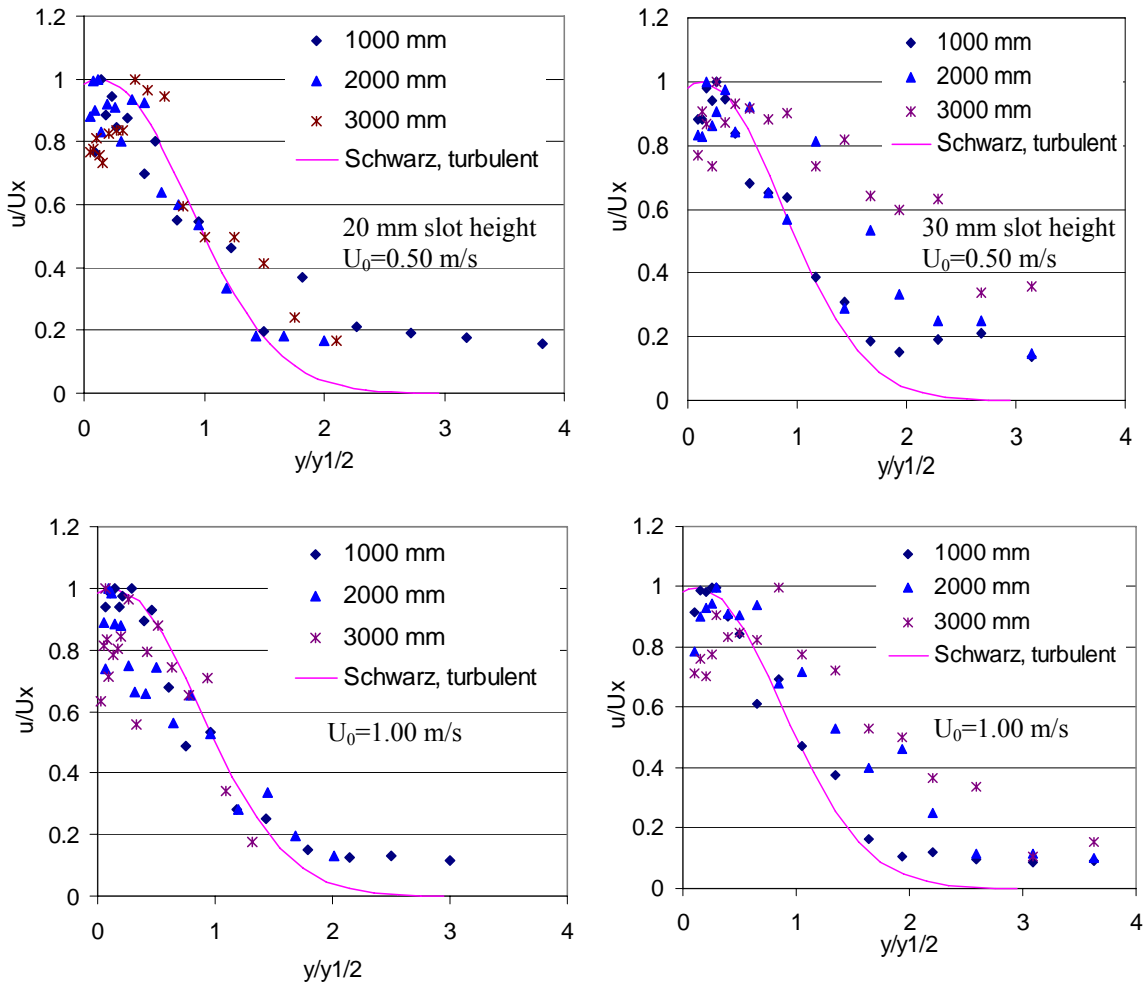
The measured velocity contours are presented in Figure 5.7 and show the whole downstream jet flow structure by 1.00 m/s slot average velocity in both isothermal and cooling conditions. With the same slot velocity, the jet issuing from the 30 mm high slot could discharge further than from the 20 mm high slot with and without the buoyant effect. In the case of the 20 mm slot the mean velocity is below 0.20 m/s beyond 1200 mm (equal to 60 slot heights), and the jet is consumed by both wall shear and free shear.

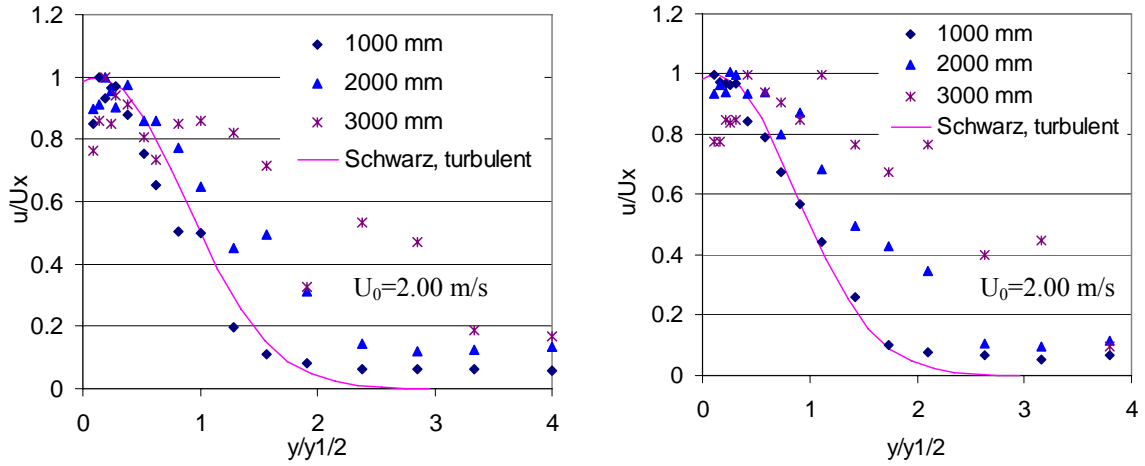


**Figure 5.7** Measured jet velocity distributions by 1.0 m/s average slot velocity.

Paper (IV) studied the whole buoyant jet flow field by measurement and modelling. The whole jet region is divided into three different flow regions due to the interaction of inertial force, gravitational force and buoyant force. To specify the three regions in (IV), the velocity profiles at three different downstream distances are compared with isothermal turbulent jet profiles to show the velocity distribution difference in the three buoyant regions. One novel superimposing velocity model has been set up to predict the maximum jet velocity decay in (IV).

To clarify the difference between different buoyant jet regions, the measured velocity profiles are collected and compared with the theoretical turbulent velocity profile by the equation derived by Schwarz and Cosart (1961). The measured data are presented in Figure 5.8 and show the measured air velocity distribution and the theoretical profiles. At a slot velocity of 0.50 m/s with the 20 mm slot height, the measured velocity profile fits the theoretical profile closer at a distance of 2000 mm than 1000 mm and 3000 mm from the jet slot. The similarity characteristics were displayed clearly by the 2 m/s slot velocity at the point 1 m from the slot.





**Figure 5.8** Measured velocity profiles and theoretical profiles by three different slot velocities.

### 5.3.2 Calculation results

Besides the Grimitlin model, another vertical non-isothermal air jet model, originally derived by Regenscheit (1970), has been used to calculate the vertical air jet velocity. The similar form of the equation was also described in Hagström et al. (1999). The original Regenscheit model takes the form of:

$$\frac{u}{u_0} = \sqrt{\frac{x_0}{x}} \pm \sqrt{\frac{Ar}{K_m} \left[ 2.83 \sqrt{\frac{x}{x_0}} - 1 \right]} \quad (63)$$

$$x_0 = \frac{h}{K_m} \quad (64)$$

where  $u$  is the airflow velocity (m/s),  $u_0$  is the initial air jet velocity (m/s),  $x_0$  is the jet core distance,  $h$  is the air jet slot height (m), and  $K_m$  is the dynamic characteristics factor of the jet, which was suggested as 0.2 by Regenscheit (1970).

In (VI) and (VII), the Regenscheit model was modified to calculate the near-wall jet velocity using the following equation:

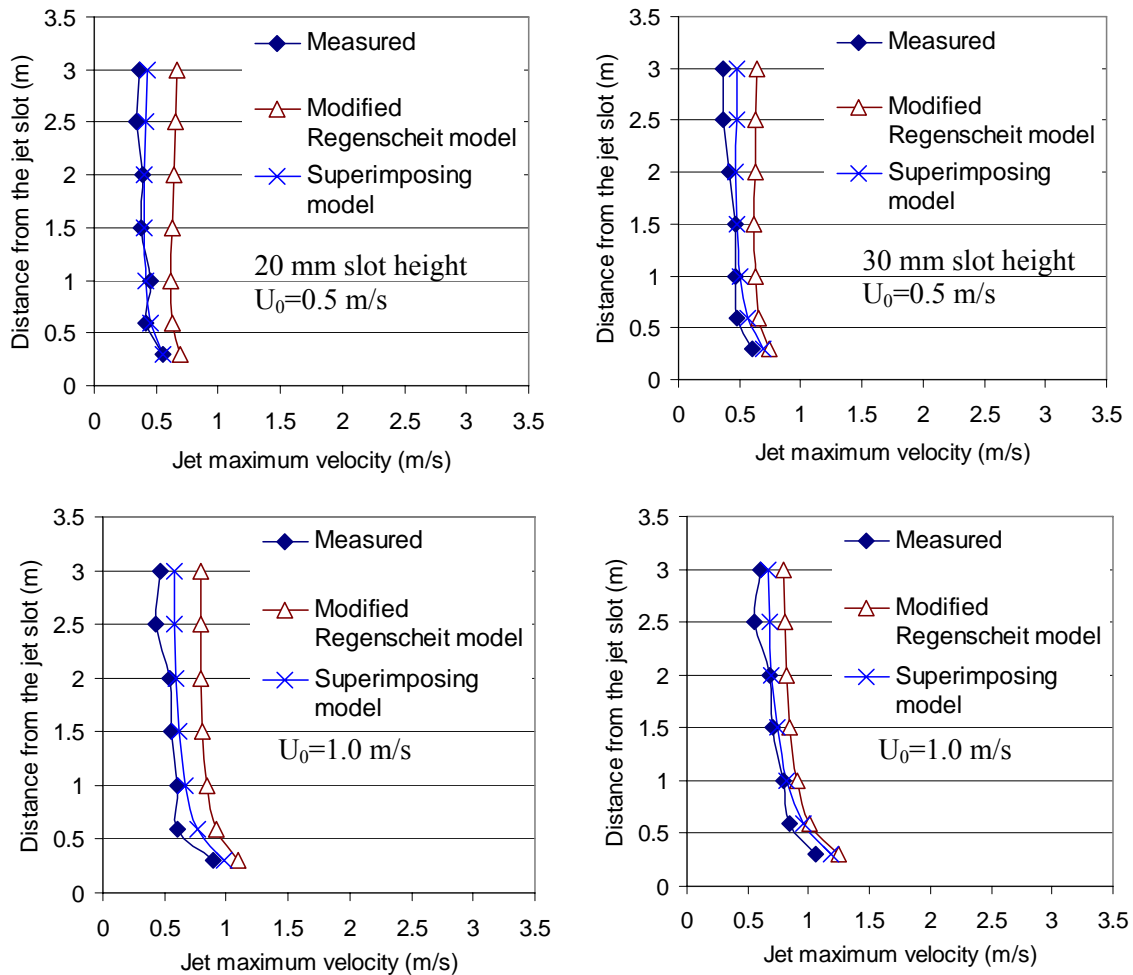
$$\frac{v_y}{v_0} = \left[ \frac{K \cdot h}{x+y} \right]^{0.5} \pm \left( K \cdot Ar \cdot \left[ 2.83 \left[ \frac{x}{K \cdot h} \right]^{0.5} - 1 \right] \right)^{0.5} \quad (65)$$

where  $K$  is the jet dynamic coefficient which should be determined by experiment for a given jet supply device,  $y$  is the distance from the jet slot to the impinged wall (m). The value of  $K$  was about 5.0 in the report by Klobut and Palonen (1992), which is equal to the corresponding coefficient, and  $K_m$  is 0.2, in the original literature of Regenscheit (1970).

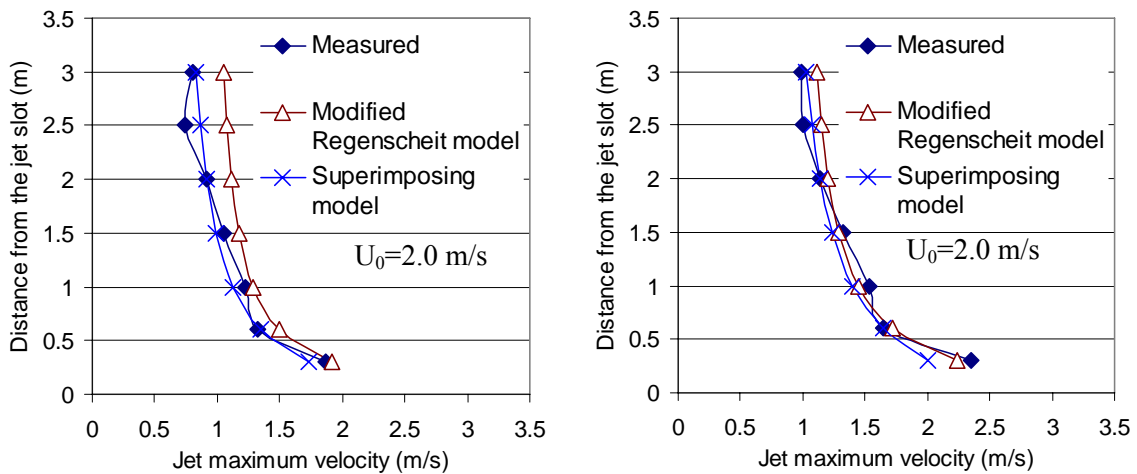
Under isothermal conditions, it was found that the velocity of the wall-bounded plane jet may be calculated by using the isothermal jet model multiplied a factor of square root 2 (considering the wall-bounded effect) as a semi-empirical model (I). When

modelling the turning jet after the corner impingement, the distance in the equation should also include the horizontal distance from the jet slot to the impinged wall, as presented in Equation 49 in (IV) and (VI). The modified Regenscheit model was validated in (IV), (VI) and (VII).

The measured and calculated results are presented in Figure 5.9 and show the performance of the Modified Regenscheit Model and the Superimposing Model under non-isothermal ( $-3^{\circ}\text{C}$ ) conditions in (IV). Most of the results by the Regenscheit model scatter outside the margins of the measurement results. The comparison shows that the superimposing model could predict the maximum velocity more accurately than the Modified Regenscheit model at slot velocities from 0.5 m/s to 2.0 m/s with both the 20 mm and 30 mm slot heights. The Regenscheit model more often predicts higher maximum velocities compared with the measurement result, except in the case of a 2.00 m/s slot velocity with a 30 mm slot height.

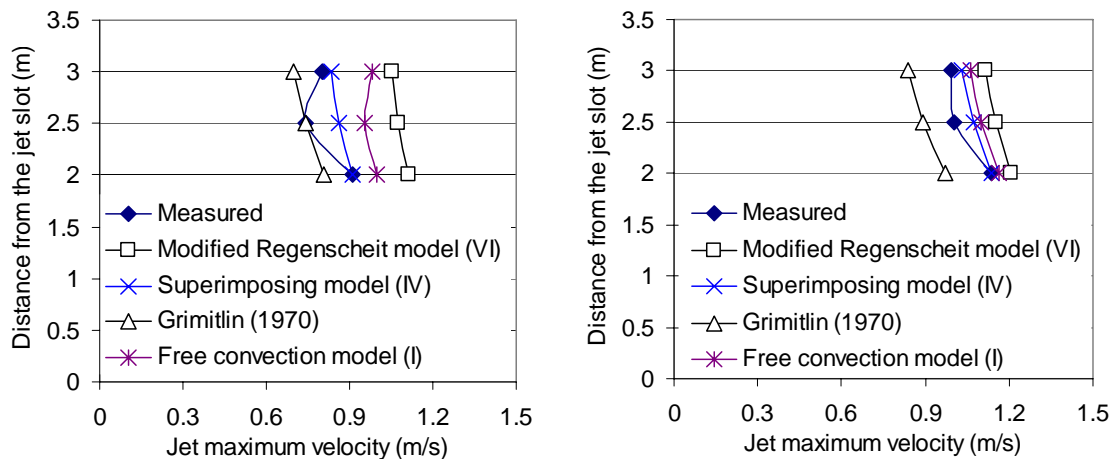






**Figure 5.9** Measured and calculated maximum velocity decay in the downward jet region by three different slot velocities.

The calculated results under non-isothermal ( $-3^{\circ}\text{C}$ ) conditions using various existing model are presented in Figure 5.10 and show a comparison with the measured data in the fully developed jet region obtained in (IV). At the same slot velocity, the performance of the various models changes slightly compared with measured data. Figure 5.10 shows that the Grititlin model underestimates the maximum jet velocity in the fully developed jet flow field. Contrastingly, the modified Regenscheit model and free convection model overestimate the jet velocity. The superimposing model obtains slightly better agreement with the measured maximum jet velocity than the other models in this study.

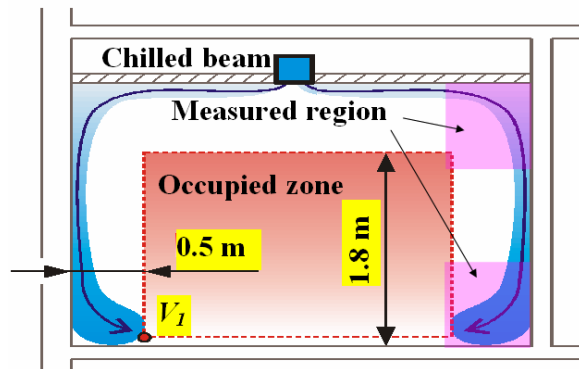


(a) (b)  
**Figure 5.10** Maximum jet velocity calculations in the developed region using various models. (a) the slot height is 20 mm,  $U_{\text{slot}}=2.0$  m/s, (b) the slot height is 30 mm,  $U_{\text{slot}}=2.0$  m/s.

## 5.4 Jet velocity distribution in the corner region

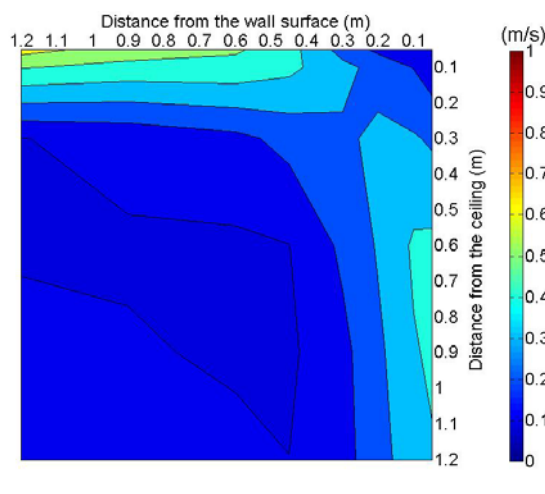
### 5.4.1 Measurement results

The turning jet behaviour and the velocity prediction in the corner region were studied in (II). In fact, two corner regions were recognized in a ventilated room in (VI). The first is the upper ceiling-wall corner and the other is the lower wall-floor corner. After turning at the ceiling-wall corner, the downward air jet approaches the wall-floor corner region by attaching to the wall surface. The two corner regions in a room are presented in Figure 5.11 and show the measured jet region in the first test chamber with the chilled beam.

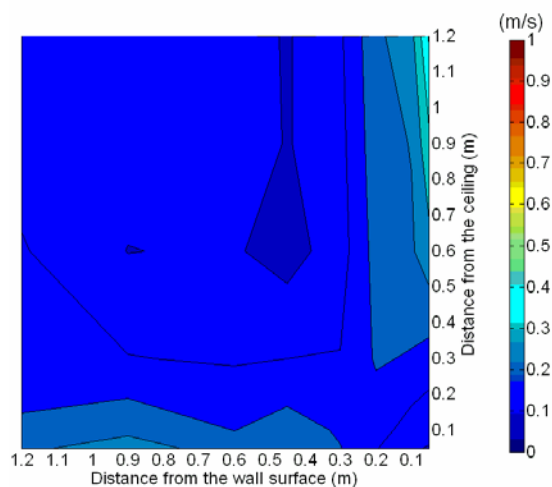


**Figure 5.11** The corner region measured in the first chamber.

The air velocity measurement results are presented in Figures 5.12 and 5.13 and show the distribution of the jet velocity in the two corner regions. In Figure 5.12, the airflow is approaching the wall beneath the ceiling at a velocity of 0.65 m/s, decreasing along the surface of the ceiling. In the corner region, the non-zero vorticity regions are distinguished by a constant air velocity region in both the upper corner and the lower corner, which is about 0.22 m/s. Figure 5.13 shows that the airflow reattaches to the floor after the separation from the wall surface with a similar pattern as in the ceiling-wall corner.



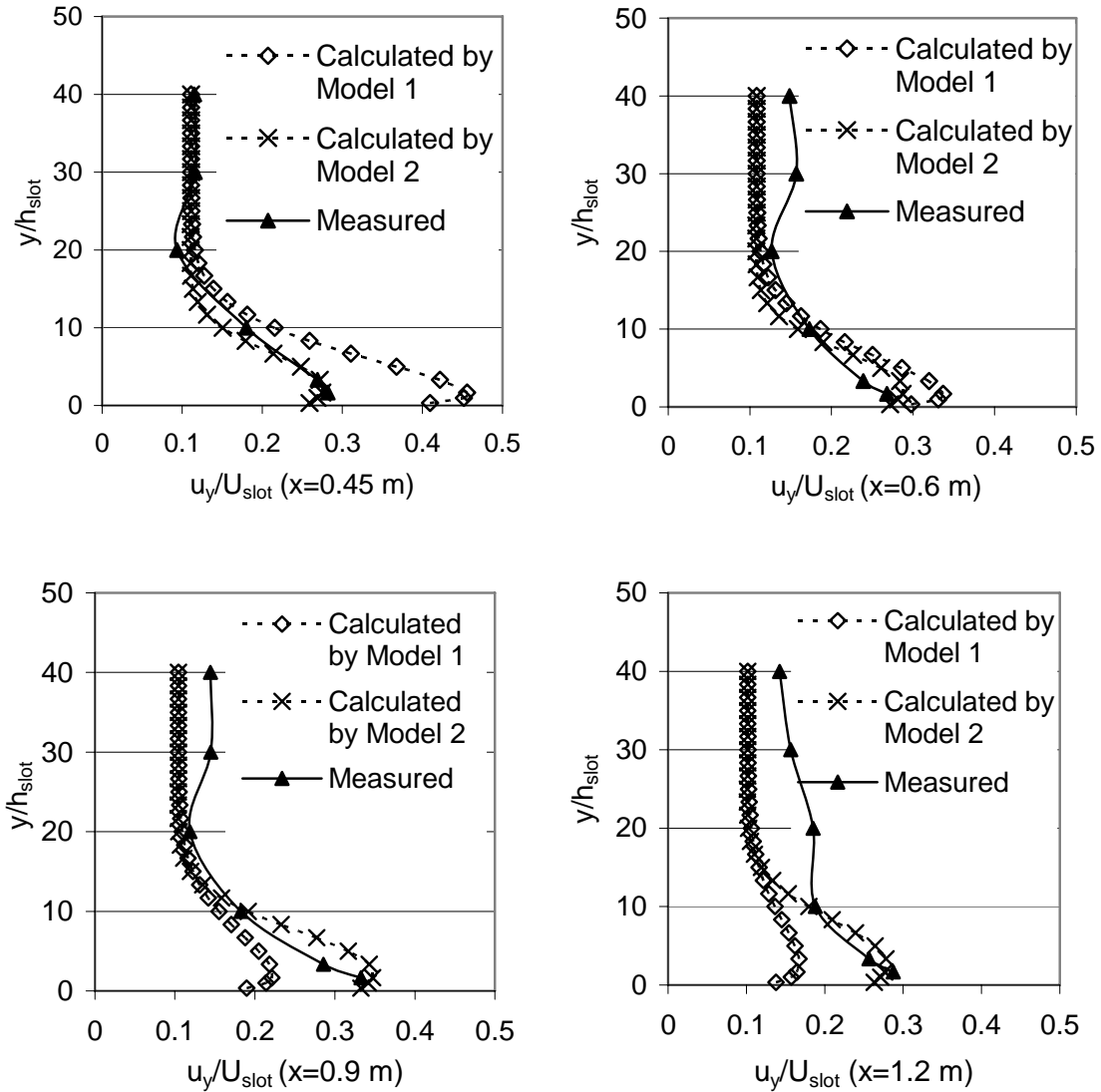
**Figure 5.12** Measured air velocity distribution in the ceiling-wall corner.

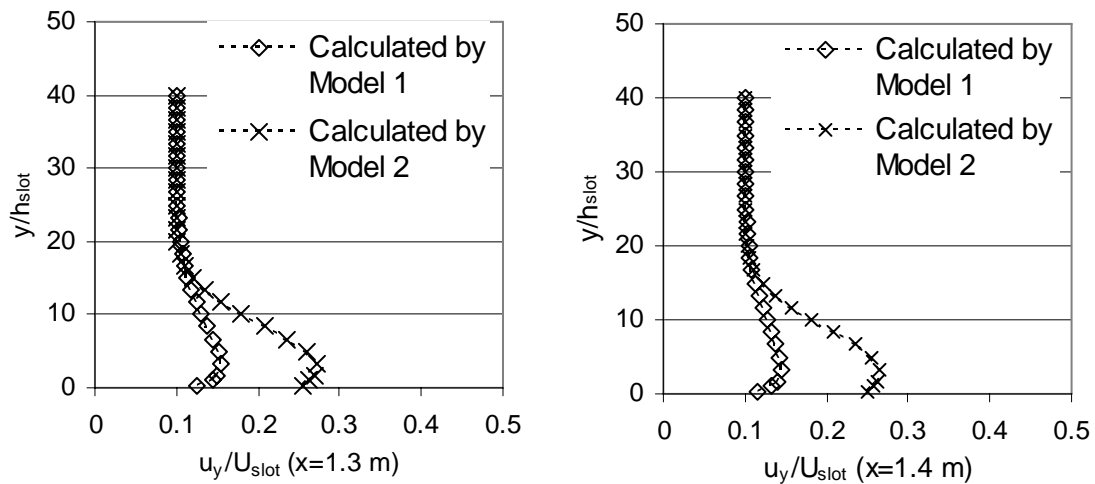


**Figure 5.13** Measured air velocity distribution in the wall-floor corner.

### 5.4.2 Calculation results

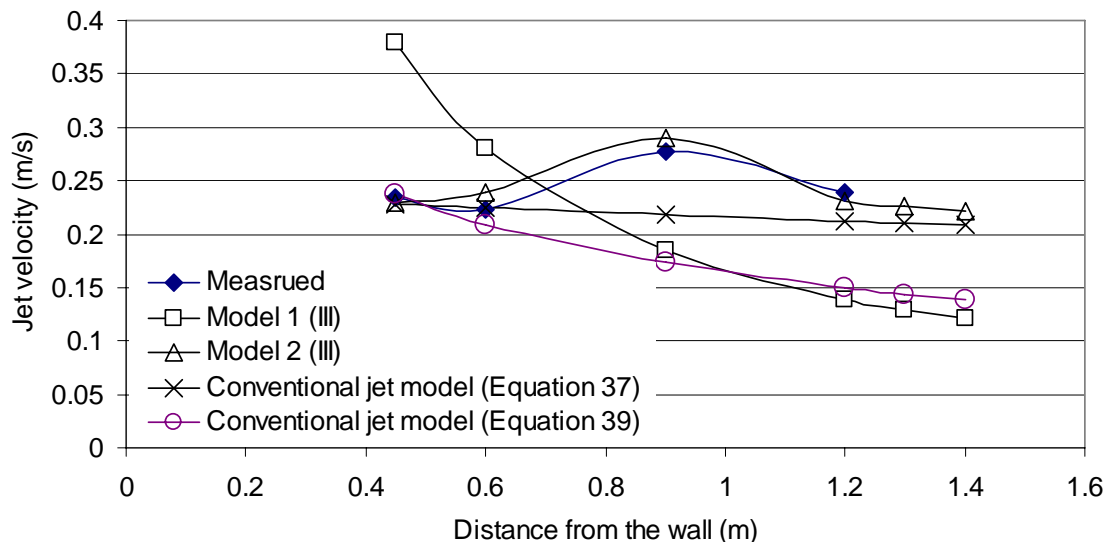
The measured and calculated results are presented in Figure 5.14 and show the performance of the Model 1, Model 2 in (II). The results illustrate that the calculated corner jet velocity profiles by both models could obtain a good agreement with the measured results at a distance of 0.9 and 1.2 m from the wall surface in the near floor region. By Model 2, the calculated maximum air velocities at different heights fitted closely to the measured results when the air jet was approaching the corner region at a height of 0.6 m from the floor.





**Figure 5.14** Measured and calculated velocity profiles in the wall-floor corner region.

The performance of the existing jet equations are presented in Figure 5.15 and show a comparison with the measured results at the floor region obtained in (II), neglecting the effect of the corner zone on the jet flow development. Except for the Model 2 set up in (II), all the other three models failed to obtain good agreement with the measured data. After two corner impingements, the measured data shows a slightly increasing trend of the jet velocity at a distance of 0.9 m from the wall. Contrastingly, most of the models predict a continuously declining trend downstream of the wall. Far beyond a distance of 1.2 m from the wall surface, Model 1 and the conventional model, Equation 39, similarly underestimate the maximum jet velocity decay. Under the same conditions, Model 2 and Equation 37 have a comparable performance at a distance of 1.2 m from the wall surface.

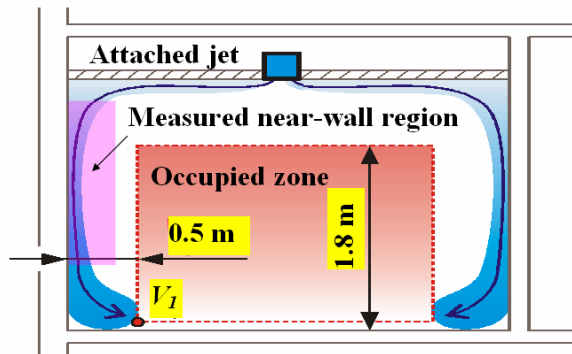


**Figure 5.15** Measured and calculated velocity profiles in wall-floor corner region.

## 5.5 Jet velocity distribution after the corner impingement

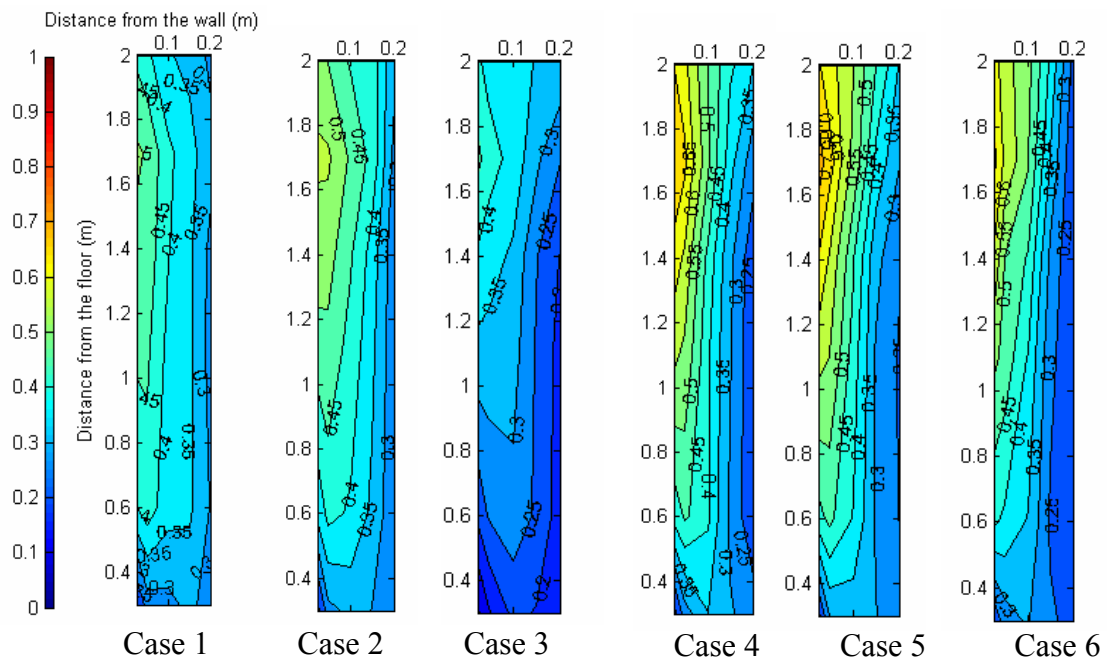
### 5.5.1 Measurement results

The near-wall region jet velocity distributions after the corner impingement were shown and discussed in (I, VI and VII). In the near-wall region studies, the jet velocity distribution with an active chilled beam was measured and modelled in the first chamber. The velocity and temperature of the attached jet were measured at six different heights and six distances from the wall in the near-wall region and the wall-floor corner region. The experiment used two airflow rates of 20 and 28 L/s with three cooling loads of 0, 40 and 100 W/m<sup>2</sup>. Figure 5.16 shows the measured region in the room equipped with the chilled beam.



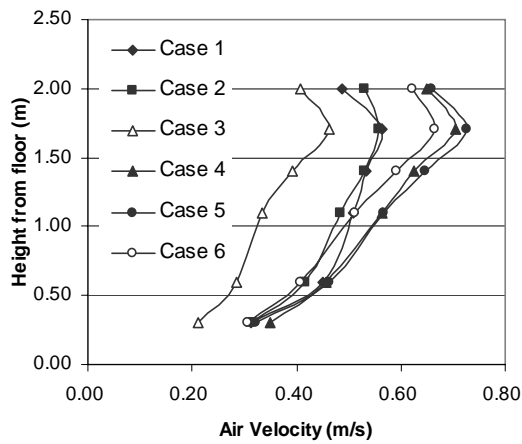
**Figure 5.16** The measured position in the near-wall region by the chilled beam.

The velocity contours are presented in Figure 5.17 and show the near-wall region air velocity distribution in six cases. With the larger airflow rate of the chilled beam, the airflow could attach to the wall surface further in both isothermal and non-isothermal cases. The corresponding air velocity is higher in the non-isothermal cases than in the isothermal ones.

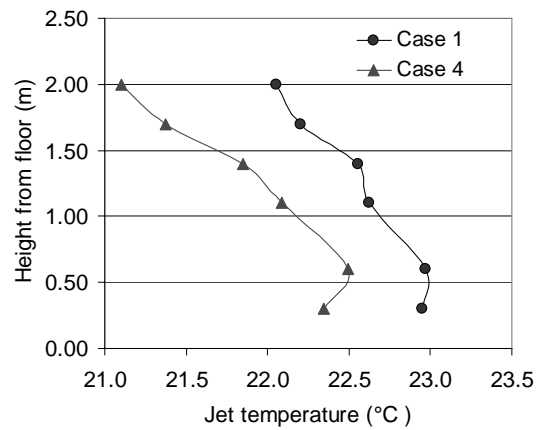


**Figure 5.17** Near-wall region air velocity distribution in six cases.

The measured maximum jet velocities are presented in Figure 5.18 and show the similar maximum velocity decay trend in six cases. It shows that in all cases the velocity increases from a height of 2.0 m to 1.7 m from the floor, and after that decreases almost linearly to a height of 0.6 m from the floor. The velocities at the heights of 2.0 and 0.3 m show the different trend compared to other points due to the corner effect. The maximum velocities occur very close to the wall surfaces, 0.025 to 0.05 m from the wall. Figure 5.19 shows the measured jet temperature in Case 1 and Case 4. In two cases the jet temperature increases quasi-linearly from a height of 2.0 m to 0.6 m from the floor. After that a slight decrease occurs from a height of 0.6 m to 0.3 m from the floor. The jet temperatures from the locations where the maximum velocities were measured are used at each measurement height. In the non-isothermal measurement, room temperatures of 23.9 and 23.5 °C, in the middle of the room at a height of 1.5 m from the floor, were used as the reference room temperature for Case 1 and Case 4, respectively.



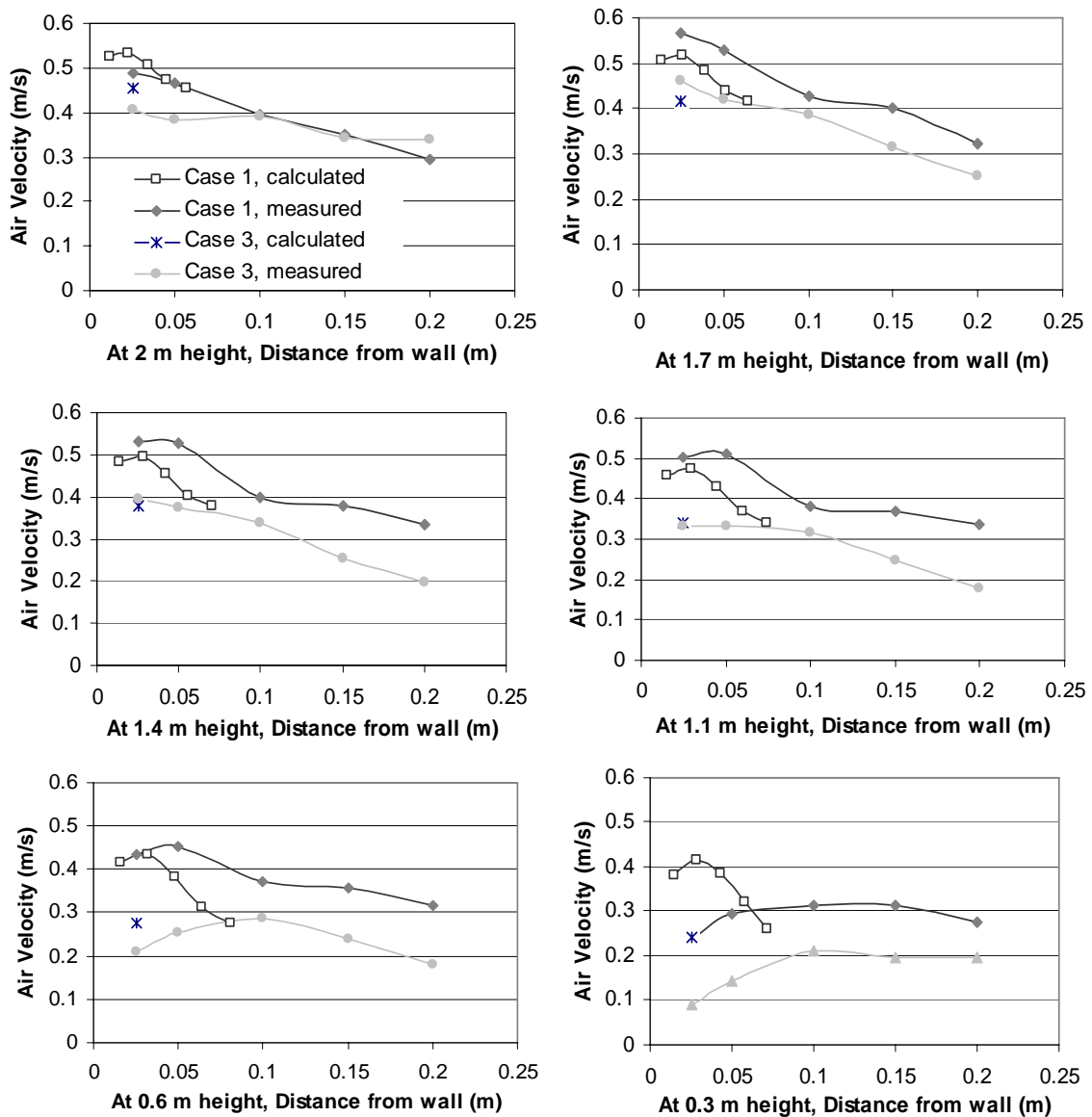
**Figure 5.18** Measured maximum air velocity in six cases.



**Figure 5.19** Measured jet temperature in two cases.

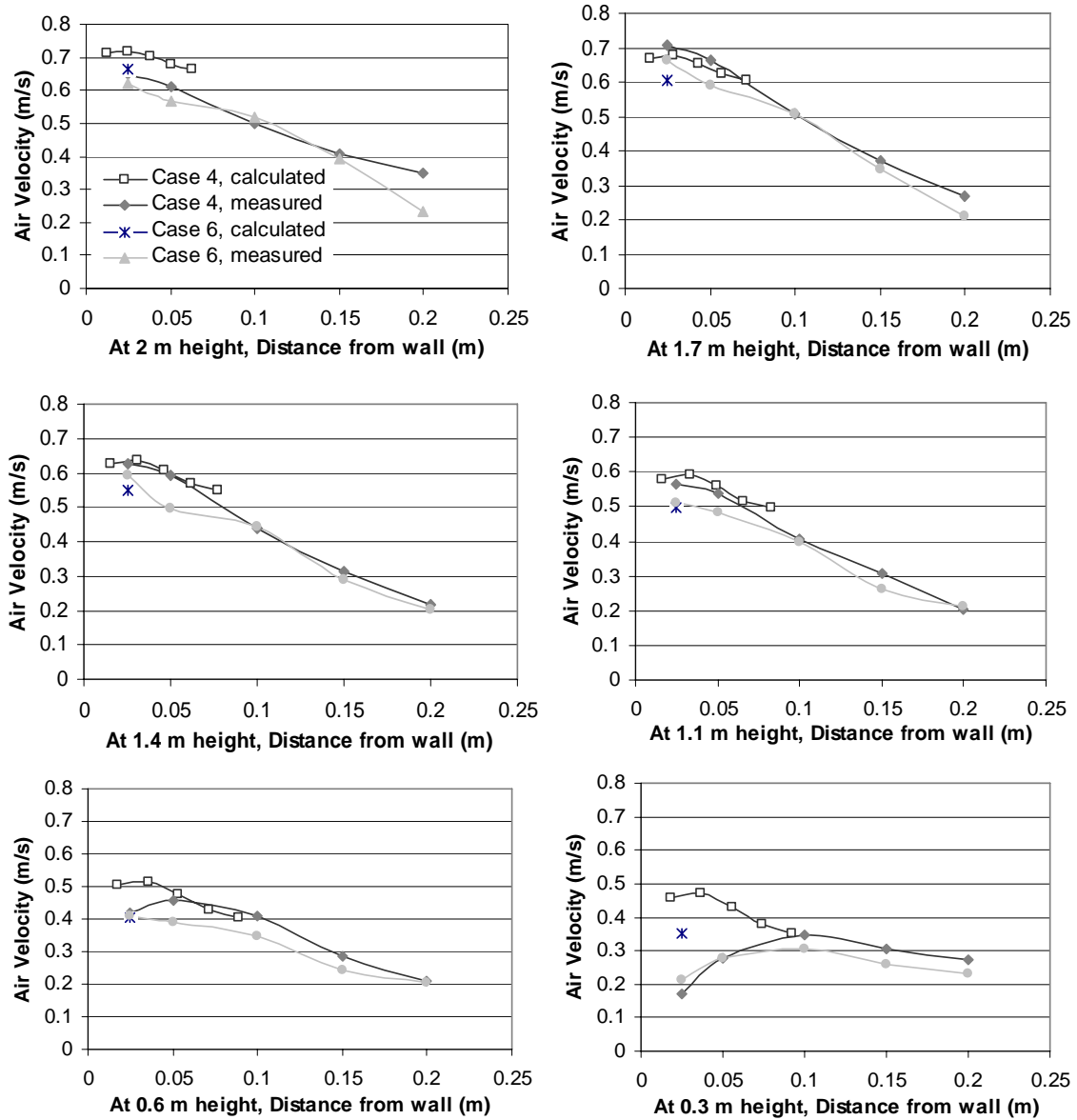
### 5.5.2 Calculation results

The measured and calculated results are presented in Figure 5.20 and show the performance of the free convection model in the near-wall region. The best agreement in maximum air velocities is at heights of 1.7 to 0.6 m from the floor. Not so good agreement at 2.0 and 0.3 m from the floor can be explained by the corner effect that is not taken into account in the free convection jet modelling. The calculated maximum air velocity is 0.53 m/s at a height of 2 m, while the measured maximum air velocity is 0.57 m/s at a height of 1.7 m.



**Figure 5.20** The calculated jet velocity by Equation 53 and the measured air jet velocity in Case 1 and Case 3.

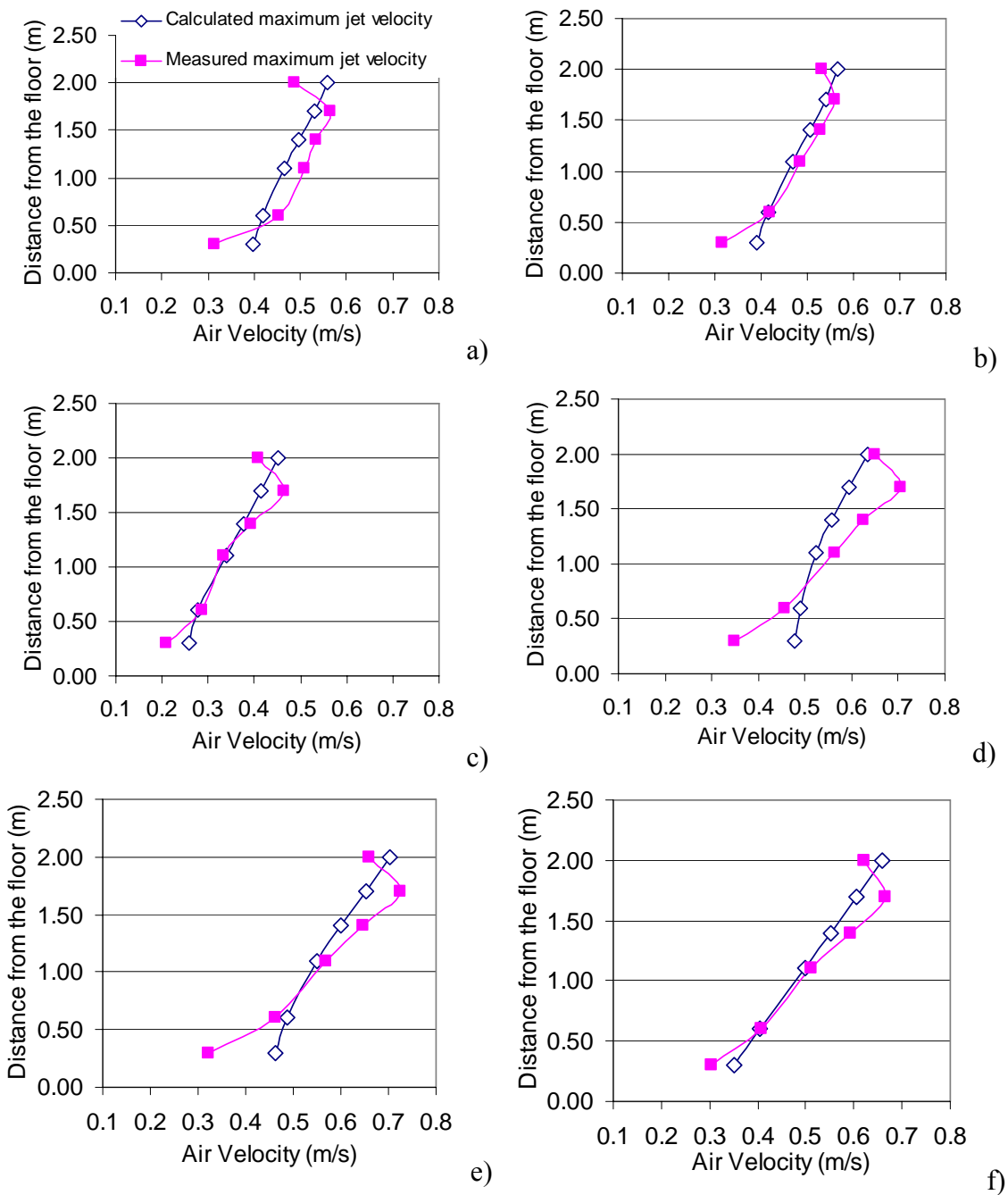
Figure 5.21 shows the results in case 4 and case 6. The agreement is very good at heights from 1.7 m to 1.1 m. The deviation is only 0.01 m/s. At 0.6 and 2.0 m from the floor, the model overestimates the velocity by about 0.04 m/s. The 0.3 m height is again beyond the range of the model.



**Figure 5.21** The calculated jet velocity by Equation 53 and the measured air jet velocity in Case 4 and Case 6.

The measured and calculated results are presented in Figure 5.22 and show the performance of the  $K$  function (VII) using the Regenscheit model. All the calculated velocity profiles feature an approximately quasi-linear decline due to the distance from floor in six cases. The linear declining trend shows a certain agreement with the measured data between 0.6 to 1.7 m from the floor. Above 1.7 m and below 0.6 m, the calculated result can not match the variation of the measured velocity. The positions beyond this region are definitely located in the upper wall-ceiling corner and the lower wall-floor corner. Considering the effect of the corner, the conventional air jet model could only predict the downward air velocity distribution with a  $K$  function.

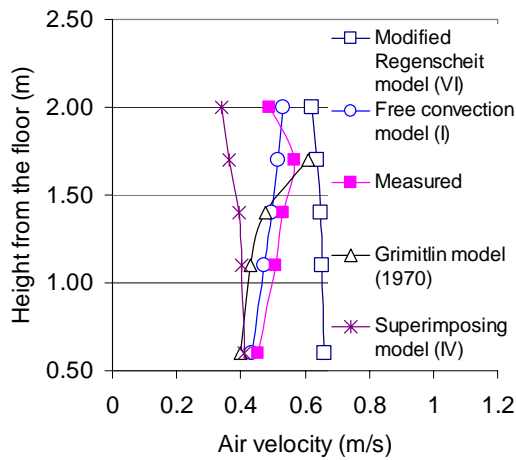




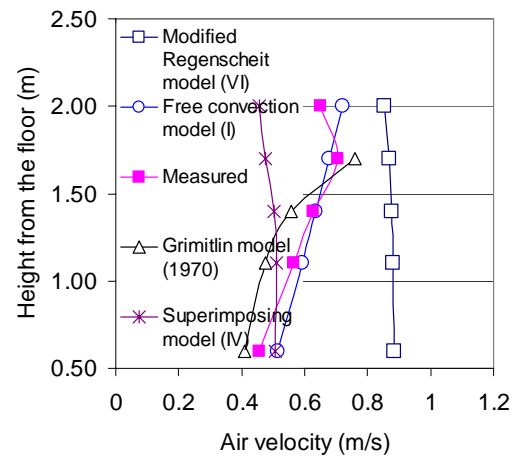
**Figure 5.22** Measured and calculated maximum velocities by a  $K$  function in six cases. a) Case 1. b) Case 2. c) Case 3. d) Case 4. e) Case 5. f) Case 6.

The calculated results are presented in Figure 5.23 and 5.24 and show a comparison with the measured data under non isothermal conditions. The presence of the corner leads to the poor performance of the chosen existing models at heights of 0.6 to 2.0 m from the floor. After the impingement of the jet flow in the corner, all the chosen models except the free convection model set up in (I) fail to predict the jet velocity decay. When the jet flow issues downward to the floor and approaches a height of 0.6 m from the floor, all the models except the modified Regenscheit model could get a good agreement with the measured data. Thus, the free convection model shows the best overall performance in this study. In addition, with various room geometries, the jet

model for the corner region jet flow, Equations 28 to 32, may be used to determine the final velocity entering the occupied zone after jet corner impingement.



**Figure 5.23** The measured and calculated results (Case 1).



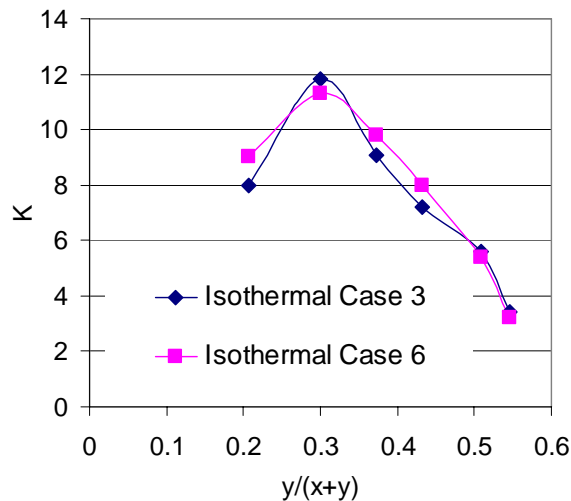
**Figure 5.24** The measured and calculated results (Case 4).

## 6 DISCUSSION

### 6.1 The limitation of the conventional jet model

In the isothermal jet studies, the conventional jet model was constructed on the basis of the jet momentum preservation from the slot. The effect of viscosity would be neglected when modelling the maximum velocity decay. The finalized jet velocity model, as presented by Rajaratnam (1976), Awbi (1991) and Hagström (1999), applied the diffuser jet dynamic characteristics coefficient which describes the intensity of the jet velocity decay along the jet. Basically, Equation 36 is for free jet velocity prediction and could still be used for the attached plane jet velocity due to the symmetry consideration with multiplying by the square root of two (I and VI). Therefore the critical point to use the conventional jet model would be the determination of the jet dynamic characteristics coefficient, the  $K$  value.

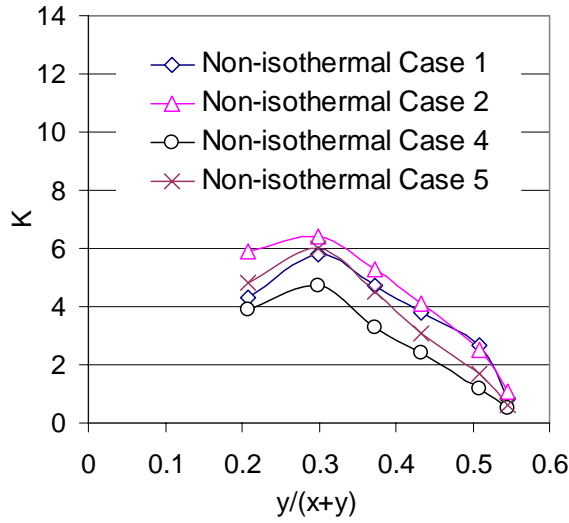
In previous studies, the  $K$  value was suggested to be a constant (Rajaratnam 1976, Awbi 1991 and Hagström 1999). However, paper (VII) states that with the same air supply device the  $K$  value is not a constant even in isothermal situations. Figure 6.1 shows the  $K$  values derived from the isothermal measured data and shows that a similar trend in the variation of the  $K$  value is shown in the two isothermal cases with different airflow rate. As shown in Figure 6.1, the airflow rate has a slight effect on the  $K$  value under two isothermal conditions. Moreover, the conventional isothermal jet model with a constant  $K$  value could not obtain agreement in the jet calculation using a chilled beam. Furthermore, the variation of the  $K$  value also resulted in the degraded performance of the conventional non-isothermal jet model, which employs a constant  $K$  value, and the conventional isothermal jet model.



**Figure 6.1**  $K$  value derived from the isothermal measured data.

In the non-isothermal cases, it was assumed in this study that the attached plane jet near the wall surface can be considered as a combination of the isothermal downward jet flow and a non-isothermal jet flow. The isothermal jet velocity may be expressed as the same as Equation 49 in (I). The non-isothermal part used the Equation 50 for the near-wall region jet velocity calculation presented by Miettinen and Aitta (1992). In earlier studies, the  $K$  value should be a constant also in the non-isothermal jet calculations (Klobut and Palonen 1992).

The  $K$  values derived from the non-isothermal measured data are presented in Figure 6.2, which shows that the  $K$  value is not a constant in all four non-isothermal cases. It is found that the  $K$  value displays a similar variation trend, increasing slightly and decreasing continuously down to the floor at different airflow rates and different cooling loads. The lowest  $K$  value was obtained in the case of the highest cooling load. The  $K$  value under non-isothermal conditions is lower than in the isothermal cases. At two supplied airflow rates, it seems that the airflow rate has less effect on the variation of the  $K$  value than the cooling load. Considering a realistic air distribution, the reason might be that air accelerates in the corner region from a horizontal ceiling to a vertical wall on which the air jet is bounded. With the non-isothermal air jet model, however, the characteristic of the square root of two results in an approximately monotonously increasing or decreasing air velocity profile. The monotonous profile with a constant  $K$  value definitely does not fit to the measured data.



**Figure 6.2**  $K$  value derived from the non-isothermal measured data.

Furthermore, the  $K$  value depends on the jet slot position and the initial velocity distribution. Thus the determination of the  $K$  value plays an important role in the prediction of the air velocity distribution. In the attached plane jet applications, forming a  $K$  function might be a choice to obtain agreement between measured and calculated results due to the effect of the room size and the air jet temperature difference on the  $K$  value. Paper (VI) shows that the conventional non-isothermal buoyancy jet equation could not predict the attached plane jet of the active chilled beam. The calculated results fitted the measured data well using a new  $K$  function in (VII), which is defined as:

$$K^* = C_0 + C_1 K^{**} \quad (66)$$

where  $C_0$  and  $C_1$  are constants, and  $K^{**}$  is defined as:

$$K^{**} = \frac{1}{1 + \text{EXP}(-(a_0 + a_1 K + a_2 y^* + a_3 T^*))} \quad (67)$$

where  $a_i$  ( $i=0,1,2,3$ ) is a calculation constant,  $y^* = y/H$  is the room size character factor,  $y$  is the vertical distance from the initial point,  $H$  is the room height,  $T^* = (T_\infty - T_s)/T_\infty$  is the temperature character factor,  $T_s$  is the supply air temperature and  $T_\infty$  is the ambient temperature. By measured data of case 1 and case 3, parameters  $a_0$ ,  $a_1$ ,  $a_2$  and  $a_3$  in Equation 66 and 67 were found to be 0.122, -0.336, 3.54 and 39.1, respectively;  $C_0$  and  $C_1$  are 11.4 and -10.3, respectively.

In the results section, Figure 5.22 already showed the improvement of the conventional Regenscheit model using the  $K$  function. The most attractive part of the model may be the validation of the model by the new measured data obtained from the first chamber. However, as for a new ventilated condition, the capabilities of the  $K$  function to improve the model to predict the velocity distribution is still not clear and definitely need more measured data and further research.

On the other hand, the initial condition of the attached plane jet depends on the design of the jet diffuser. The dynamic characteristics of the jet vary with the type of jet diffusers. Therefore the conventional jet model could not directly be used to predict the

jet velocity of the chilled beam in a room. The application of the conventional jet model for prediction of the maximum jet velocity should include identification of the dynamic characteristics of the jet.

## 6.2 The attached plane jet thickness

An attached plane jet is produced when the flow is bound by the wall on one side and the flow direction at the exit from the opening is parallel to the surface. Firstly, the air jet produced by the air diffuser was considered as laminar flow in the Reynolds number analysis. In laminar flow studies, almost one hundred years ago Blasius found a celebrated solution for laminar-boundary-layer flow. From the similarity solution of the laminar-boundary layer, a value of 99% boundary layer thickness is obtained as (White 2006):

$$\delta_{99\%} \approx 3.5 \sqrt{\frac{2\nu x}{U}} \quad (68)$$

where  $U$  is the average air-jet velocity at the jet slot,  $\nu$  is the kinematic viscosity of the fluid, and  $x$  is the distance from the position of the jet slot.

Poreh et al. (1967) studied the maximum velocity  $U_m$  of an impinging jet; beyond that they formulated an equation for the wall-jet boundary layer thickness as:

$$\frac{\delta}{b} = 0.098 \left( \frac{r}{b} \right)^{0.9} \quad (69)$$

Paper (III) studied the jet thickness by attached plane jet experiments. As shown in the jet visualization results, the jet volume flow grows by entraining the ambient air when leaving the jet slot. The variation of the boundary-layer thickness with distance has been presented earlier by Schwarz and Cosart (1961) to be proportional to the distance from the virtual origin. The correlation may be written as:

$$y_{1/2} = C_2 (x + x_0) \quad (70)$$

where  $C_2$  is a parameter that should be determined by test, and the averaged  $C_2$  is given by experimental results as 0.0678 at Reynolds numbers varying from 13000 to 41000 in the experiment. With experimental results in a three-dimensional turbulent wall jet, Rajaratnam and Pani (1974) reported the half-width  $y_{1/2}$  linear variation as:

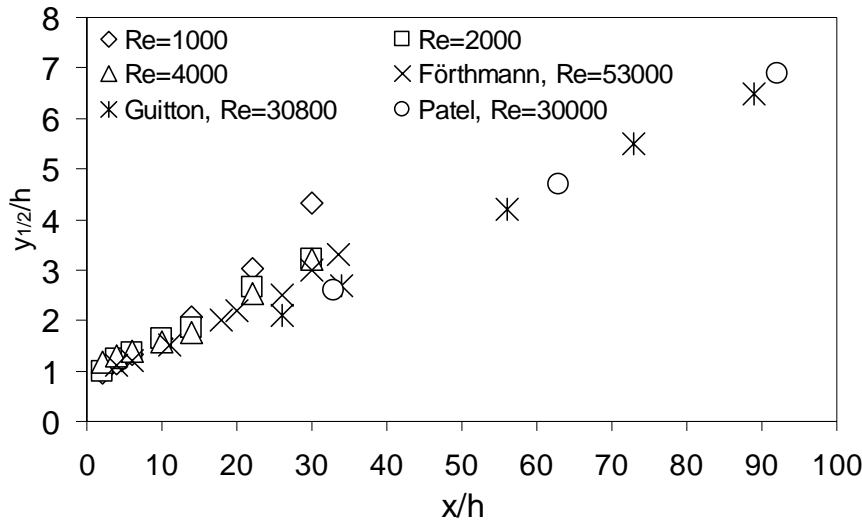
$$\frac{y_{1/2}}{h} = 0.9 + 0.045 \frac{x}{h} \quad (71)$$

The relationship in Equation 71 reveals that the virtual origin is located about 20 slot heights behind the nozzle. In addition, Launder and Rodi (1981) obtained the jet growth rate for the turbulent attached plane jet as:

$$\frac{dy_{1/2}}{dx} = 0.073 \pm 0.002 \quad (72)$$

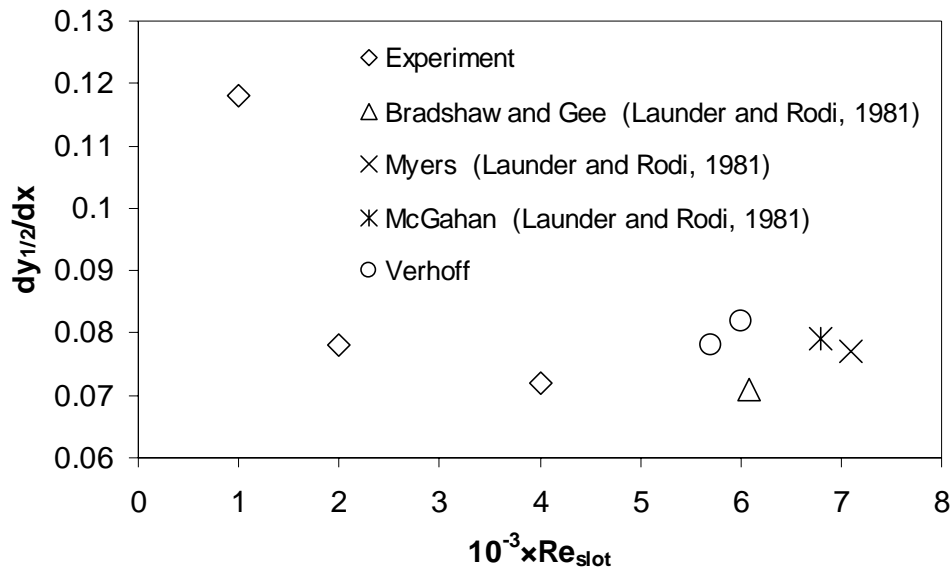
For a turbulent attached plane jet, Topp and Nielsen (2000) derived a linear form of the maximum velocity decay as the same as Equation 70.

Figure 6.3 shows the growth of the half-width of the attached plane jet in both lower Reynolds number and higher Reynolds number jet flow. It shows that the growth of the jet half-width with a lower Reynolds number is faster than with a higher Reynolds number jet. In particular, the attached jet with the lowest Reynolds number presents the largest difference compared with other Reynolds number jets.



**Figure 6.3** Attached plane jet thickness growth in stagnant surroundings.

Figure 6.4 shows the dimensionless spreading rate defined in terms of the jet half-width plotted against the slot Reynolds number. The figure shows that the spreading of the jet is significantly influenced by the low frequency oscillations of the jet caused by shear layer instability. The reason might be that large vortices are formed in the shear layers at the fundamental frequency of the instability, which leads to sub-harmonic low frequency oscillations due to vortex pairing and merger at larger axial distances (Hsiao and Sheu 1994). Consequently, the far-field flow structure of a low Reynolds jet is dominated by large vortices which give rise to a higher level of flow intermittency, larger entrainment of ambient fluid, and faster jet decay, as compared to the high Reynolds number turbulent jets.



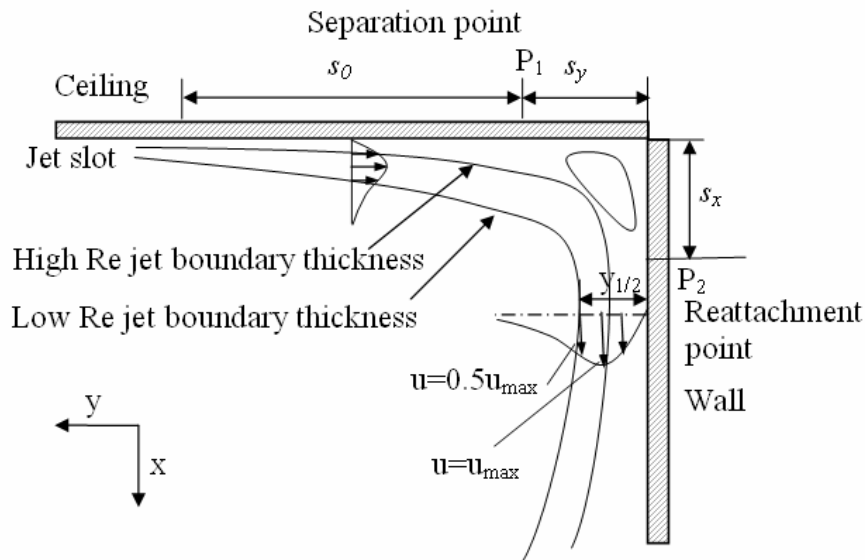
**Figure 6.4** Dependence of the jet thickness growth rate on the Reynolds number.

In the earlier studies, Suresh et al. (2008) also observed that for low Reynolds numbers  $Re < 2000$ , characteristics such as velocity profiles, turbulence intensities, maximum velocity decay, and length scales are strong functions of the Reynolds number and axial distance. At high Reynolds numbers, the state of turbulence becomes independent of inlet Reynolds number and axial distance, in the far field. For the transitional Reynolds number regime studied here, the overall spread rate of the jet is also strongly influenced by the Reynolds number because of changes in the eddy formation and interaction processes.

Figure 6.4 shows that the jet spreading rate for all these cases falls within the range of Equation 73 for Reynolds numbers 2000 to 8000, which is slightly wider than the range defined by Equation 72. Equation 73 takes the expression as:

$$\frac{dy_{1/2}}{dx} = 0.075 \pm 0.003 \quad (73)$$

Compared with the spread rate of the higher Reynolds number jet reported by Launder and Rodi (1981 and 1983), the spread rate of the low Reynolds number attached plane jet varies in a wider range. The unsteadiness of the attached plane jet may contribute to the difference between different experiments. The jet flow pattern is presented in Figure 6.5 and shows the jet boundary thickness variation approaching the corner. Due to the different Reynolds number, Figure 6.5 indicates that the jet boundary thickness grows in a different way to the measured results shown in Figure 6.3 and Figure 6.4. A jet at a relatively low Reynolds number may entrain more ambient air into the jet, thus resulting in the different behaviour from the high Reynolds number jet. The different jet development characteristics may also require identification of the jet flow pattern from a different jet slot in practical jet applications. Therefore, in jet modelling the jet velocity model should be validated at different jet Reynolds numbers.



**Figure 6.5** The jet boundary thickness variation approaching the corner.

### 6.3 The corner effect on jet flow

In a ventilated space, the room geometry poses an unavoidable difficulty in the jet velocity distribution. The corner situation might be one of the most common disturbance conditions for the jet flow. Paper (VI) shows that the conventional non-isothermal jet equation could not predict the attached plane jet produced by an active chilled beam after turning at the corner. In (VII) the  $K$  function is derived to compensate the non-isothermal jet model. To improve the performance of the jet equation with an attached jet, Paper (II) studied the corner effect on the jet flow. It was found that to avoid the lower corner effect the calculation should be stopped at a height of 0.60 m from the floor with the models described in (I) and (VII). Under the experimental conditions, the velocity at 0.60 m from the floor may be used as an estimate of the velocity entering the occupied region (I). With various room geometries, Equations 28 to 32 should be used to determine the final velocity entering the occupied zone after the jet impingement in the corner region.

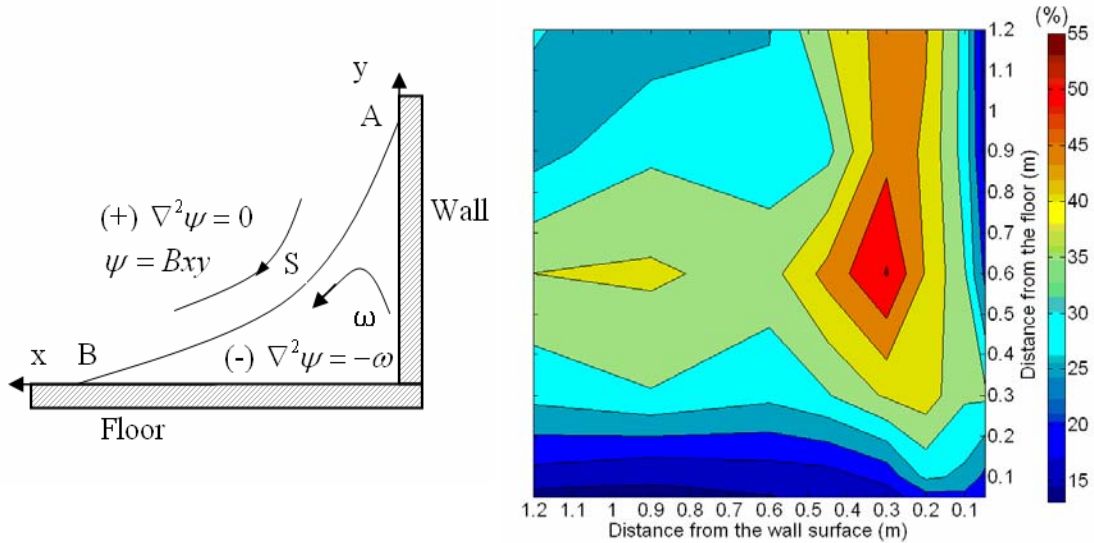
In (II), the returning corner jet model is constructed to estimate the air velocity distribution affected by the wall-floor corner. Based on the experimental results in (II), the air velocity profile performs the similarity characteristic in the near-wall region and the near-floor region at the wall-floor corner. The corner contains a non-zero vorticity region, which occurs similarly in stagnation-point flow as well (White 2006).

Figure 6.6 shows the airflow configuration in the non-zero vortex corner. On the boundary of the non-zero vorticity region, Moore et al. (1988) pointed out that a vortex sheet separates an irrotational '+' region from a region '-' of uniform vorticity  $\omega$  (in). McLachlan (1991) also presented the closed streamline characteristic of an incompressible fluid with low viscosity in a corner region.

The measured turbulence intensity distribution is presented in Figure 6.7 and shows that the turbulence intensity changes in a way similar to that of the mean air velocity as a



symmetrical distribution in a corner region. Especially the contour of 30% turbulence intensity could get a good agreement with the air velocity contour of 0.20-0.25 m/s.



**Figure 6.6** Illustration of the rotational corner flow. **Figure 6.7** Measured corner airflow turbulence intensity.

#### 6.4 Jet potential core

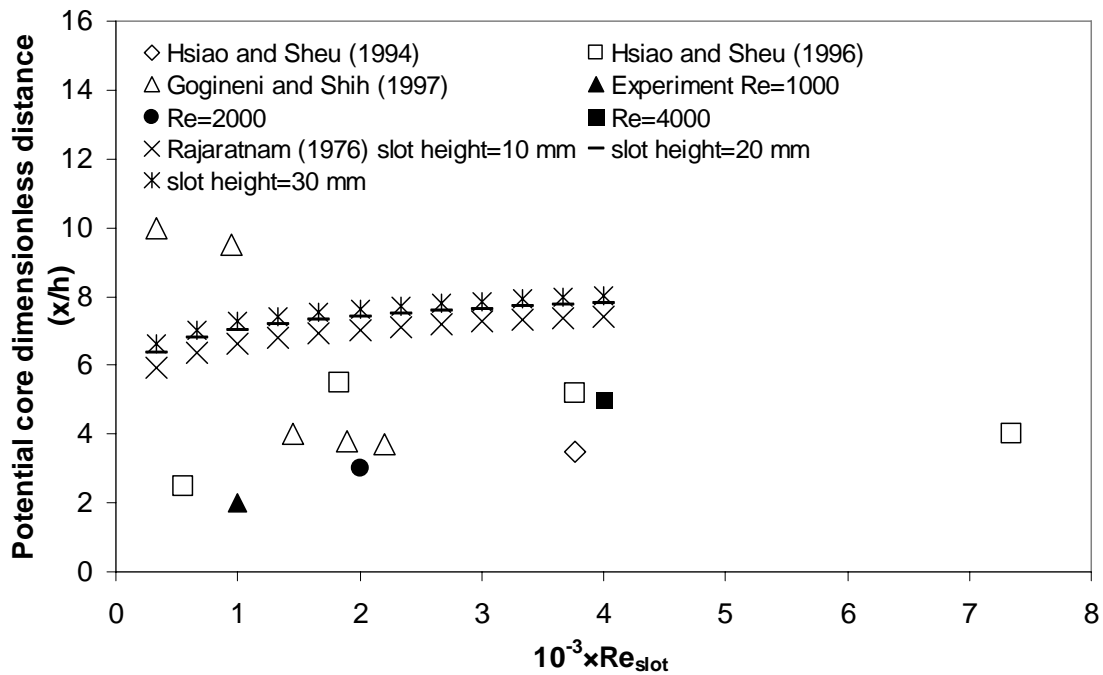
In the starting region of the jet, the potential core has been studied for many decades; Papers (III and IV) were striving to reveal the process by which the jet's potential core develops. With regards to the length of the jet's potential core, Rajaratnam (1976) assumed that the velocity distribution in the boundary layer follows the one-seventh power law; the rate of growth of  $\delta$  is given by the expression:

$$\frac{\delta}{x_0} = \frac{0.37}{(U_0 h / \nu)^{1/5}} \quad (74)$$

where  $\delta$  is the boundary layer thickness,  $x_0$  is the length of the potential core,  $U_0$  is the jet exit velocity,  $h$  is the jet slot height and  $\nu$  is the kinematic fluid viscosity. Then the potential core equation was deduced to estimate the length of the potential core as:

$$0.0875 \frac{x_0}{h} + 0.37 \left( \frac{x_0}{h} \right)^{4/5} \frac{1}{(U_0 h / \nu)^{1/5}} = 1.0 \quad (75)$$

A Fortran program was used to calculate the potential cores in the case of a 10 mm jet slot height. The calculated results were compared with the data from previous studies as well as and the measured data in Figure 6.8. Figure 6.8 shows the dimensionless distance of the jet's potential core versus the Reynolds number. The length of the potential core in the measurement was selected by setting the constant jet velocity to approximately  $0.99U_0$ .



**Figure 6.8** Dependence of the jet's potential core on the Reynolds number.

The calculated potential core length by the Rajaratnam (1976) equation displays longer values than others, except two points by Gogineni and Shih (1997). In the case of the Reynolds number 4000, the measured data obtains a good agreement with that of Hsiao and Sheu (1994 and 1996). When the Reynolds number is lower than 4000, the measured potential cores were shorter than the results found in the literature. Therefore, the length of the jet's potential core depends mostly on the jet's initial Reynolds number. At a low turbulent intensity level, the potential core regions are compared in Table 6.1 using different initial Reynolds numbers. Table 6.1 shows that the potential core regions differ from each other significantly at different initial Reynolds numbers even at a very low turbulent intensity level. In addition to the Reynolds number, the jet slot characteristics, including the aspect ratio and the profile of the jet slot velocity, might also result in the difference of the length of the potential core. As for the jet application in a room, the length of the potential core will definitely affect the jet transitional process and the modelling of the jet velocity in the fully developed region.

**Table 6.1** Summary of the jet's potential core at low Reynolds numbers.

Reference	Re <sub>s</sub>	Jet height (mm)	Potential core region (x/h)	Aspect ratio	Remarks
Hsiao and Sheu (1994)	3770	11	<3	27	Turbulence intensity <0.5%
Shih and Gogineni (1995)	1000	5	<12	20	PIV, turbulence intensity 0.3%
	1000		<3		
Hsiao and Sheu (1996)	550	2.7~14.7	<2.5	20-111	Turbulence intensity <0.7%
	1830		<5.5		
	3770		<5.2		
	7350		<4		
Gogineni and Shih (1997)	330	5	<11	20	PIV technology
	950		<9.5		
	1450		<4		
	1900		<3.8		
	2200		<3.7		
	3800		<1		
Levin et al. (2005)	3080	3	<4.33	166	Turbulence level <0.05%

### 6.5 The buoyant jet regions and self similarity

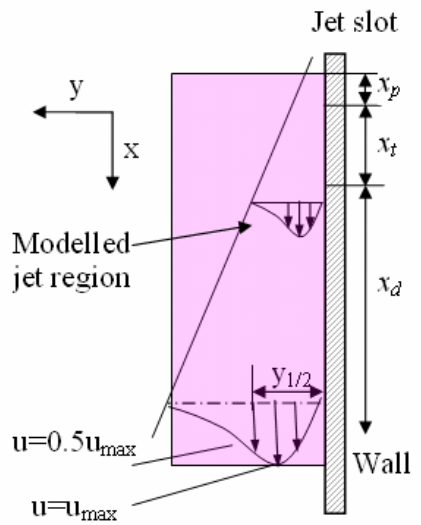
By the three-region definition of the buoyant jet structure, present studies could not specify the distinguishing points that separate the buoyant jet regions. Paper (IV) dealt with the clarification of the different characteristic in each jet flow regions. At different jet slot velocities, the inner layer, which is attached to the wall surface, could be observed below the maximum jet velocity line in (III) and (IV). The measurement results showed that the intermediate region of the buoyant jet does exist when the inner layer extends downstream of the jet slot. The furthest distance that the inner layer extended is approximately 500, 1500 and 2500 mm corresponding to average slot velocities of 0.50, 1.00 and 2.00 m/s, respectively. The observation of the extended inner layer confirms that the initial momentum flux and the buoyancy flux are of comparable importance in the intermediate region (So and Aksoy 1993).

As defined by Chen and Rodi (1980) and So and Aksoy (1993), if the relative influence of the momentum and the buoyancy is used as the critical criteria to classify the jet regions, the non-buoyant region refers to the situation in which the momentum completely dominates the jet behaviour. Abdulhadi and Pedersen (1971) and Quintana et al. (1997) already confirmed that the buoyant jet has the characteristics of self-similarity within a distance of 12 to 50 slot heights downstream of the jet slot. However, the self-similarity characteristics of the attached buoyant jet could not guarantee a similar modelling process in the jet application in the room (I-V). Figure 6.9 and 6.10 show the different jet development processes in the attached jet application. The difference of the jet flow development process needs corresponding considerations in the jet modelling.

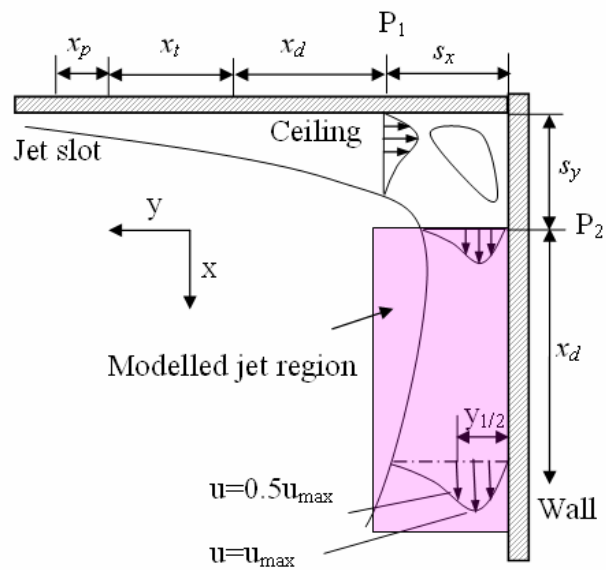
Figure 6.9 displays the general downward attached jet development pattern. In isothermal conditions, the jet velocity could be modelled by the conception of the two-zone jet division: the developing zone and developed zone (III). Other present studies show that the characteristics of the jet flow development are dependent on the Reynolds number, especially when the Reynolds number is smaller than 6250 (Suresh et al. 2008). As shown in Figure 6.9, the jet's potential core is followed by the jet transitional region and the fully developed region.

Contrastingly, the buoyant jet may include three regions: the non-buoyant region, the intermediate region, also called the transitional region, and the buoyant region in the straight downward attached jet flow. An earlier study showed that the non-buoyancy region refers to the same region as a jet's 'starting length' (Chen and Rodi 1980). Basically, the jets in a quiescent ambient can be classified according to the relative importance of the initial momentum flux and the initial specific buoyancy flux (So and Aksoy 1993). In addition, it has been found that the relative influence of inertia and buoyancy forces resolves the stratified flow characteristics in a room (Awad et al. 2008). With respect to the buoyant jet modelling, Paper (IV) shows the superimposing method to resolve the effect of the buoyant force and gravitational force on the jet's downward behaviours. The superimposing model directly deals with the downward jet issuing from the jet slot by the concept of the virtual origin and the three-jet-region division. This method may contribute to the downward jet modelling, in which the jet's virtual origin needs identification.

Figure 6.10 illustrates the jet development pattern with the effect of a corner. Papers (I) and (II) proved the fact that the jet flow in the corner region needs a special modelling process. The corner jet model was derived in (II) and validated by measurement results. In Paper (I), it is assumed that the attached jet near the vertical wall surface can be treated as a combination of the isothermal downward air jet flow and the free convection flow. Unlike the straight downward jet flow pattern shown in Figure 6.9, in which the buoyant force always acts in the same direction as the gravitational force (in cooling cases), the near-wall region jet flow pattern in Figure 6.10 depends significantly on the upstream jet flow pattern before the jet turns at the corner. The horizontal jet flow is influenced by the gravitational force, which acts perpendicularly to the attached jet flow. When the jet reattaches to the wall surface, the jet flow may be considered as a mix of the turning jet and the free convection flow (I). Therefore, near-wall jet velocity modelling differs from conventional vertical jet modelling (I and IV).



$x_p$  Jet potential core distance  
 $x_t$  Jet transitional region distance  
 $x_d$  Jet fully developed region distance



**Figure 6.9** Jet regions modelled in the downward attached jet flow. **Figure 6.10** Jet regions modelled in the turning downward attached jet flow.

In the buoyant jet cases, the measured data indicates that the distance of the non-buoyant region might be proportional to the slot Reynolds number and inversely proportional to the initial Archimedes number. Moreover, the maximum velocity in the non-buoyant region could be calculated by the isothermal jet equation within this region. Beyond this region, in the intermediate region, the superimposing model could be applied to predict the maximum velocity decay in the downstream jet flow field (IV).

The superimposing model was validated with measured data at velocities of 0.5, 1.0 and 2.0 m/s. However, at the beginning of the jet flow and after 2.0 m downstream of the slot, the difference between the calculated results and the measured data can still be seen. The different characteristics of the three buoyant jet regions might contribute to the difference. Moreover, the size and the details of the jet outlet may also result in the error between the predicted results and the measured results. As explained by Malmström (1996), the jet outlet can influence the velocities and the temperatures in the resulting jet through three different mechanisms: initial jet momentum, jet spread and the form of temperature profile.

## 7 CONCLUSIONS

The turbulent attached plane jet may be applied in ventilated and air-conditioned spaces to create a draught-free indoor environment. However, the measured data shows that the existing jet model could not be used to predict the velocity decay of the attached plane jet in a room with the corner effect. This study was carried out to improve the existing modelling and calculation method applied to predict the jet velocity in both ventilated and air-conditioned rooms.

In this study, it was identified that the draught model is originally validated for a horizontal back flow for sedentary activities at a thermal sensation close to neutral. The limitation of the model is that the impact of large-scale velocity fluctuations, the airflow direction, the frequency of jet fluctuation and the exposure duration of the occupant may not be evaluated by the model. Moreover, in (V) and (VIII), it was shown that the most critical situation for the sensation of a draught is when the flow is from behind at neck level. Those velocities from the front that caused the same sensation as a flow from the back were about 1.5 times higher (V). Considering the effect of the draught location, the literature review showed that about 1.5 times higher velocities at ankle level, compared to neck level, will cause the same draft sensations in (VIII).

Before jet impingement in the corner, it was found the turbulent attached plane jet will become turbulent in a very short distance, e.g. at 2 slot heights downstream of the jet slot in (III). In addition, the turbulent attached plane jet was found to show the self-similarity characteristic earlier than the previous studies. The potential core exists in the attached plane jet and extends to 2-5 slot heights downstream of the jet slot. However, the measured potential core is shorter than the earlier results. As for the jet modelling, the similarity exponents of the maximum velocity in the two models (III), -0.5 and -0.48, could be used to predict the maximum velocity decay after a distance of 30 slot heights downstream of the jet slot in the developed region.

In the downward origin jet, the distance of each jet region could be dependent on the initial conditions, including the slot Reynolds number and the initial Archimedes number (IV). At different jet slot velocities, the inner layer which is attached to the wall surface could be observed below the maximum jet velocity line. The superimposing model in (IV) could predict the maximum velocity decay beyond the non-buoyant region in the range of 667-4000 Reynolds numbers based on the jet slot height and the jet slot velocity. The velocity profile displays self similarity characteristics like an isothermal turbulent attached jet at the point of 1.00 m from the slot. The profile with a 2 m/s slot velocity fits the theoretical profile very well. To specify the starting point of the buoyant region, more detailed measurement results may be needed.

The measurement results indicate that the modelling of the impingement jet should be carried out for prediction of the downward near-wall region jet velocity. With the corner effect, the turning jet models were set up in (I) and (II) to predict the jet velocity decay after impingement in the ceiling-wall corner and the wall-floor corner. The jet velocity distribution was studied in (II) by modelling and experiments. It was revealed that the turning air jet reattaches to the floor surface with entrained ambient air after impingement in the corner; at the same time, the rest of the air at low speed in the ventilated room does enforce the free shear at the free boundary of the attached jet (II).

The non-zero vorticity region model set up in (II) could predict the jet separation point and reattachment point in the jet impingement region. The calculated and measured results show the corner-jet velocity profiles by the corner models obtain satisfactory agreement with the measured data in (II).

By using the horizontal jet in the first chamber, the measurement results showed that the jet velocity decreases almost linearly when the jet turns down along the wall surface at the ceiling-wall corner in (I). The free convection model was able to predict the maximum jet velocity along the wall surface with good accuracy at a height of 0.60 to 2.00 m from the floor. The velocity distribution was almost symmetric in the corner and, thus, it was reasonable to stop the calculation at a height of 0.60 m. Under the experimental conditions, the velocity at a height of 0.60 m may be used as a reasonable estimate of the velocity on the floor when the airflow enters the occupied region at 0.60 m away from the wall (I). With various room geometries, Equations 28 to 32 should be used for determination of the final velocity entering the occupied zone after jet impingement in the corner region.

The models validated in this study provide a solid basis for comprehensive and systematic indoor airflow design using the attached plane jet. In different jet regions of the attached plane jet, the corresponding model can be used directly to predict the jet velocity distribution. In addition, the models can be used to select the airflow rate for linear slot diffusers, to design the initial supply air velocity and to determine the final air velocity entering the occupied zone. The data obtained in the work could be used to validate the corresponding CFD simulation for further attached plane jet product development. The superimposing model established here could be used as the practical one-equation method to predict the maximum jet velocity decay in the preliminary stage of product development, and in room air distribution design especially by attached plane jet application, i.e. the chilled beam. The data and the models specified in this study could be applied to improve the accuracy of the calculation by CFD software in the study of indoor airflow.

## REFERENCES

- Abdulhadi, R. and Pedersen, C. O. (1971). The behavior of a downward-directed heated wall jet. ASHRAE Transactions, Vol. 77(2), pp:222-229.
- Abrahamsson, H. (1997). On turbulent wall jets. PhD thesis, Department of Thermo and Fluid Dynamics, Chalmers University of Technology, Göteborg, Sweden.
- Abramovich, G.N. (1948). Turbulent free jets of liquids and gases. Moscow: Gosenergoizdat.
- Alamdari, F., Butler, D. J. G., Grigg, P. F. and Shaw, M. R. (1998). Chilled Ceilings and Displacement Ventilation. Renewable Energy, Vol. 15, pp:300-305.
- Albright, L. D. and Scott, N. R. (1974). The low-speed non-isothermal wall jet. J. Agric. Engng Res. Vol. 19, pp:25-34.
- ASHRAE (2004). ANSI/ASHRAE Standard 55-2004, Thermal Environmental Conditions for Human Occupancy. Atlanta: American Society of Heating, Refrigerating, and Air-conditioning Engineers, Inc.
- Awbi, H. B. (1991). Ventilation of Buildings. E& FN SPON, total pages 313.
- Awbi, H. B. and Hatton, A. (1999). Natural convection from heated room surfaces. Energy and Buildings, Vol. 30, pp:233-244.
- Awbi, H. B. and Hatton, A. (2000). Mixed convection from heated room surfaces. Energy and Buildings, Vol. 32(2), pp:153-166.
- Bajura, R. A. and Szweczyk, A. A. (1970). Experimental investigation of a laminar two-dimensional attached plane jet. Phys Fluids, Vol. 13(7), pp:1653-166.
- Ballestini, G., Carli, M. D., Masiero, N. and Tombol, G. (2005). Possibilities and limitations of natural ventilation in restored industrial archaeology buildings with a double-skin facade in Mediterranean climates. Building and Environment, Vol. 40, pp:983-995.
- Barenblatt, G. I., Chorin, A. J. and Prostokishin, V. M. (2005). The turbulent wall jet: A triple-layered structure and incomplete similarity. Proc Natl Acad Sci U S A. Vol. 102(25), pp:8850-8853.
- Cao, G.Y., Kurnitski, J. and Seppänen, O. (2008). Effect of occupant thermal plume on air flow pattern and temperature distribution in an office room. In: Proceedings of Indoor Air 2008, Copenhagen, Denmark, August 17-22, 2008.
- Chen, J. C. and Rodi, W. (1980). Turbulent buoyant jets-A review of experimental data. HMT, Pergamon, London, 4.
- Costelloe, B. and Finn, D. (2003). Indirect evaporative cooling potential in air-water systems in temperate climates. Energy and Buildings, Vol. 35(6), pp:573-591.
- DIN4715-1. (1995). Chilled surfaces for rooms-Part 1: Measuring of the performance with free flow – Test rules, November 1995.



- EN 13779:2007. (2007). Ventilation for non-residential buildings-Performance requirements for ventilation and room-conditioning systems. European Committee for Standardization, Brussels.
- EN 13182:2002. (2002). Ventilation for buildings. Instrumentation requirements for air velocity measurements in ventilated spaces. European Committee for Standardization, Brussels.
- Fanger, P. O. (1970). Thermal comfort. Copenhagen: Danish Technical Press.
- Fanger, P. O. and Christensen, N. K. (1986). Perception of draught in ventilated spaces. *Ergonomics*, Vol. 29, pp:215-235.
- Fanger, P. O., Melikov, A. K., Hanzawa, H. and Ring, J. (1988). Air turbulence and sensation of draught. *Energy and Buildings*, Vol. 12, pp:21-39.
- Faulkner, D., Fiski, W. J., Sullivan, D. P. and Wyon, D. P. (1999). Ventilation efficiencies of desk-mounted task/ambient conditioning systems. *Indoor Air*, Vol. 9, pp:273-281.
- Fredriksson, J., Sandberg, M. and Moshfegh, B. (2001). Experimental investigation of the velocity field and airflow pattern generated by cooling ceiling beams. *Building and Environment*, Vol. 36, pp:891-899.
- Förthmann, E. (1934). Über turbulente strahlausbreitung. *Ingenieur-Archiv*, 5(1):42-54; translated as (1936). Turbulent jet expansion. National Advisory Committee for Aeronautics, Technical Memorandum, No. 789, National Aeronautics and Space Administration, USA.
- Glauert, M. B. (1956). The Wall Jet. *J. Fluid Mechanics*, Vol. 1, pp:625-643.
- Gogineni, S. and Shih, C. (1997). Experimental investigation of the unsteady structure of a transitional plane wall jet. *Experiments in Fluids*, Vol. 23, pp:121-129.
- Griefahn, B., Künemund, C. and Gehring, U. (2001). The impact of draught related to air velocity, air temperature and workload. *Applied Ergonomics*, Vol. 32, pp:407-417.
- Griefahn, B., Künemund, C. and Gehring, U. (2002). Evaluation of draught in the workplace. *Ergonomics*, Vol. 45 (2), pp:124-135.
- Grimitlyn, M. 1970. Zurluftverteilung in raumen. *Luft und Kältetechnik*, no. 5, pp:246-256.
- Hagström, K., Siren, K. and Zhivov, A. M. (1999). Calculation methods for air supply design in industrial facilities. Helsinki University of Technology, HVAC Laboratory, Report B60, Finland, pp:50-58.
- Hagström, K., Sandberg, E., Koskela, H. and Hautalampi, T. (2000). Classification for the room air conditioning strategies. *Building and Environment*, Vol. 35, pp:699-707.
- Hiroshi, S. and Fujihiko, S. (1964). An experimental investigation of the instability of a two dimensional jet at low Reynolds numbers. *J. Fluid Mech.* Vol. 20(2), pp:337-352.
- Hsiao, F. B. and Sheu, S. S. (1994). Double row vortical structures in the near field region of a plane wall jet. *Experiments in Fluids*, Vol. 17, pp:291-301.

- Hsiao, F. B. and Sheu, S. S. (1996). Experimental studies on flow transition of a plane wall jet. *Aeronautical Journal*, Vol. 100(999), pp:373-380.
- Houghten, F. C. (1938). Draft temperatures and velocities in relation to skin temperature and feeling of warmth. *ASHRAE Transactions*, Vol. 44, pp:289-308.
- ISO 7730 (2005). Moderate thermal environments - determination of the PMV and PPD indices and specification of the conditions for thermal comfort. International Organization for Standardization.
- Karimipannah, T. (1996). Turbulent jets in confined spaces. PhD thesis, Centre for Built Environment, Royal Institute of Technology, Gävle, Sweden.
- Karimipannah, M. T. (1999). Deflection of wall-jets in ventilated enclosures described by pressure distribution. *Building and Environment*, Vol. 34, pp:329-333.
- Kosonen, R., Horttanainen, P. and Dunlop, G. (2000). Integration of heating mode into ventilated cooled beam. In: *Proceedings of Roomvent 2000*, Reading, UK, July 9-12 2000, Vol. 1, pp:381-386.
- Kosonen, R. and Tan, F. (2005). A feasibility study of a ventilated beam system in the hot and humid climate: a case-study approach. *Building and Environment*, Vol. 40, pp:1164-1173.
- Kosonen, R. and Virta, M. (2007a). Taking flexibility into account in designing beam systems. In: *Proceedings of Clima 2007*, Helsinki, Finland, June 13-15, 2007.
- Kosonen, R., Melikov, A., Yordanova, B. and Bozhkov, L. (2007b). Impact of heat load distribution and strength on airflow pattern in rooms with exposed chilled beams. In: *Proceedings of Roomvent 2007*, Helsinki, Finland, June 10-14, 2007.
- Klobut, K. and Palonen, J. (1992). *Ilmasuihkut Kirjallisuuskatsaus*. Technology report, Helsinki.
- Kulkarni, A. A. and Joshi, J. B. (2005). Measurement of eddy diffusivity in bubble column and validation based on the intermittency models. *Chemical Engineering Science*, 60 pp:6146-6159.
- Launder, B. E. and Rodi, W. (1981). The turbulent wall jet. *Prog. Aerospace Sci.*, Vol. 19, pp:81-128.
- Launder, B. E. and Rodi, W. (1983). The turbulent wall jet - measurements and modeling. *Annual review of fluid mechanics*, Vol. 15, pp:429-459.
- Levin, O., Chernoray, V. G., Löfdahl, L. and Henningson, D. S. (2005). A study of the Blasius wall jet. *Journal of Fluid Mechanics*, Vol. 539, pp:313-347.
- Liddament, M. W. (2000). A Review of Ventilation and the Quality of Ventilation Air. *Indoor Air*, Vol. 10, pp:193-199.
- Loitzansky, L.G. (1973), *Mechanics of Liquid and Gas*, Moscow: Nauka.
- Loomens, M. G. (1998). *The Measurement and Simulation of Indoor Air Flow*. Thesis, Technische Universiteit Eindhoven.

- Mayer, E. and Schwab, R. (1988). Direction of low turbulent airflow and thermal comfort. In: Proceedings of Healthy Buildings 1988, Stockholm, Sweden, Vol. 2, pp:577-582.
- Malmström, T. G. (1996). Archimedes number and jet similarity. In: Proceedings of Roomvent 1996, Yokohama, Japan, June 17-19, 1996, pp:415-422.
- McLachlan, R. (1991). A steady separated viscous corner flow. *J. Fluid Mech.* Vol. 231, pp:1-34.
- Melikov, A. K., Langkilde, G. and Derbiszewski, B. (1990). Airflow characteristics in the occupied zone of rooms with displacement ventilation. *ASHRAE Transactions*, 96 (1), pp:555-563.
- Melikov, A. K., Popiołek, Z. and Jorgensen, F. E. (1998). New method for testing dynamic characteristics of low velocity thermal anemometers. *ASHRAE Transactions*, 104(1b):1490-1506.
- Melikov, A. K. (2004). Personalized ventilation, *Indoor Air*, 14 (Suppl. 7), pp:157-167.
- Melikov, A., Pitchurov, G., Naydenov K. and Langkilde G. (2005). Field study on occupant comfort and the office thermal environment in rooms with displacement ventilation. *Indoor Air*, Vol. 15, pp:205-214.
- Melikov, A., Yordanova, B., Bozhkov, L., Zboril, V. and Kosonen, R. (2007). Human response to thermal environment in rooms with chilled beams. In: Proceedings of Clima 2007, Helsinki, Finland, June 10-14, 2007.
- Miettinen, A. and Aitta, T. (1992). Virtaus ja Lämmönsiirto. Invent-Teknologiaohjelma, Report 8, Helsinki, pp:18-20.
- Mojola, O. O. (1976). Steady flow separation along a straight streamwise corner. *Appl. Sci. Res.* Vol. 31, pp:431-436.
- Moog, W. (1978). Dimensionierung von Luftführungssystemen. *Fortschritt-Berichte Der Zeitschriften. Reihe 6 Nr. 49 total 103 pages.*
- Moore, D. E., Saffman, P. G. and Tanveer, S. (1988). The calculation of some Batchelor flows. Sadvorskii vortex and rotational corner flow. *Phys. of Fluids*, Vol. 31(5), pp:978-990.
- Nielsen, P. V. and Möller, T. A. (1987). Measurement of wall jet flow in air conditioned room. In: Proceedings of Roomvent 87, Stockholm, Sweden, June 10-12, 1987.
- Nielsen, P. 1991. Models for the prediction of room air distribution. In: Proceedings of the 12th AIVC Conference, Ottawa, Canada, September 24-27, 1991, Vol. 1. pp:55-71.
- Nielsen, P. V. (2007). Analysis and design of room air distribution system. *HVAC&R Research*, Vol. 13(6), pp:987-997.
- Niu, J.L., Gao N.P., Phoebe M. and Zuo H.G. (2007). Experimental study on a chair-based personalized ventilation system. *Building and Environment*, Vol. 42, pp: 913-925.
- Popiołek, Z., Melikov, A. K., Jorgensen, F. E., Finkelstein, W. and Sefker, T. (1998). Impact of natural convection on the accuracy of low-velocity measurements by thermal

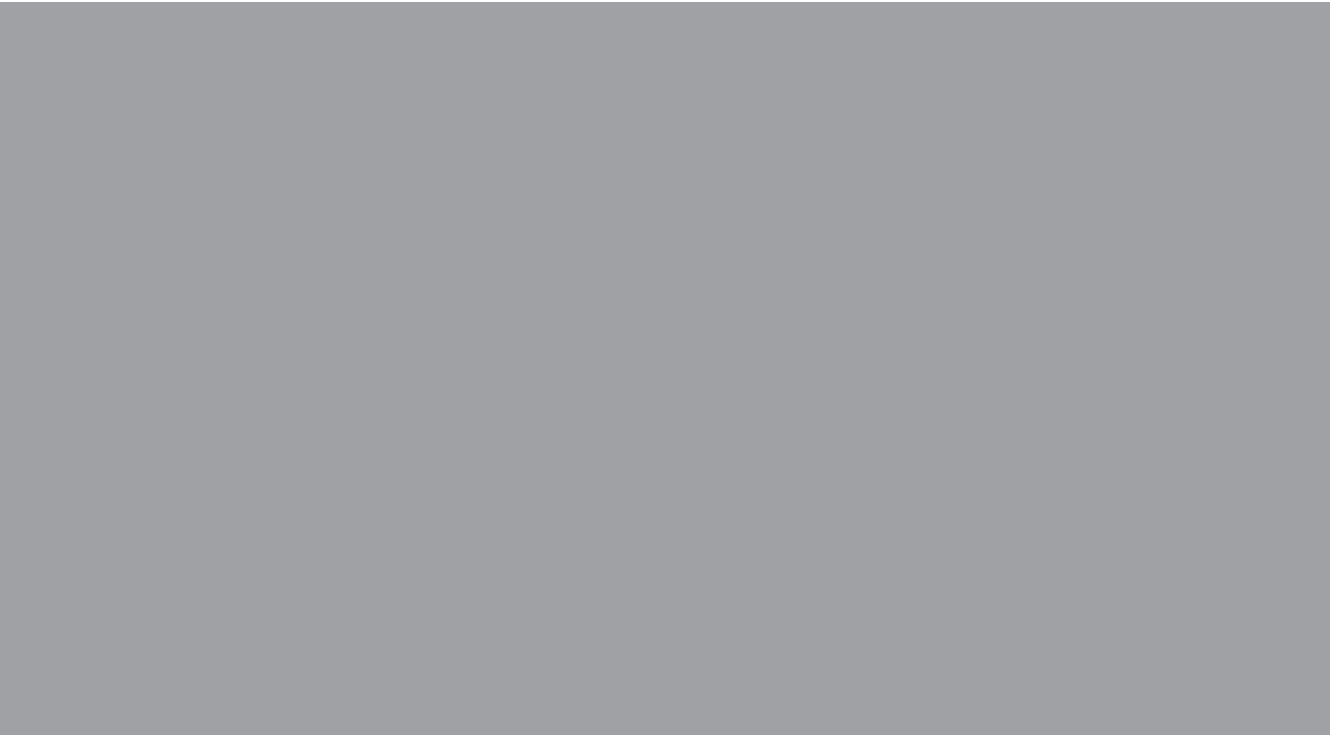
- anemometers with omnidirectional sensor. ASHRAE Transactions, Vol. 104(1B), pp:1507-1518.
- Poreh, M., Tsuei, Y. G. and Cermak, J. E. (1967). Investigation of a turbulent radial wall jet. Journal of Applied Mechanics, pp:457-463.
- Prek, M. (2006). Thermodynamical analysis of human thermal comfort. Energy, 31 pp:732-743.
- Quintana, D. L., Amitay, M. and Ortega, A. (1997). Heat Transfer in the Forced Laminar wall jet. Journal of Heat Transfer, Vol. 119, pp:451-458.
- Rajaratnam, N. and Pani, B. S. (1974). Three-dimensional turbulent wall jet. Journal of the Hydraulics Division, Vol. 100, pp:69-83.
- Rajaratnam, N. (1976). Turbulent Jets. Elsevier, Amsterdam, The Netherlands, pp:214-216.
- Regenscheit, B. 1970. Die Archimedes-Zahl Kennzahl zur Beurteilung von Raumströmung. Gesundheits Ingenieur 91(6):172-177.
- Regenscheit, B. (1975). Strahlgesetze und Raumströmung. Klima-Kälte-Technik 6.
- Riffat, S. B., Zhao, X. and Doherty, P. S. (2004). Review of research into and application of chilled ceilings and displacement ventilation systems in Europe. Int. J. Energy Res. Vol. 28, pp:257-286.
- Ruponen, M., Streblow, R. and Mustakallio, P. (2005). Room velocity control for room ventilation device. In: Proceedings of Clima 2005, Lausanne, Switzerland, October 10-12, 2005.
- Ruponen, M. and Tinker, J. A. (2007). Novel method for measuring induction rates. In: Proceedings of Roomvent 2007, Helsinki, Finland, June 10-14, 2007.
- Sandberg, M. (1987). Velocity characteristics in mechanically ventilated office rooms. In: Proceedings of Roomvent 87, Stockholm, Sweden, June 10-12, 1987.
- Sandberg, M., Wiren, B. and Claesson, L. (1992). Attachment of a cold jet to the ceiling - length of recirculation region and separation distance. In: Proceedings of Roomvent 92, Aalborg, Denmark, September 2-5, 1992, pp:487-499.
- Sato, K., Osuka, H. and Inoue, I. (1981). Maximum penetration distance of a vertical buoyant jet. International Chemical Engineering, Vol. 21(3), pp:435-443.
- Schwarz, W. H. and Cosart, W. P. (1961). The two-dimensional turbulent wall jet. J. Fluid Mech. Vol. 10, pp:481-495.
- Seppänen, O., Fisk, W. J. and Mendell, M. (2002). Ventilation rates and health. ASHRAE Journal, August 2002, pp:56-57.
- Seppänen, O. and Fisk, W. J. (2004). Summary of human responses to ventilation. Indoor Air, Vol. 14 (Suppl 7), pp:102-118.
- Seppänen, O., Fisk, W. J. and Lei Q. H. (2006). Ventilation and performance in office work. Indoor Air, Vol. 16, pp:28-36.

- Seppänen, O. (2008). Ventilation strategies for good indoor air quality and energy efficiency. *International Journal of Ventilation*, Vol. 6(4), pp:297-306.
- Shih, C. and Gogineni, S. (1995). Experimental study of perturbed laminar wall jet. *AIAA J.* Vol. 33(3), pp:559-561.
- Sigalla, A. (1958). Measurements of skin friction in a plane turbulent wall jet. *J. R. Aeronaut. Soc.* Vol. 62, pp:873-877.
- Smith, T. and Duck, P. W. (1977). Separation of jets of thermal boundary layers from a wall. *Q J Mechanics Appl Math.* Vol. 30, pp:143-156.
- So, R. M. C. and Aksoy, H. (1993). On vertical turbulent buoyant jets. *Int. J. Heat Mass Transfer*, Vol. 36(13), pp:3187-3200.
- Srebric, J., Liu, J. and Chen, Q. (2000). Experimental Validation of jet formulae for air supply diffusers. In: *Proceedings of Roomvent 2000*, July 9-12, 2000 Reading, UK, Vol. 1, pp:529-540.
- Stannov, T., Melikov, A. K., Popiołek, Z. and Jorgensen, F. E. (1998). Test method for describing directional sensitivity of anemometers for low-velocity measurements indoors. *ASHRAE Transactions*, Vol. 104(1b), pp:1481-1489.
- Subba, R. and Gorla, R. (1976). Combined natural and forced convection in a laminar wall jet along a vertical plate with uniform surface heat flux. *Appl. Sci. Res.* Vol. 31, pp:455-464.
- Suresh, P. R., Srinivasan, K., Sundararajan, T. and Das, S. K. (2008). Reynolds number dependence of plane jet development in the transitional regime. *Physics of fluid*, Vol. 20(4), DOI: 10.1063/1.2904994.
- Syehev, V. V. (1972). *Laminar Separation*. Moscow. Translated from *Izvestiya Akademii, Nauk SSSR, Mekhanika Zhidkosti Gaza*, Vol. 3, pp:47-59.
- Tetervin, V. (1948). Laminar flow of a slightly viscous incompressible fluid that issues from a slit and passes over a flat plate. *NACA TN*, No. 1644.
- Toftum, J. and Nielsen, R. (1996a). Draught sensitivity is influenced by general thermal sensation. *International Journal of Industrial Ergonomics*, Vol. 18(4), pp:295-305.
- Toftum, J. and Nielsen, R. (1996b). Impact of metabolic rate on human response to air movement during work in cool environment. *International Journal of Industrial ergonomics*, Vol. 18(4), pp:307-316.
- Toftum, J., Zhou, G. and Melikov, A. (1997). Air flow direction and human sensitivity to draught. In: *Proceedings of Clima 2000*, Brussels.
- Toftum, J. (2002). Human response to combined indoor environment exposures. *Energy and Building*, Vol. 34, pp:601-606.
- Toftum, J. and Melikov, A. (2003). Human Response to Air Movement - Evaluation of ASHRAE's Draft Criteria (RP-843). *HVAC&R Research*, Vol. 9(2), pp:187-202.
- White, M. F. (2006). *Viscous Fluid Flow*. Third edition. McGraw-Hill International Edition.

- Yang, J. W. and Patel, R. D. (1973). Effect of buoyancy on forced convection in a two-dimensional wall jet along a vertical wall. *Journal of Heat Transfer*, Vol. 95 (1), pp:121-123.
- Yu, H., Liao, C. M. and Liang, H. M. (2003). Scale model study of airflow performance in a ceiling slot-ventilated enclosure: isothermal condition. *Building and Environment*, Vol. 38, pp:1271-1279.
- Yu, H., Liao, C. M., Liang, H. M. and Chiang, K. C. (2007). Scale model study of airflow performance in a ceiling slot-ventilated enclosure: Non-isothermal condition. *Building and Environment*, Vol. 42, pp:1142-1150.
- Zboril, V., Melikov, A., Yordanova, B., Bozhkov, L. and Kosonen, R. (2007). Airflow distribution in rooms with active chilled beams. In: *Proceedings of Roomvent 2007*, Helsinki, Finland, June 10-14, 2007.
- Zhou, G. and Melikov, A. (2002a) Equivalent frequency - a new parameter for description of frequency characteristics of airflow fluctuations. In: *Proceedings of Roomvent 2002*, September, Copenhagen, Denmark, pp. 357-360.
- Zhou, G., Melikov, A. and Fanger, P.O. (2002b) Impact of equivalent frequency on the sensation of draught. In: *Proceedings of Roomvent 2002*, September, Copenhagen, Denmark, pp. 297-300.

## ORIGINAL PUBLICATIONS

- I Cao, G.Y., Kurnitski, J., Mustakallio, P. and Seppänen, O. (2008). Active Chilled Beam Wall Jet Prediction by the Free Convection Model. *International Journal of Ventilation*, Vol. 7(2), pp:169-178.
- II Cao, G.Y., Kurnitski, J., Ruponen, M., Mustakallio, P. and Seppänen, O. (2009). Plane-air-jet corner zone modelling in a room ventilated by an active chilled beam. *International Journal of Ventilation*, Vol. 7(4), pp:287-298.
- III Cao, G.Y., Kurnitski, J., Ruponen, M. and Seppänen, O. (2009). Modelling and experimental investigation of the turbulent attached plane jet in the transition process. *HVAC&R Research*, Vol. 15(3), pp:489-508.
- IV Cao, G.Y., Kurnitski, J., Ruponen, M. and Seppänen, O. (2009). Modelling and experimental investigation of a buoyant attached plane jet. *Applied Thermal Engineering*, Vol. 29(13-14):2790-2798.
- V Cao, G.Y., Kurnitski, J. and Mustakallio, P. (2007). Draught risk evaluation in rooms with chilled beams, In: *Proceedings of Roomvent 2007*, pp:101-110, June 13-15, 2007, Helsinki, Finland.
- VI Cao, G.Y., Kurnitski, J., Mustakallio, P. and Seppänen, O. (2007). Performance of chilled beam air distribution close to the wall. In: *Proceedings of Roomvent 2007*, pp:79-86, June 13-15, 2007, Helsinki, Finland.
- VII Cao, G.Y., Kurnitski, J., Mustakallio, P. and Seppänen, O. (2007). Chilled beam's air distribution measurements and plane wall jet modeling, In: *Proceedings of the 5th International Symposium on Heating, Ventilating and Air Conditioning - ISHVAC 2007*, pp:288-295, September 7-8, 2007 Beijing, China.
- VIII Kurnitski, J., Cao, G.Y. and Mustakallio, P. (2007). Draft assessment for ceiling vs. wall mounted chilled beams. In: *Proceedings of Roomvent 2007*, pp:11-18, June 13-15, 2007, Helsinki, Finland.



ISBN 978-952-248-134-4  
ISBN 978-952-248-135-1 (PDF)  
ISSN 1795-2239  
ISSN 1795-4584 (PDF)